North Sea Transnational Grid, Dynamic Wind Farm Model for simulating multi-terminal HVDC grids

E.J. Wiggelinkhuizen, J.T.G. Pierik (ECN Wind Energy) and R.T. Pinto (TU-Delft)

February 2014
ECN-E–14-006

Acknowledgement

The work reported is part of the project ”North Sea Transnational Grid” of ECN and TU-Delft. The project is financially supported by NL Agency under the EOS-LT program.

Contract No.:	019945 (SES6)
Project title:	North Sea Transnational Grid
Work Package:	WP3: NSTG multi-terminal converter operation and control
Project partners:	TUD-EPP
ECN project number:	5.0376

Abstract

The NSTG project aim is to determine the best solution (modular, flexible, most cost effective) for a high capacity transnational offshore grid. In WP3 of this project a control system for a multi-terminal DC (MTDC) grid with wind farms connected to it has been developed and tested both in simulations and on laboratory scale. The tested MTDC system can be considered as an elementary block of the Transnational Grid. The development of the MTDC controller using the novel DVC (Distributed Voltage control) power flow control method in combination with a multi-objective power flow optimizer as part of WP3b has been described in [16] together with the laboratory validation as part of WP4. This report describes a non-linear dynamic wind farm model and its simulation in the MTDC grid, which is referred to as WP3a.

The modeled wind farm consists of variable speed turbines with a permanent magnet generator and full-rated voltage source converter. The individual wind turbines and array cables are aggregated to a single string of wind turbines or even to a single wind turbine connected to an AC bus through a single AC cable. The wind farm is connected to the DC grid via a single transformer and an AC/DC converter, which is a voltage source converter in this case. The models and the controls of the wind farms, the HVDC converters and the passive components are described with their implementation in Matlab/Simulink®. The model assumes symmetrical voltages and does not contain switching elements, harmonic filters and protection systems. However the dynamics and physical limitations relevant for the grid stability are modeled. To evaluate the wind farm model response it has been connected to an onshore grid model through a HVDC-VSC station.

Simulations have been performed for different cases including normal operation, restricted power flow and ac grid faults leading power imbalances in the MTDC grid. The simulations showed that using the DVC method the DC-power flow showed good accuracy and dynamic performance. Also the DC-voltages in the MTDC network were kept within safe limits by the DVC converter control combined with the power limitation of the wind farm during ac-grid voltage dips.

Keywords: offshore wind energy; HVDC; power electronics; DC-grids; dynamic simulation.

Contents

1	**Introduction**	**5**
1.1	Scope	5
1.2	Structure of the report	6
2	**NSTG structure and technologies**	**7**
2.1	Structure of NSTG	7
2.2	Wind turbine types	9
2.3	Combinations of wind farm and converter types	10
2.4	Control design	12
3	**MTDC model desciption**	**13**
3.1	MTDC topology	13
3.2	Modeling assumptions	15
4	**Wind farm model description**	**17**
4.1	Wind farm model	17
4.2	Wind turbine model	21
4.3	Wind turbine model blocks	22
4.4	Wind turbine generator control	23
4.5	Wind turbine grid converter	25
4.6	HVDC control	26
5	**Simulations**	**29**
5.1	Power Flow Control	29
5.2	Case descriptions	30
6	**Conclusions**	**39**
A	**Model parameters**	**43**
A.1	Wind farm model	43
A.2	Wind farm control	43
B	**Implementation**	**47**
B.1	Simulation environment	47
B.2	Block structure	49

B.3 Wind farm 51
B.4 Wind turbine 55
B.5 MTDC model 75

C Suggested improvements and next steps 81
C.1 Wind Farm dynamic models 81
C.2 DVC power flow control with measurement errors 83
C.3 DC loop flows 86

Index 89

1

Introduction

The integration of a large share offshore wind energy in the European electricity system requires a significant effort for the development of an offshore grid infrastructure. With the increasing wind farm sizes and distances to the onshore grid connection points, the technical and economical limits of High Voltage AC (HVAC) cables are reached at a certain point. With the development of High Voltage DC (HVDC) systems it has become feasible to build long transmission links to offshore wind farms, to interconnect wind farms and even to establish transnational interconnections for international exchange of wind power.

In the NSTG project three scenarios for the NSTG are studied, representing different stages in the development of this grid, cf. [9]. Besides a good technical performance and economical feasibility the NSTG should be flexible and modular. This means that wind turbines and converters of different technologies and with different ratings can be connected and that the grid design is suitable for stepwise extension. It is likely that the NSTG will expand in steps, each time applying newer generations of power electronic converters and cable technology. Further, the NSTG will not only be connected to different national grids, but also to HVDC interconnectors, generating units, loads and storage systems.

1.1 Scope

In the NSTG project all connections in the NSTG between the wind farm substations and the national grid connection points are DC. In the final scenario all wind farms, which are aggregated to one or two nodes per country, are interconnected through a DC ring and also directly connected to the nearest onshore connection point through a full rated DC connection, cf. figure 1.

Different technical solutions and control strategies for the NSTG will be evaluated. For MTDC converters several AC/DC converters technologies are considered, including Voltage Source Converters, Current Source Converters (CSC) combinations of these types. Also different combinations of wind turbine types and converters and their implications for system design and operation are discussed. Detailed technical design aspects of the components, such as specific wind turbines types and converters, protection systems

Figure 1: North Sea Transnational Grid and wind farm locations (photo: NASA)

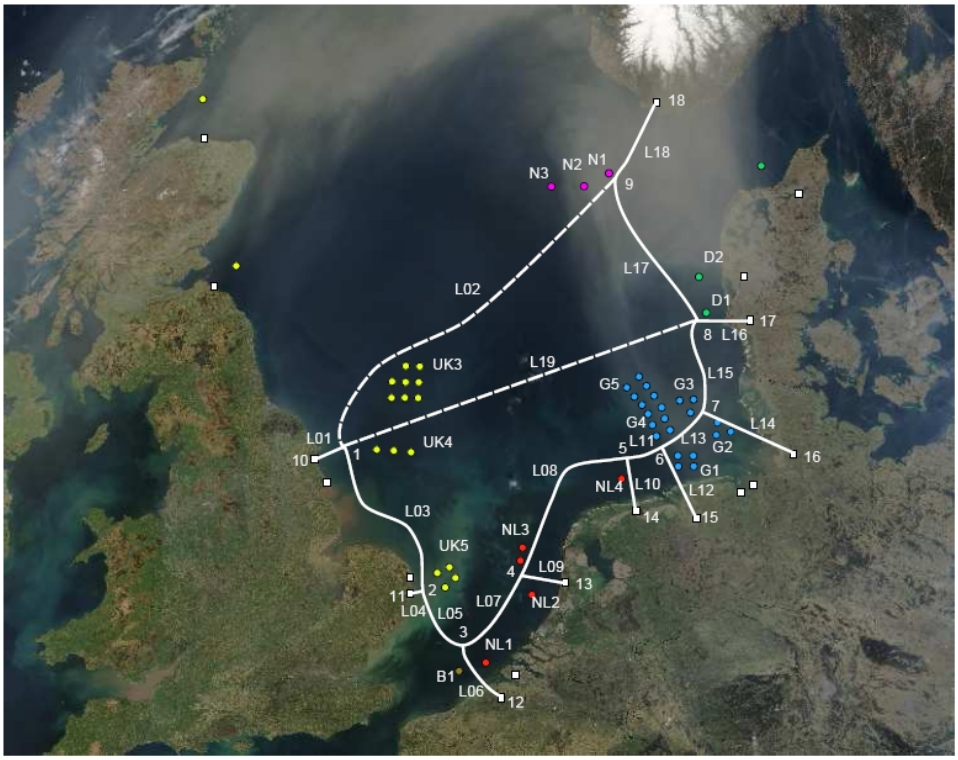

and harmonics, are not considered here.

For the most promising solution an MTDC controller has been developed in WP3b and tested in WP4. The MTDC controller should preserve the power balance in the DC-network via the setpoints of the connected AC/DC converters, such that the DC voltage at all nodes is kept stable and within safe operational limits. Therefore the selected control algorithm, called Distributed Voltage Control (DVC) developed by TU-Delft, applies a Multi-Objective Optimisation Algorithm (MOOA), tailored for this application by TU-Delft as part of WP5.

This report deals with the wind farm models that will be used to develop and test the MTDC controllers. The development and testing of the MTDC controller will be reported separately.

1.2 Structure of the report

A summary of the current and future wind farm technology options to be interconnected through the NSTG is presented in sections 2.2 and 2.3. This includes fixed-speed and variable speed concepts with and without converter. Also different converter types and grid topologies are discussed, as these influence how the wind farm is operated and which technology combinations are suitable.

In section 2.4 a selection is made of the most promising technology combinations for the NSTG, for which a controller will be designed and tested.
Sections 3 and 4 describe the models of the MTDC network and wind farm.
Section 5 describes the simulation cases and presents the results.
Section 6 summarizes the conclusions and next steps.

2

NSTG structure and technologies

2.1 Structure of NSTG

For exploiting of the large wind energy potential in the North Sea the NSTG is considered to connect large wind farms located far offshore to the onshore grid and to strengthen the transnational energy trading capacity by long DC-interconnectors. Starting from the existing and already planned offshore wind farms, onshore grid connection points and HVDC interconnectors, the NSTG will expand gradually, as outlined in [9].

There are many possibilities for the internal structure of the NSTG and it is not yet determined how this grid will develop, cf. [7]Figure 2 illustrates some basic topologies from which the NSTG can be composed. In Figures 2 b) to e) each gray line represents a pair of cables, while in Figure 2 a) the individual poles are shown instead. The DC/DC-converter blocks in Figures 2 b) to e) are shown as gray boxes, indicating that these converters are only required for interconnection of HVDC systems with different voltage levels.

The topologies a) and b) can be regarded as primarily a transnational interconnector for trading to which one or more a wind farms feed in. If not yet fully loaded, connecting a wind farm to such interconnector increases the utilisation of the existing infrastructure. In some cases this may result in net cost benefits. In scheme a) the classical LCC-HVDC technology is applied. The feed-in to about 20% of the interconnector rated power can be realised by means of a series-connected DC/DC-converter [1]. The tap in the HVDC line can be made at either the positive or the negative pole or as parallel device. Despite the limited power rating this converter carries the (constant) nominal current and should have galvanic isolation to withstand the maximum voltage of a single pole. In case of a VSC-HVDC link, as shown in scheme b), the DC-voltage level of the interconnector and the WF grid may not match, therefore a DC/DC-converter is included to match this difference. Several concepts for tapping have been patented but no full-scale system has been built so far.

The scheme in Figure 2c) can be a cluster of wind farms far offshore that is connected

Figure 2: Possible basic topologies in the NSTG

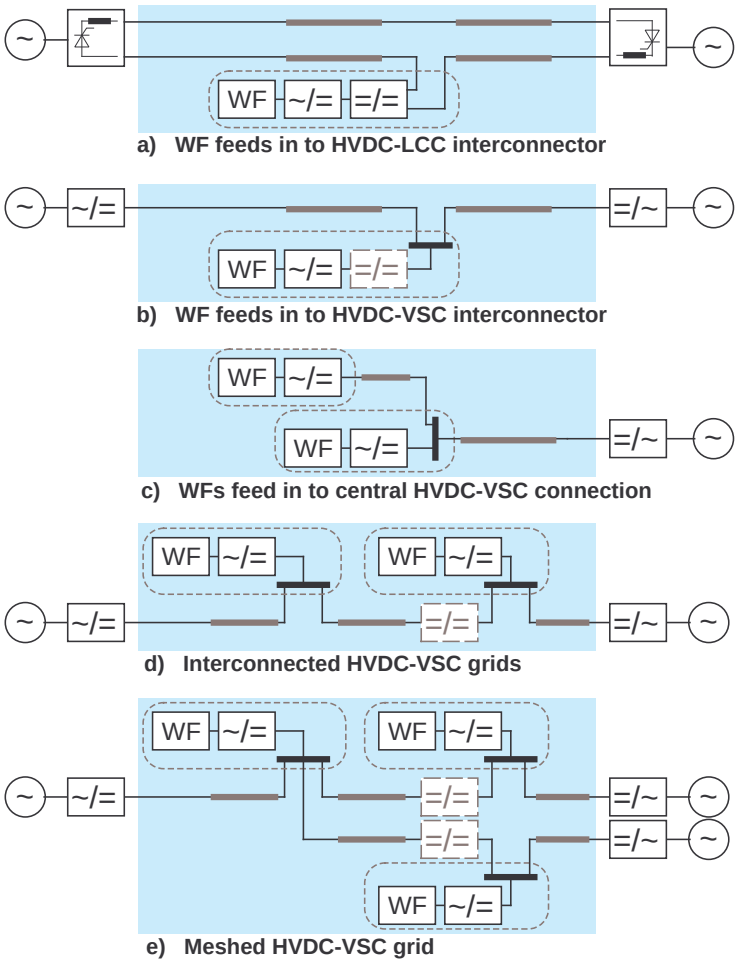

via a central point through a strong HVDC link. For example this could be an offshore HVDC hub as extension of the national grid, such as in the German offshore zone, or a HVDC backbone to alleviate onshore congestion problems, such as proposed for the Irish sea. A problem is that the connection capacity should be sufficient to connect not only the existing wind farms, but also to include planned wind farm installations.

The schemes d) and e) are examples of more complex structures, which may be built in the Southern part of the North Sea, e.g. at the East coast of the UK, where numerous large wind farms are planned. Scheme d) can be seen as an interconnection of two already existing wind farms, each one connected to the nearest onshore grids through HVDC. A DC/DC- converter may be required to match the difference in rated voltage of the two systems.

For developing the control for the NSTG a relatively small meshed multi-terminal DC system will be considered, representing a section of the NSTG. To be representative the studied MTDC system will consist of at least two wind farms or wind farm clusters with different power output profiles and at least two onshore grids which should be interconnected to enable trading.

In section 2.2 the basic technology options for wind turbines are described, followed by an evaluation of possible combinations of wind turbine types and converter technolo-

Figure 3: Possible basic topologies in the NSTG

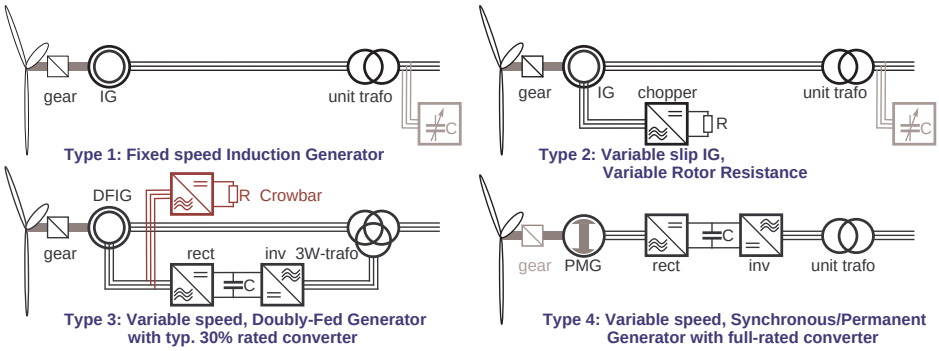

gies for integration in the NSTG. The model of the selected combination(s) is described in section 4, including the wind farm controller design.

After having developed the controllers for the simplified NSTG topology, it should be verified that these are suitable for more complex MTDC systems and in combination the different wind farm technologies.

2.2 Wind turbine types

The wind farm characteristics are mainly determined by the type of wind turbines that are applied. Wind turbines are usually categorized as follows, see also figure 3, cf. [6] and [20]. Please note that only wind turbines with AC voltage connection are considered.

Fixed Speed Induction Generator (FSIG) type is usually directly connected to a central AC/DC converter. The aerodynamic power limitation is usually aerodynamic (active) stall. The dynamic properties of stalling the blades are usually not very accurate, so not suitable for power regulation, but rather for fast power reduction in case of braking. Advantages are the simple and cost effective design, while drawbacks are the lack of controllability of active and reactive power, generation of harmonics and higher blade loading. By changing the grid frequency in the wind farm, controlled by the turbine or wind farm converter, (partial) variable speed operation is possible.

A variant of this wind turbine type for a limited variable speed operation is FSIG with variable rotor resistance. This type is mentioned here only for completeness and will not be considered further, because of the lower efficiency and higher maintenance requirements.

Doubly Fed Induction (or Asynchronous) Generator (DFIG/DFAG) with partial converter in the rotor circuit and pitch to vane aerodynamic control operates at variable speed and has good control capabilities, i.e. independent control of active and reactive power. Because of the small converter and lower top mass it is less costly than a full rated wind turbine, however the rotor circuit is sensitive to voltage dips, and adequate protection by a controlled chopper circuit is required. Crowbar protection without a controlled chopper, as applied in older types, is only effective for very short grid dips and therefore considered insufficient. Other drawbacks are the extra maintenance due to the generator slip rings and also the lower efficiency in partial load due to the increased slip. The

Figure 4: Wind farm technologies and grid connection options

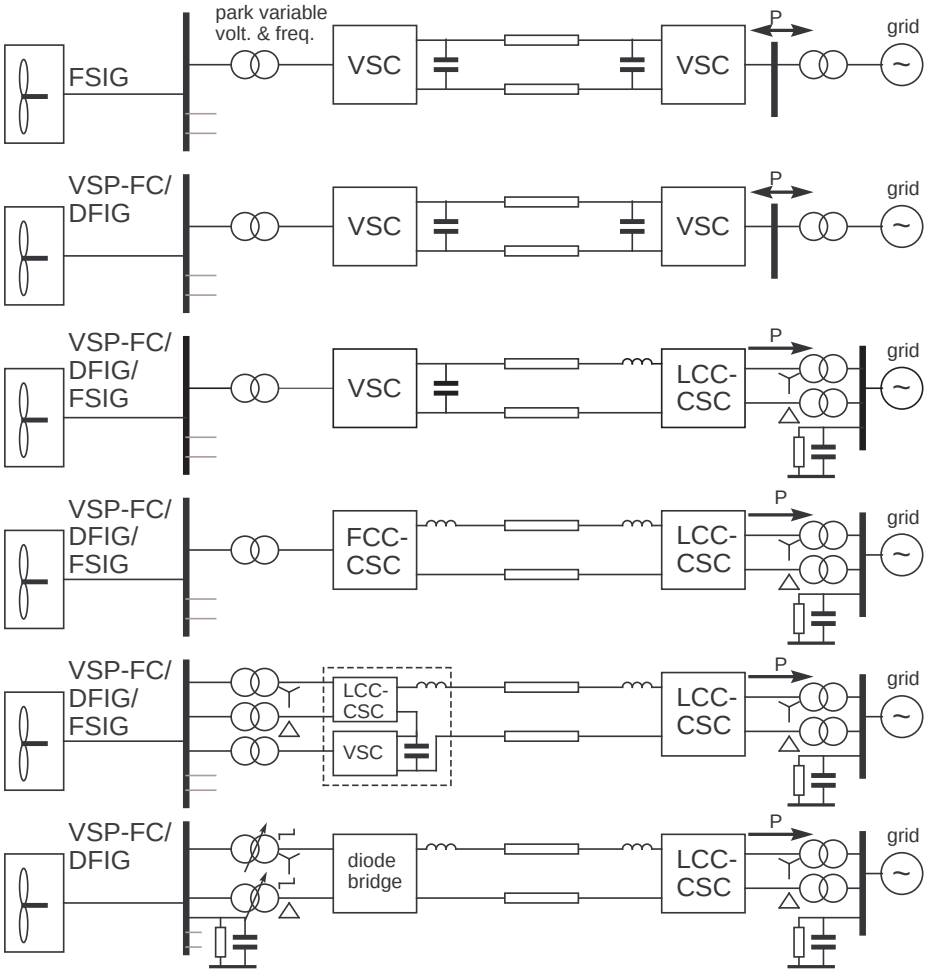

reactive power control capability, which is related to the converter size, is limited.

Synchronous or Permanent Magnet Generator with Full Rated converter (SGFC/PMGFC) has rapidly gained popularity thanks to its superior control capabilities. These capabilities are mainly important for reducing loads and to contribute to the grid frequency and voltage stability. Drawbacks are the higher costs of the full rated converter and of the active material in case of a PM generator, the higher top mass and the limited fault current contribution.

A more detailed overview of wind turbine types and their main electrical and control characteristics is provided by [15] and [24]. In [24] also hybrid wind farms are proposed to optimize costs as well as control capabilities.

2.3 Combinations of wind farm and converter types

Figure 4 shows possible combinations of different wind farm and converter technologies for grid connection, see also [23], [4] and [3]. For simplicity a point-to-point HVDC link is considered.

The most common converter technology to use to connect offshore wind farm is Voltage

Source Converters (VSC) as shown in the upper two schemes. VSC with forced commutated IGBT switches are fully controllable, although losses are still relatively high and protection against DC-faults is difficult. In the case of FSIG type wind turbines the VSC at the WF side controls the voltage and frequency to a setpoint can be adjusted by the WF control. In this way the wind farm can operate at collective variable speed at below-rated wind speeds, which is an improvement compared to operation at fixed speed, although the power control is still limited and issues like reactive power compensation and harmonics remain [24].
The third scheme shows a hybrid HVDC connection with a VSC at the WF side and an onshore line commutated current source converter (LCC-CSC) based on thyristors. With this combination converter losses and costs could be reduced. The LCC-CSC converter requires a strong grid connection and a large area to install the harmonics filters. As indicated in the figure, the power flow is unidirectional.
The fourth option is to have a CSC also at the WF side, however with forced commutation (FCC), so that the converter is fully controllable and produces less (low-order) harmonics. This type of converter is not commonly used, but could be built using reverse-blocking IGBT switches. A series-connected hybrid converter (SHC) at the WF side could be used, although it is obviously more complex and also not yet available. A SHC combines a classical thyristor converter with a relatively small IGBT VSC converter, about 30% of the total rated power. The VSC acts as an active harmonic filter and improves the control capabilities, including fault handling. The losses are expected to be close to those of a LCC converter. [18]
Final option that is presented is a passive diode bridge, which is simple and cheap, although it requires that the WF controls the active power, grid voltage and frequency. Further it needs harmonic filters, although less than thyristor converters. Multi-phase switching can be applied to reduce low-order harmonics, but this requires extra phase-shifting transformers and a well-balanced grid voltage. According to [2] the wind farm can only operate at optimum power under the condition that the rectifier is in voltage clamping mode, i.e. the WF voltage control is saturated. A solution, which is proposed for further investigation, is to apply tap changers in order to maintain this condition. Special attention is required for accurate and fast the active power control in the wind farm.

Selection

For the wind turbine type a Variable Speed Pitch-controlled type with full-rated converter is chosen because this type shows good control capabilities, which are especially needed for balancing the power in the MTDC grid. Looking at the specific operating conditions of a wind farm connected through a VSC, DFIG wind turbines are expected to show similar dynamic performance. The Fixed speed types without converter have poor control capabilities and need additional equipment to preserve power quality.
DFIG wind turbines connected via HVDC are supposed to behave similar to wind turbines with full-rated converters, except for short-circuit current and asymmetrical faults. However, the AC-voltage in the wind farm is controlled by the HVDC converters, therefore asymmetrical faults are less likely and also the short-circuit current contribution is less relevant than with an AC grid connection.

From the different HVDC converter technologies it is clear that at the wind farm a forced-commutated converter is required because of its superior controllability and smaller footprint. For the moment hybrid converter types are considered to be too complex and their feasibility is uncertain, while the expected behaviour should be like a VSC. From

the viewpoint of the protection a combination of VSC and forced commutated CSCs seems interesting, but when only considering dynamic behaviour for power flow control design, it is expected to be similar to a DC grid with only VSCs. Therefore VSC technology is chosen for modeling the MTDC grid.

Other components

It should be noted that several components that are required in the technical design have been omitted here, such as array cables, protection, grounding, balancing, switches, harmonics filters, platforms, auxiliary power supplies, measurement and telecommunication. For a proper dynamic wind farm simulation these simplifications can be justified, these components should be considered in case of detailed wind farm design, as most of these impose design limitations and some may also influence the dynamic behaviour.

2.4 Control design

The presented combinations of wind farm and converter technologies all have different capabilities and dynamic characteristics. Therefore the control design for the wind farm converter as well as for the wind turbine electrical system of each combination is also different.

In general the wind farm converter is set supply the AC voltage and frequency according to fixed setpoint values. Under normal conditions all available power from the wind farm is converted to DC, so the power flow control should be performed by neighbouring stations in the MTDC network or, in case of a point-to-point HVDC link, by the receiving converter station. For VSC stations this is equivalent to controlling the DC voltage, while for CSC stations this means DC current control. In the following we assume only VSC stations in the MTDC network.

In case of power imbalance in the DC network, or more specific, DC over-voltage, the WF power output should be reduced almost instantly. Because reducing the generator torque needs some time and because of limitations of the converters, chopper-controlled braking resistors are needed to dissipate the excess power. The WF power reduction can be accomplished in different ways, depending on the type and design of the VSC station and the wind farm. This is treated in more detail in section 4.

The wind turbine model is based on an existing 6MW demo turbine including the controller [22]. The wind turbine grid-side VSC control has been adapted to operate in combination with a VSC, in particular the reactive current injection during voltage dips. The VSC control settings in the MTDC grid have been copied from the settings derived in WP3b. The controller optimisation using the linearized models has not been implemented in this model.

In the next sections models for wind farms and converters will be described.

3

MTDC model desciption

In the next paragraphs the wind farm configuration in an MTDC system is presented and modeling assumptions are motivated. Then the WF model structure is presented and the functional blocks and their operation are described. Finally some aspects of the implementation in Simulink™ are described.

3.1 MTDC topology

To study the control of a multi-terminal DC-grid, a simplified topology has been chosen, representing a part of this grid, located in the southern part of the North Sea, see Figure 5.

It comprises three grid connection points in different countries, named UK, NL and DE in Figure 5, and three offshore wind farms, indicated by the red dots, named UK1, NL1 and DE1. The lines represent HVDC transmission cables and the intermediate nodes N4, N5 and N6 are cable T-joints. The size and location of the wind farms connected to the NSTG have been derived by clustering the main offshore wind farms in the three

Figure 5: Topology of the modeled MTDC grid

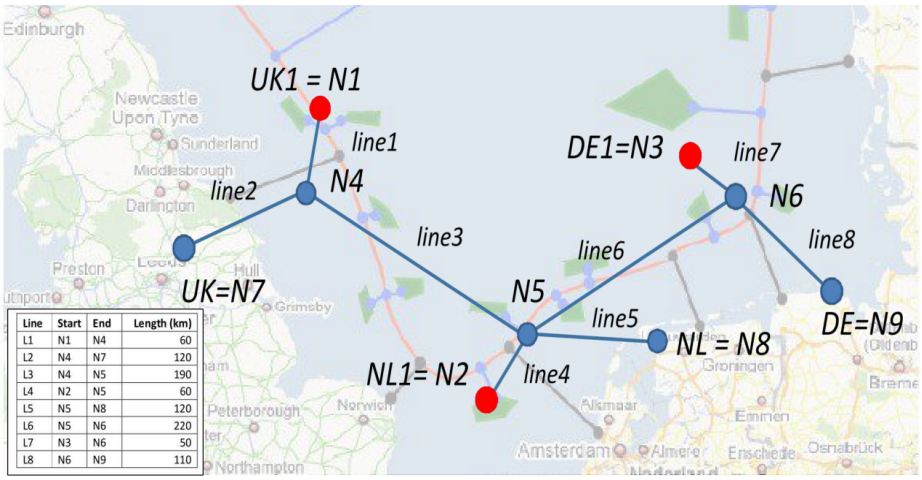

Line	Start	End	Length (km)
L1	N1	N4	60
L2	N4	N7	120
L3	N4	N5	190
L4	N2	N5	60
L5	N5	N8	120
L6	N5	N6	220
L7	N3	N6	50
L8	N6	N9	110

Figure 6: Components of the modelled MTDC grid (DE nodes)

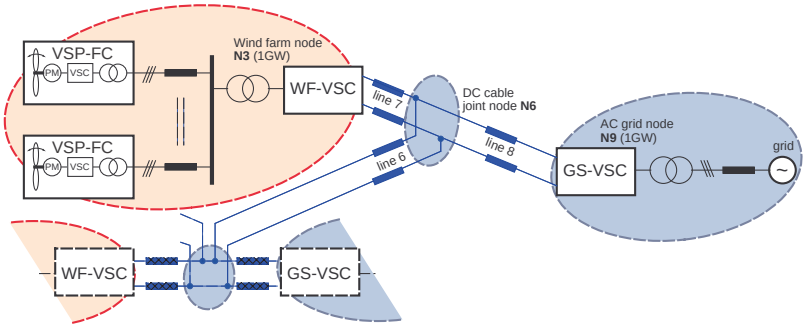

national regions in the southern part of the North Sea, also including wind farms in the construction and planning phase. These locations are used to derive the line lengths.

MTDC system rating

For simplicity, each wind farm node and each onshore node in the small MTDC grid represents a single voltage-source converter (VSC) station of 1GW. Also the nominal power of each of the wind farms is chosen as 1GW, see Figure 6, so that the capacity is sufficient to transport all wind power to the nearest country. Trading offshore wind power or onshore generated power to other countries via line3 and line6 in Figure 5, is possible up to the available capacities of the VSC stations of the three countries.

DC network model

Figure 7 shows a more detailed scheme of the same MTDC network. The rated power of each of the wind farms and of each converter is chosen equal to 1GW. The nominal interconnection voltage is chosen equal to 640kV (cable pair of +/-320kV), as this is the highest voltage for which offshore cables are currently available, so that transmission losses over longer distances are minimized.

In the model of the MTDC network each DC cable connection is represented by a single Π-section. At each node half the capacitance of the connected cables is added to the VSC station capacitance. The voltage is assumed to be perfectly balanced.

AC Network model

As the focus is on the control of the MTDC grid, the models of the three terrestrial AC grids are highly simplified. Two AC grids (NL and DE) are modelled as an infinite bus behind a short circuit series impedance, while the UK AC grid is modelled as a single synchronous generator with a series line impedance and a shunt resistance to model a 3-phase fault. These AC grids do not have other loads or generation units connected. The short-circuit power is chosen equal to 5000MVA.

The AC-side of each VSC shows a current smoothing inductor Z_{sm} and a shunt capacitance C_f representing the harmonics filtering, which are both specified in p.u. of the VSC base power. The AC grids are connected to a constant reference voltage u_{gref} through a short-circuit impedance Z_g in series with the transformer leakage inductance Z_{leak}. All impedances are frequency dependent, but for simplicity the symbol Z is used and the same holds for the series admittances Y of the DC-cables.

Figure 7: Model of the MTDC network including AC-grids

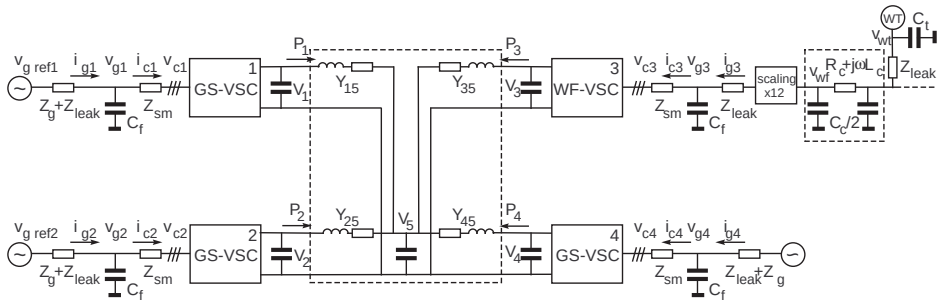

3.2 Modeling assumptions

A number of simplifications have been carried through in the models to reduce the computation time when simulating wind farms with a large number of turbines and converters and also because the required information, such as control parameter and protection settings, is not available. The models have been implemented in Simulink and are based on earlier work in which dynamic wind farm models have been developed and demonstrated, cf. [12, 13, 14] and also partly verified, cf. [10, 11].

The models only consider symmetrical AC-voltages and currents, represented as dynamic phasors. Devices for protection and balancing are not included. Non-linear magnetic effects, such as transformer core saturation and hysteresis losses, are not modelled either. The cable models consist of lumped frequency-dependent network elements. Converters are modelled as non-switching and lossless, only a low-pass filter is included to represent the switching delay. At the DC-side voltage ripples from converter switching and voltage unbalance are neglected. The dynamic behaviour of measurement devices, also including PLLs for estimating the grid voltage angle and rotor flux position, is represented by low-pass filters.

This means that electromagnetic phenomena, such as inrush currents, switching transients and harmonics, cannot be accurately represented in the models. However the aim is to develop and evaluate wind farm controllers, so the dynamic response in the frequency range of concern, typically up to 20 Hz. should be modeled accurately.

DC grid operation

The wind farm converter (WF-VSC) operates as rectifier and controls the wind farm AC voltage to a fixed reference, while the power production is determined by the wind farm. The grid side converters (GS-VSC) together control the power flow in the DC-network such that the DC node voltages and line currents stay within safe operating limits and electrical losses are minimized. Compared to point-to-point HVDC systems, the DC voltage at the WF-VSC may show more variation due to changing power flows in the MTDC network.

For this power flow control a new method, called Distributed Voltage Control (DVC), is applied here. Compared to other possible control methods it shows good dynamic response as well as good scalability, i.e. that it is applicable for complex networks, and fail-safe operation, cf. [16].

4

Wind farm model description

For the developing wind farm controllers to be applied in MTDC systems, a dynamic wind farm model is used which consists of one or more identical wind turbine models. In most cases only a single turbine model is applied, but for some detailed studies a string with five wind turbines has been modelled, for instance to study the AC voltage profile and interaction of turbines via the grid. The wind turbine models are variable speed with permanent magnet generator and a full rated voltage-source converter. The turbines are connected to a central power collection bus through a string feeder. The output power of a single string feeder is upscaled to match the total wind farm output power. A transformer matches the voltage level of the wind farm collection grid to that of the wind farm converter station.

To model the effect of spatial smoothing of the output power of wind turbines in a wind farm different wind inputs are applied for each of the wind turbines in the model. In this way also a more realistic response is obtained during fault events and activation of wind farm power curtailment, because the different operating conditions of the modelled wind turbines lead to different dynamic responses.

4.1 Wind farm model

The upper scheme in Figure 8 shows the wind farm electrical layout in which each five wind turbines are connected to a string feeder. Because of the large size of the wind farm the model it should be simplified, which is done by aggregating components, as shown in the lower scheme. The collection grid is represented by a single cable, the power generated by a single string is upscaled with a factor of N_{par}, which is the number of parallel strings, and the wind turbines are represented by a single VSC. The power input of this VSC $P_{e_aggr}(t)$is generated by combining the outputs of three detailed wind turbine models.

Figure 9 shows how the three output power series $P_1(t)$, $P_2(t)$and $P_3(t)$ are generated. Depending on the position of a wind turbine in the farm a different power output series is selected and a delay time Δt is added, which is indicated in Figure 10, cf. [8]. The

Figure 8: Wind farm component aggregation

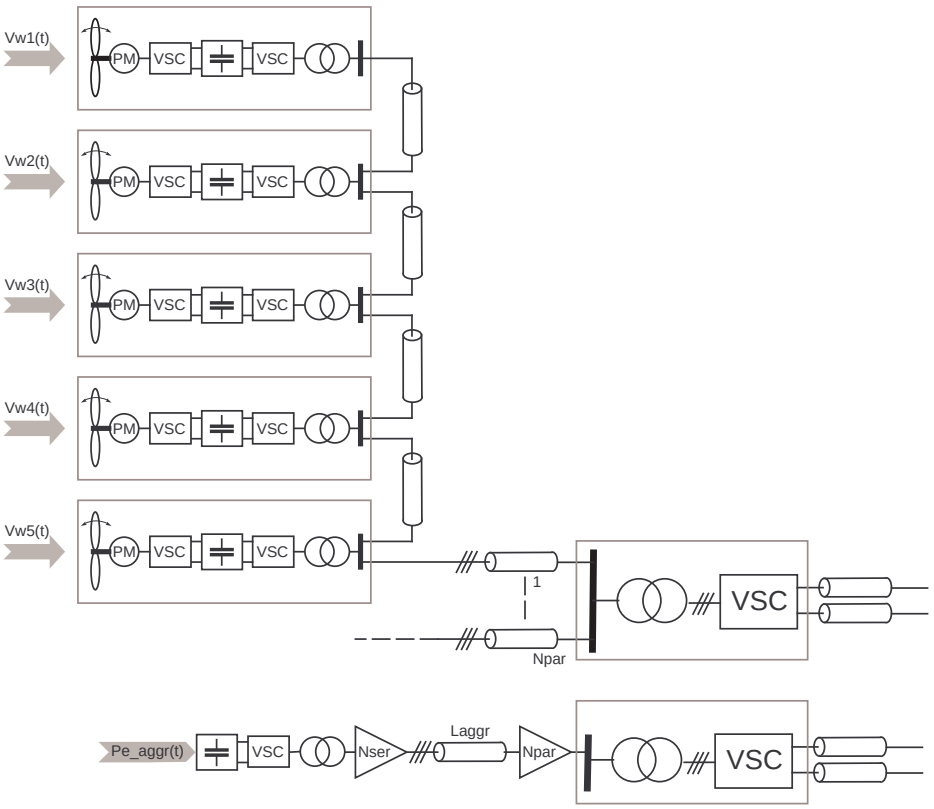

Figure 9: Wind farm smoothing, step 1: generation of wind turbine power series

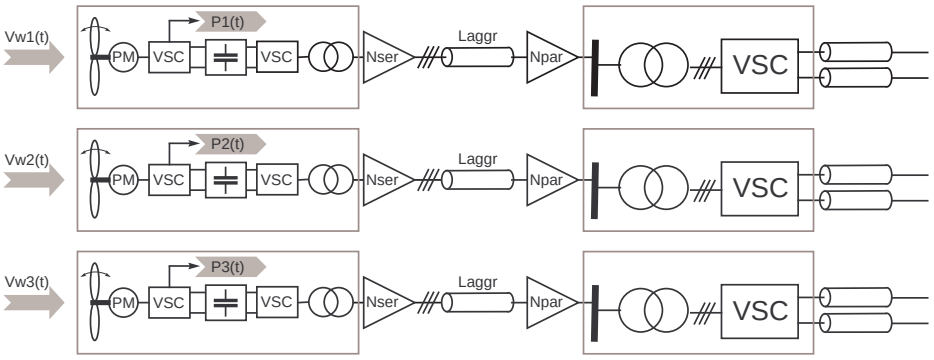

wind speed deficits in the wind farm due to wake effects are only estimates, as more accurate calculations are complicated and need detailed information of the turbines, the wind farm layout and the atmospheric conditions. Depending on the simulation case different undisturbed wind speed series are applied.

The delay time is inversely related to the average wind speed, which leads to a sufficiently low correlation between the power outputs. According to the theory the resulting power output variance is reduced by a factor of $\sqrt{N}$ compared to the output variance of a single wind turbine. An extra low-pass filter has been added, to smoothen the power output steps in the output $P_{e\_aggr}(t)$ caused by the sampling rate of the wind turbine controller output.

Figure 10: Wind farm smoothing, step 2: combining wind turbine power

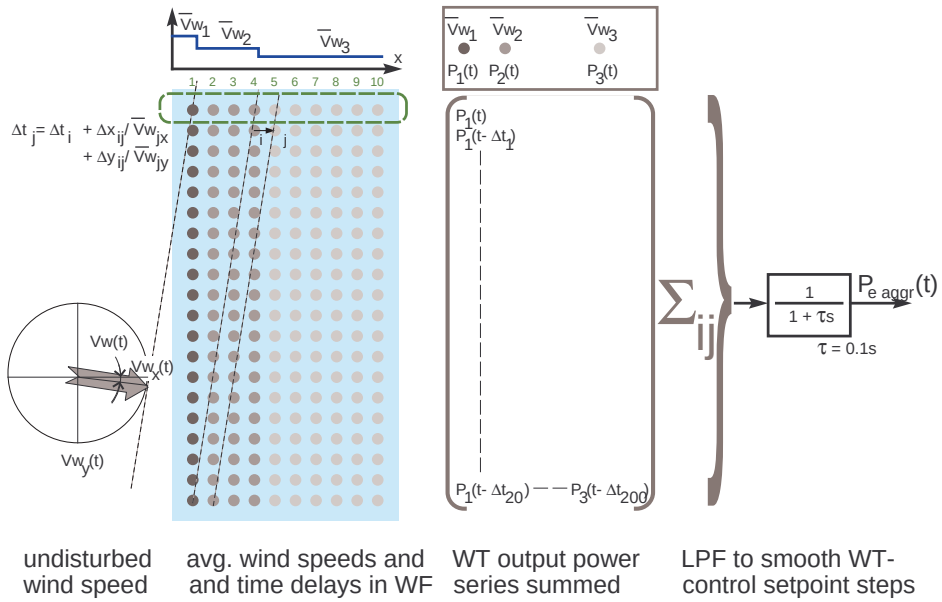

Figure 11: Wind farm power per wind turbine

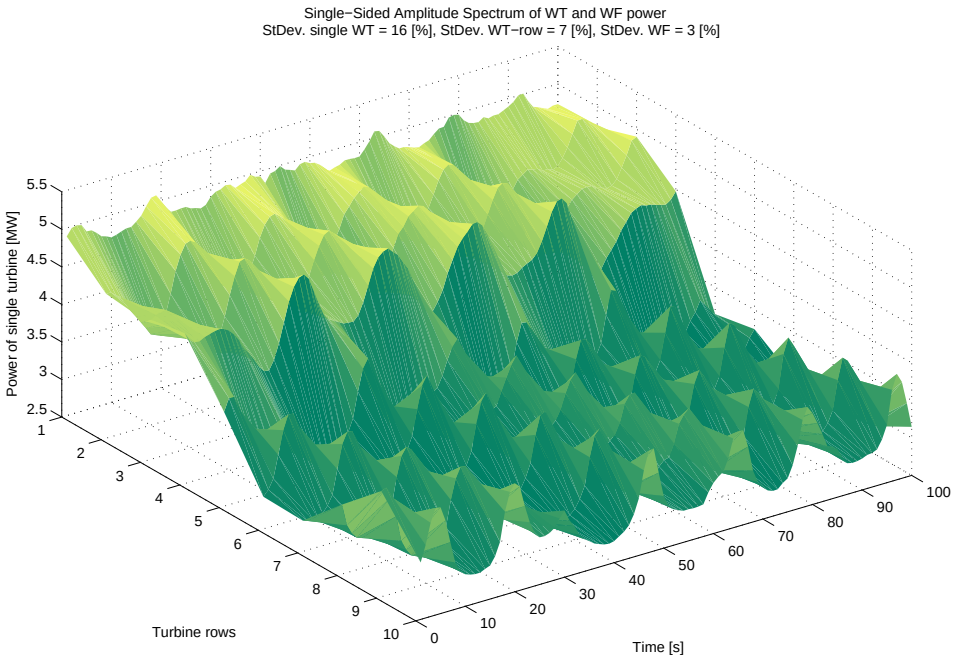

Figure 12: Wind farm power per line of 20 wind turbines

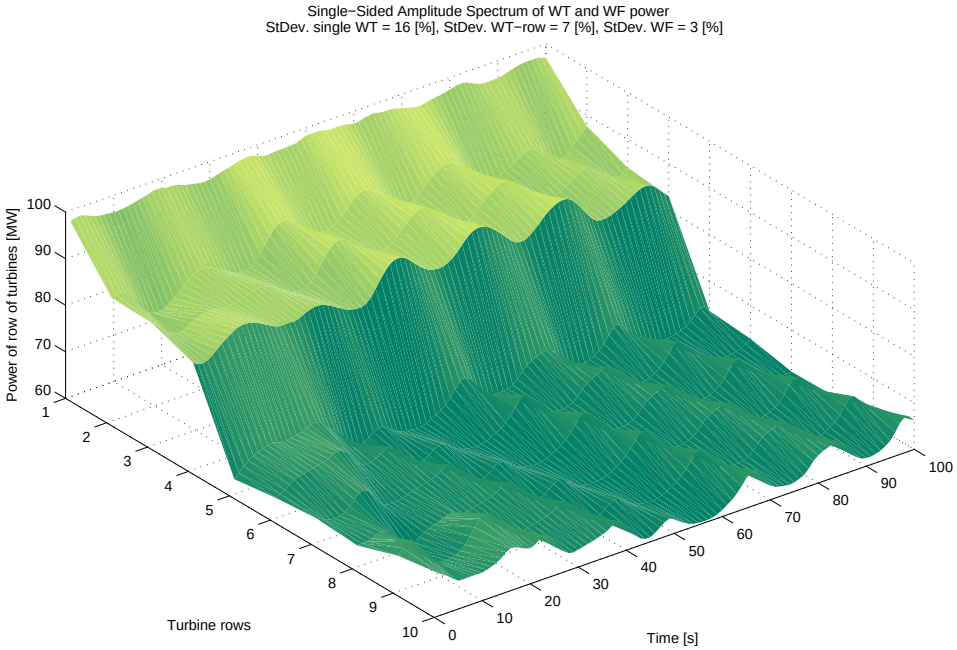

Figure 13: Wind turbine and wind farm power

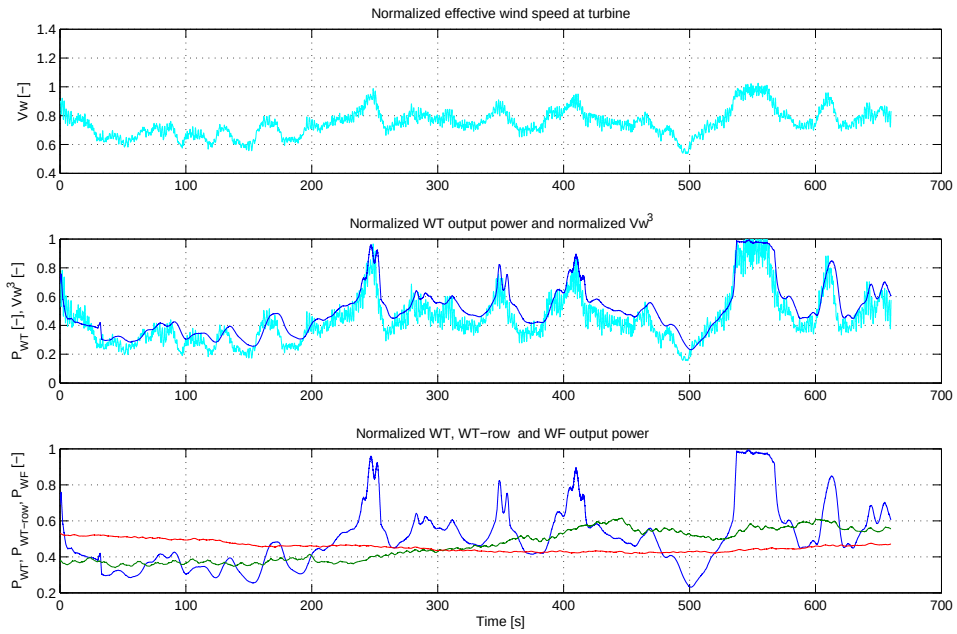

Figure 11 shows the output power in time of the individual turbines that are in the upper row of Figure 10, while Figure 12 shows the power in time of each vertical line of turbines in Figure 10. Figure 12 shows that summing the power outputs per 20 turbines significantly reduces the power output variations, because of the spatial smoothing. The power variations around rated wind speed, in row 1, are relatively small, because the wind turbine control limits the output power. Also for low wind speeds, in rows 4 to 10, these variations are small compared to the variation in rows 2 to 4, because the optimum power varies with the cube of the wind speed.

Figure 14: Wind turbine and wind farm power spectra

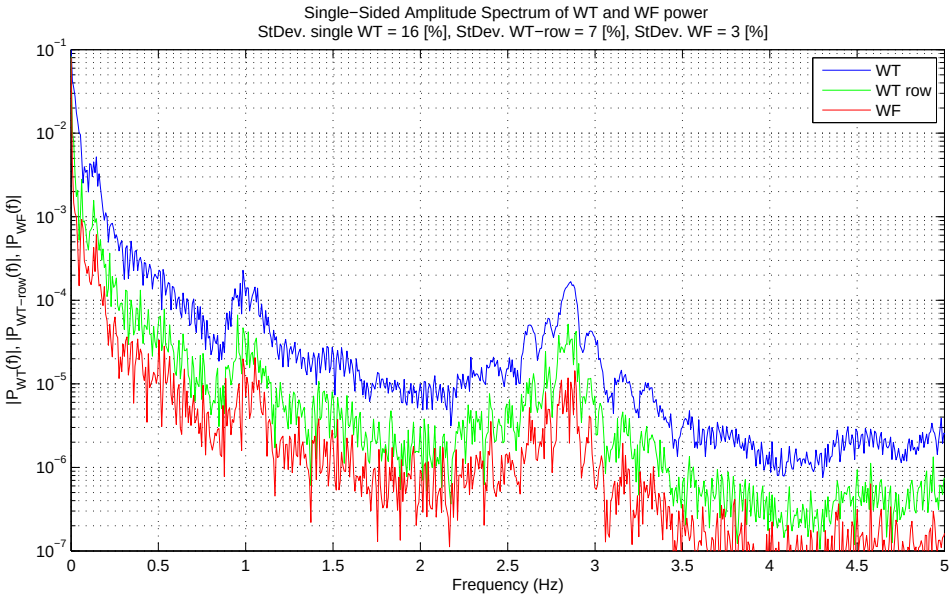

Figure 15: Wind turbine schematic overview

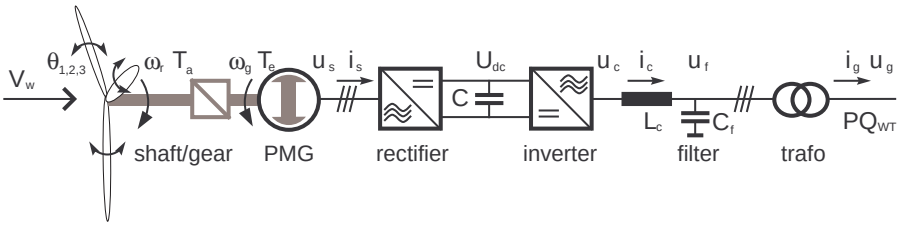

Figure13 also illustrates the smoothing effect of the wind farm. The upper plot in this figure shows the wind speed of an individual wind turbine, normalised to the rated wind speed. The middle plot shows that the wind turbine power output closely follows the cubic wind speed. The third plot shows the smoothing effect per row of 20 turbines (in green) and of the complete wind farm of 200 turbines (in red). The normalized power spectra in Figure 14 show the expected reduction in output power variation of about one order of magnitude. Because of the relatively short simulation time, the comparison of the values in lower end of the spectrum, under about 0.1 Hz., is less accurate.

4.2 Wind turbine model

The applied wind turbine type is variable speed, collective pitch controlled with a permanent magnet generator that is connected through a full-rated converter, cf. Figure 15.

Below rated wind speed the wind turbine controller sets the generator torque T_e to maintain optimum tip speed ratio operation, so ω_r is proportional to the wind speed V_w, while the blade pitch angle Θ is kept fixed at working position. Above rated wind speed the collective pitch angle is increased towards vane position in order to limit the aerodynamic power, while the generator torque control is set to keep the output power P_{WT} close to the rated power. At the same time these controls should keep the rotor speed within a limited range, which requires careful design of the controller, as the re-

Figure 16: Wind turbine model blocks

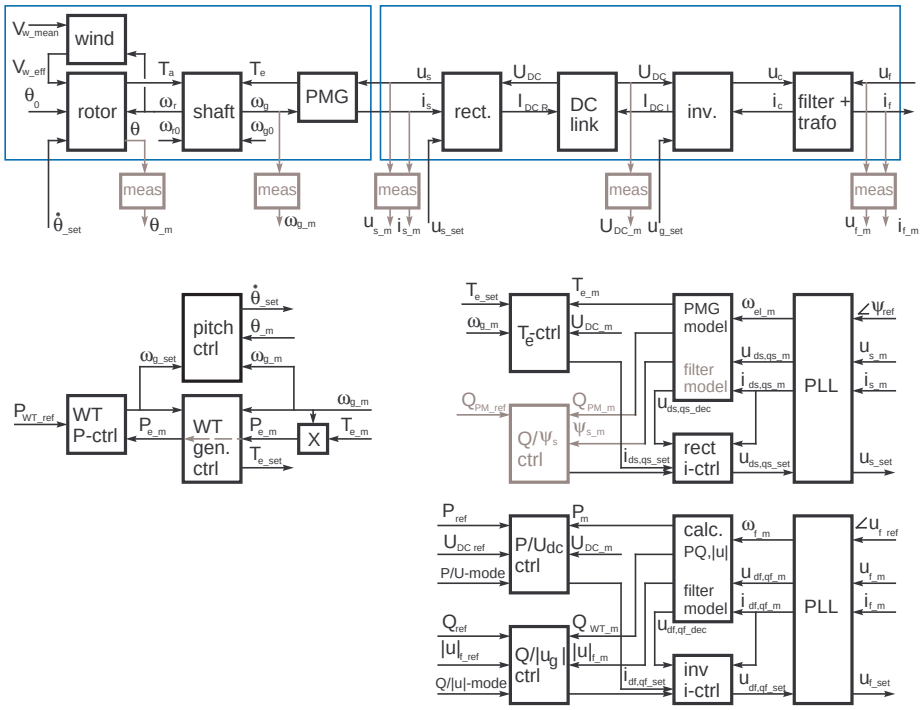

sponse of the aerodynamic torque to a pitch angle variation is slow, especially close to working position. Secondly, controlling the torque to maintain constant power output implies that the generator torque set-point decreases with increasing rotor speed, which is a positive feedback to the rotor speed and in-plane blade deflections.

The wind turbine converter is a back-to-back voltage source converter. The rectifying converter controls the generator torque T_e according to the set-point from the wind turbine controller. The inverter controls the DC-link voltage U_{DC} and the reactive power output Q_{WT}, or the AC-voltage $|u_g|$, according to a given set-point.

4.3 Wind turbine model blocks

Figure 16 shows the elementary blocks in the wind turbine model. In this scheme the block **wind** generates a rotor-effective wind speed V_{w_eff}, which includes turbulence, wind shear, rotational sampling, tower shadow and tower movements. In the block **rotor** the aerodynamic torque T_a and thrust force F_a are calculated using a Blade Element Momentum (BEM) rotor model, based on a set of torque and thrust coefficients as a function of tip-speed ratio and pitch angle. This block also includes a dynamic inflow model, pitch actuator models and a tower model. The block **shaft** holds a 2-mass shaft model. A detailed description of the WT model and the WT controller design is available from [22].

In the generator model, also used in [12], parameters from a 2MW multi-pole generator from a direct drive wind turbine have been used, cf. [21]. For upscaling to a 6MW turbine the current and electrical torque are multiplied with a factor of three and an ideal gearbox is inserted to compensate for the difference in rated rotational speed.

The converter is modelled as non-switching voltage sources, assuming only symmetrical

Figure 17: Wind turbine and rectifier control

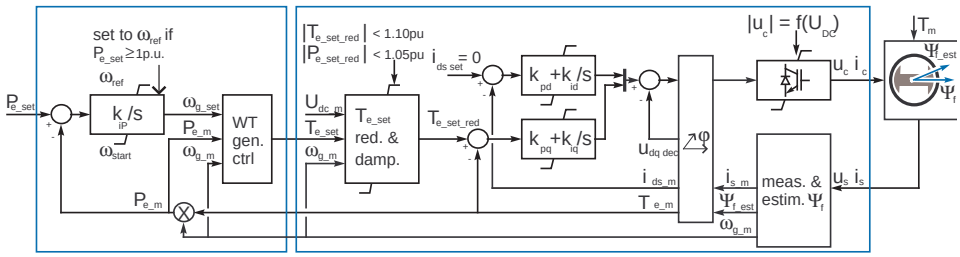

voltages, so that these can be represented by their positive sequence values in a rotating dq-frame.

The control input of the rectifying converter is given by the torque controller, which also includes damping control. With the reactive power fixed to zero this is equivalent to a current setpoint $i_{s\,set}$ perpendicular to the rotor flux ψ_s. The control input of the inverter is the grid current i_f, where active and reactive power are decoupled using vector control based on the estimated rotor flux angle.

The measurement and control blocks are described in the following subsections. The parameters of the wind turbine and the other wind farm components are listed in Appendix A.

4.4 Wind turbine generator control

Figure 17 shows the schematics of the modelled generator control. The WT controller provides the torque setpoint $T_{e\,set}$ to the rectifying converter. The inner control loop controls the torque T_e through the stator current $i_{q\,s}$, while $i_{d\,s}$ is controlled to zero, cf. [19]. i_{ds} is aligned with the rotor flux and thus linked to the reactive power.

External regulation of the active power output is modelled with an integral controller that will slowly vary the rotor speed set-point $\omega_{g\,set}$ if $P_{e\,set} < 1pu$. The series filter inductance and filter capacitance between the converter and the generator have been neglected, but this does not seriously influence the control response. The converter voltage amplitude $|u_c|$, for the fundamental frequency, is limited dynamically to $U_{dc}/2$.

Under normal operating conditions the rectifier setpoint $T_{e\,set\,red}$ equals the electrical torque setpoint $T_{e\,set}$ from the wind turbine controller. In case of a DC-overvoltage in the converter, the rectifier torque set-point $T_{e\,set\,red}$ is reduced in order to restore the power balance in the DC-link. Also a damping torque is added when rotor angle oscillations are measured. These oscillations can be induced by transient events, such as grid loss or WT control actions. The generator itself provided little damping.

The rotor flux position $\angle\,\Psi_{f\,est}$ is estimated from the measured voltages, currents and angular speed and the generator parameters. The PLL which is commonly applied for this is modeled as a low-pass filter, assuming a small tracking angle so that PLL is operating in its linear range. The block $\angle\,\varphi$ aligns the control inputs and outputs to the estimated rotor flux angle.

$$L\,di_{ds}/dt + R\,i_{ds} = d\Psi_d s/dt - v_{ds} - \omega_g\,\Psi_{qs} = d\Psi_d s/dt - v_{ds} - \omega_g(L\,i_{qs} + \Psi_{qf}) \quad (4.1)$$

$$L\,di_{qs}/dt + R\,i_{qs} = d\Psi_q s/dt - v_{qs} + \omega_g\,\Psi_{ds} = d\Psi_q s/dt - v_{qs} + \omega_g(L\,i_{ds} + \Psi_{df}) \quad (4.2)$$

assuming $R << sL$ and steady-state, $d\vec{\Psi}/dt = 0$, $d\vec{i}_s/t = 0$:

$$\omega_g\,\Psi_{qf\,est} = -v_{ds} - \omega_g\,L\,i_{qs} \quad (4.3)$$

$$\omega_g\,\Psi_{df\,est} = \quad v_{qs} - \omega_g\,L\,i_{ds} \quad (4.4)$$

$$\angle\,\Psi_{f\,est} = \arctan(\frac{-v_{ds} - \omega_g\,L\,i_{qs}}{v_{qs} - \omega_g\,L\,i_{ds}}) \quad (4.5)$$

With the estimated flux the decoupling voltages $-\omega_g\,\Psi_{qf\,est}$ and $\omega_g\,\Psi_{df\,est}$ are calculated and added to the controller output voltages to eliminate the cross-coupling terms in (4.1) and (4.2). The PI-controllers for the electrical torque and $i_{d\,s}$ are set to a bandwidth of 125 rad/s.

In case of a high DC-link voltage the generator torque setpoint is decreased gradually, according to the scheme in figure 18. Fast rising DC-link voltages are emphasized using a high-pass filter in order to detect the DC-voltage rise at an early stage. The speed of the torque reduction is chosen proportional to the energy stored in the DC-link with a factor $1/(\omega_g\tau_{red})$ to obtain a DC-voltage decrease time constant of τ_{red}. After the power balance has been restored and the grid-side inverter starts to ramp-up active power, the dc-voltage decreases below a theshold $U_{dc\,raised}$ and the generator torque is slowly ramped-up. During the reduction of the generator torque and also shortly after the recovery a low-pass filter is enabled in order to smoothen the oscillations in the torque setpoint from the turbine controller, while this controller acts on the rotational speed and does not contribute to the damping. Instead a damping torque is added, which is calculated from the derivative of the measured rotational speed. This damping torque however results in an oscillating generator power to the dc-link, which should be compensated by means of a controlled braking resistor. Also the remaining effect of the damping torque on the dc-link voltage is estimated in the factor k_{comp} and subtracted from the measured dc-link voltage to prevent interaction of the damping torque with the the power reduction block.

Figure 18: Generator torque reduction and damping

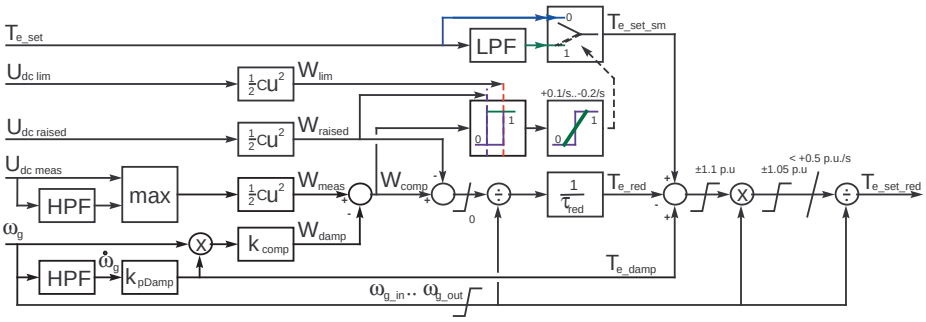

Figure 19: Wind turbine converter control

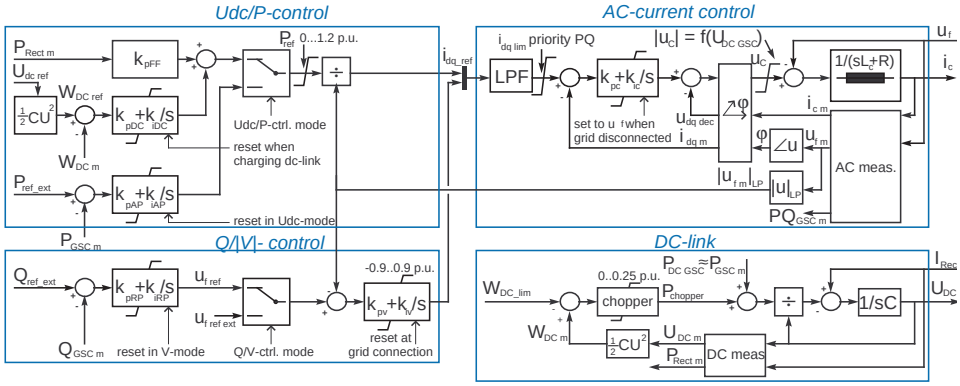

4.5 Wind turbine grid converter

Figure 19 shows the model of the wind turbine grid converter and its control. The AC-grid current is controlled in a similar way as for the generator-side converter. The outer control loop provides the current setpoints $i_{d\,ref}$ and $i_{q\,ref}$, which are calculated from the active and reactive power setpoints and the measured grid voltage. The active current setpoint is either controlled by an external power reference $P_{ref\,ext}$ or follows from the DC-voltage controller. This controller acts on the energy stored in the DC-link W_{DC} rather than on the DC-voltage directly, so that the control loop is linear. The DC-voltage control involves a feedforward of the measured power from the rectifier P_{rect} to improve the dynamic response.

The reactive current control is implemented in the model as a fast AC-voltage control in cascade with a slow reactive power controller. Depending on the Q/V-control mode the AC-voltage control can also follow an external voltage setpoint.

A common dq-reference frame is used, in which the filter voltage u_f is aligned to the q-axis. For simplificy the voltages and currents of the AC-current controller, either in control dq-coordinates or in grid dq-coordinates, are shown as single lines. Also the controllers, filters and other blocks for these quantities in d and q are shown as single blocks.

The bandwidth of the current control loop, which is limited by the converter switching delay, is set to 2 krad/s. The bandwidth of the outer loops controlling active and reactive power is set 120 rad/s, as derived in [16].

The dynamic response of the PLL that is commonly used in converters for voltage angle estimation is modelled using a low-pass filter with 20ms time constant. The same filtering is also applied for the measured values of $|u_f|$, P_{WTC} and Q_{WTC}. The setpoints for active and reactive power are filtered similarly. These filters also prevent high-frequency oscillations of the grid voltage that can occur because small grid voltage variations are amplified by the controller that maintains the active power.

The control mode settings are determined by the operating mode control, cf. Figure 20. For example, the DC-voltage control is disabled when the DC-link is being charged, or the external reactive power setpoint is overruled during AC-voltage drops.

In case of a voltage drop at the WT terminals the WT inverter current increases, which

Figure 20: Wind turbine grid-side converter operational mode

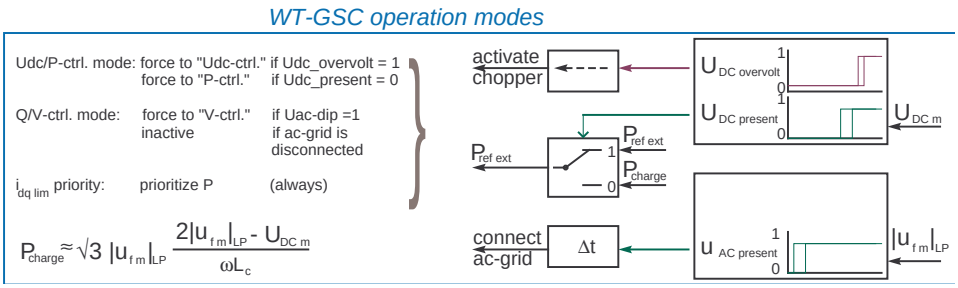

Figure 21: HVDC Wind Farm Converter

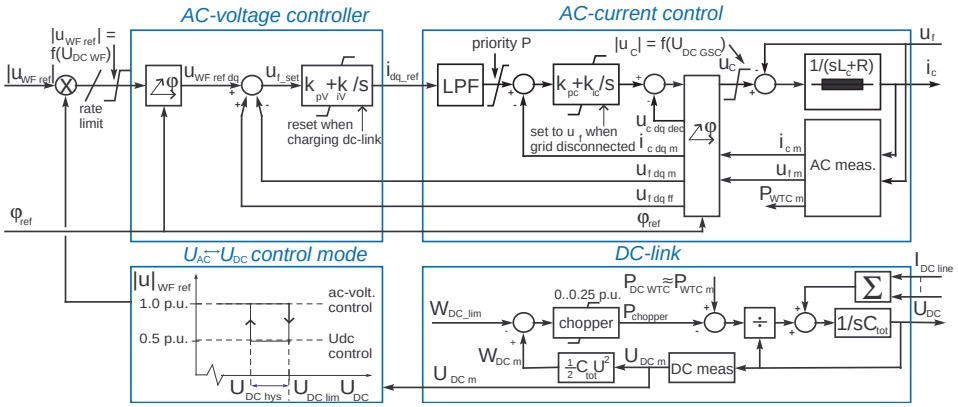

may lead to current limit operation. During an ac-voltage drop the WT controller usually prioritizes the reactive current for maximum voltage support. However in this case the WT is not directly connected to a public AC-grid, but the AC-voltage is controlled by the HVDC-WF converter. Therefore other priorities than AC-voltage support may be chosen, e.g. maximizing active current, as indicated in the figure with “prioritize P”.

4.6 HVDC control

The figures 21, 22 and 24 show the control schemes of the modelled HVDC components: the Wind Farm Converter (WFC), the Grid-Side Converter (GSC) and the controlled braking resistor. The DC-capacitance C_{tot} is equal to the station capacitor plus half the capacitances of all connected cables.
Under normal operating conditions the WFC controls the ac-voltage amplitude and frequency to a constant reference values $|u_{WF\,ref}|$ and φ_{ref}. This outer control loop sets the reference values $i_{d\,ref}$ and $i_{q\,ref}$ of the inner current control loop. The feedforward term $u_{f\,dq\,ff}$, equal to $j\omega L_{leak}\, i_{cm}$, compensates for the voltage difference of the transformer. In case of a single HVDC link, a feedforward term $P_{DC\,WFC}(R_{cable}/U_{DC}^2)$ can be included to estimate the DC-voltage at the GSC, so that the voltage setpoints and limits of both converters are comparable. Based on the measured DC-link voltage the WFC reduces the WF voltage to 0.5 p.u. as a measure to limit the WF active power, until the DC-voltage drops below $U_{DC\,lim} - U_{DC\,hys}$.

The HVDC-GSC model is similar to the WT-GSC model, but with different operational mode settings. For instance, during an AC-grid voltage dip the HVDC-GSC prioritizes the reactive power for voltage support. Also, an external active power limitation is implemented, e.g. for grid frequency support, while for the WT external power control is im-

Figure 22: HVDC Grid Side Converter

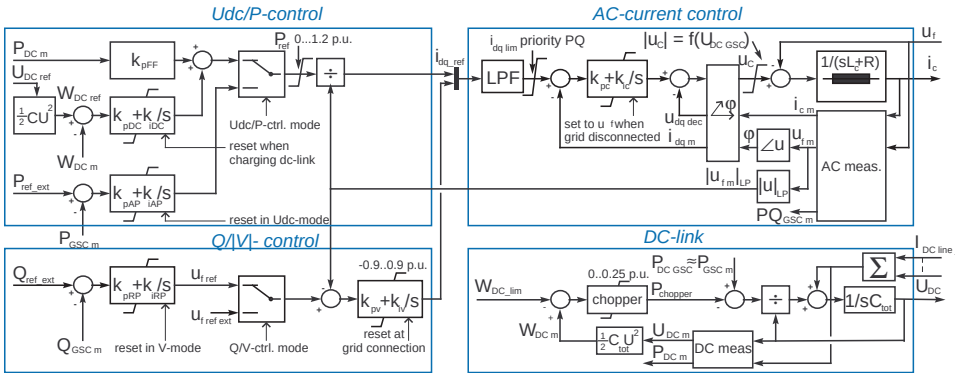

Figure 23: HVDC Grid Side Converter operation

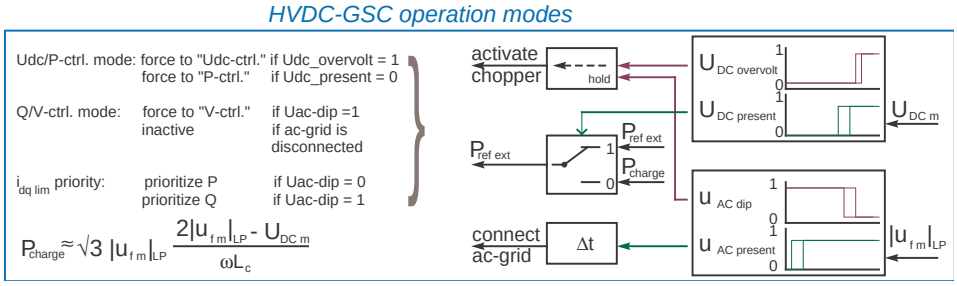

Figure 24: HVDC DC-link with chopper

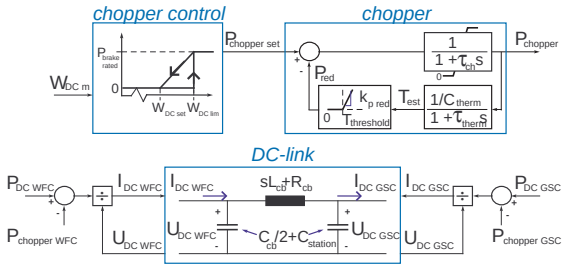

plemented by lowering the aerodynamic power through the rotor speed angular speed setpoint. Another minor difference is that the generator sign convention is chosen at the DC side for both HVDC converters, while for the WT-GSC the generator sign is chosen for the AC side.

A model of a chopper-controller braking resistor to limit fast DC voltage rise is shown in figure 24. In the modeled MTDC system choppers are only implemented in the grid side converter of each wind turbine. Depending on the MTDC network configuration and the wind farm capabilities also choppers could be included at some nodes in the network, if necessary. Therefore in the schemes of figure 21 and 22 choppers are included.

The detection of DC-overvoltages is implemented as follows. A high-pass filter circuit is included to emphasize a steep increase of the DC-voltage for early activation of the dump load. The maximum peak power set to 0.25 p.u. is relatively small, because of the high costs of the chopper and also the continuous power of the load is limited using a simple thermal model.

5 Simulations

For a number of cases under different operational conditions simulations have been performed for the MTDC grid, including the dynamic wind farm models. These cases are described and the results presented. The simulation results presented include the complete wind farm model and therefore differ slightly from the results published in [17] where a simpler wind farm representation is used. Here also a somewhat more detailed converter operational mode setting has been applied.

5.1 Power Flow Control

For controlling the power flow in the MTDC network the so-called Direct Voltage Control (DVC) method is applied [16]. In this method the optimal power flow (OPF) is solved repeatedly, which directly provides all DC node voltage set-points. The solver uses a Genetic Algorithm that finds the optimal DC node voltages for a set of objective functions and constraints. Because of the required calculation time the optimisation has been performed offline for the moment. The voltage setpoints from the power flow optimization are calculated for each 5 sec. interval.

The chosen objective function for the optimisation is to minimize the transmission losses in the DC network while complying with the power flow restrictions set by the involved TSOs. At a later stage the objective function may also include converter losses. The constraints are set to maintain N-1 security. Here N-1 security is defined differently compared to AC grids, namely, that in case when a single converter station or DC line fails that all generated wind power can be exported without curtailing the wind farms output or transnational energy trade or violating any of the network constraints. Strictly, curtailing the wind farms in case of a failure does not mean that the power flow solution will cause network instability in case of a single failure.

The given inputs to this OPF are the prescribed active power set-points of the different countries, the produced wind power per node and the MTDC network parameters and constraints. In this method it is possible to select multiple slack nodes, i.e. nodes for which no power setpoint is prescribed. This showed to reduce the losses as well as to increase the stability in case of perturbations, e.g. grid congestions or converter outages.

Compared to other methods, such as droop control or voltage margin, it combines good dynamic properties and applicability for complex networks. Also the needs for fast telecommunication are modest. Furthermore it can easily handle constraints, for instance settings from system operators or network limitations. Also the method can be applied within an optimization strategy, considering for instance transmission losses minimization and profits from energy trading. Finally, in case of congestions or loss of telecommunication, setting the DC-voltages results in less severe overvoltages compared to imposing power setpoints.

5.2 Case descriptions

The case studies aim to show how the DVC method performs when facing some of the most common situations when controlling a MTDC grid for integration of OWFs, viz.: start-up procedures; normal operation; operation under wind curtailment; and operation under a contingency in one of the ac network nodes. TSOs may influence the power flow in the MTDC network through setting or restricting the power at the respective VSC station in order to establish international energy trading or to help resolving congestions in the terrestrial grid. This situation leads to higher transmission losses in the DC system, but are aimed to obtain a benefit for the overall power generation and transmission and trading system. These power restrictions may also lead to wind curtailment. The type failure that is simulated is relevant to situations in which a converter station fails, or symmetrical ac-line fault occurs. Although asymmetric line faults may lead to power variations 3-phase faults are usually seen as most severe for HVDC systems. DC faults are not considered as the dynamic models are not suited to simulate transients and harmonics.

Table 1 contains the detailed description of all the examined case studies and their subcases.

Black start of the MTDC system

For the black start it is considered that the converter station linked to the UK grid *UK1* is connected first, followed by the station *NL1* after 250 ms and then by station *DE1* after another 250 ms. First the IGBT switches are blocked, so that the DC grid is charged via the anti-parallel diodes or through a separate pre-charging circuit. At about 500 ms. the DC voltage level is such that the IGBT switches of the *UK1* converter are unblocked and the wind farm *WF-UK*AC grid voltage is established ramped up. The lower left graph in Figure 25 shows the DC-link charging power of the modeled wind farm and the AC active and reactive power at the AC grid filter. The lower right figure shows the internal DC link voltage ans the AC grid voltage in the wind farm.

The results of case study 1, show that the complete start-up procedure of the MTDC network can be performed very fast, i.e. in less than a second. In reality, such start up does not need to be this fast. However, since voltage-source converters do not have the means to block DC faults, and the development of high-power high-current DC short-circuit breakers is yet incipient, this rapid black-start the MTDC network might be very useful in helping to clear DC faults.

Normal operation of wind farm with HVDC grid connection

In this case study, the British, Dutch and German OWFs are producing wind energy with an average value of 0.5 pu, 0.8 pu and 0.5 pu, respectively. Figure 26 shows the simulation results for case study 2. On the left-hand side of Figure 26 the OWF-VSC and GS-VSC active power is displayed, while on the right-hand side the dc-side voltage is given.

Table 1: Description of the analysed case studies

Case Study		Description
1. Start-up Procedures	**1a.** MTDC Start-up	During the start-up procedure, the MTDC system voltage is charged from zero to the rated system voltage value by the GS-VSC terminals.
2. Normal Operation	**2a.** Priority	Priority is given to the country where the wind energy is being produced, i.e. all the power goes to the rightful country; while there is no energy trade.
	2b. Proportional Sharing	The sum of all the energy being produced by the OWFs is equally divided amongst all the countries through energy trade via the MTDC network.
	2c. Power flow Reversal	The power flow of the German node is reversed. At first the power is flowing from the MTDC network into Germany and, in a later stage, this power flow is reversed.
3. Wind Curtailment	**3a.** Low-wind Scenario	The MTDC system behaviour is analysed during wind curtailment in a scenario where the wind energy generation is low.
	3b. High-wind Scenario	The MTDC system behaviour is analysed during wind curtailment in a scenario where the wind energy generation is high.
4. AC Contingency	**4a.** Low-wind Scenario	The MTDC system behaviour is analysed during an ac fault at the UK node in a scenario where the wind energy generation is low. In this case study the MTDC network is N-1 secure.
	4b. High-wind Scenario	The MTDC system behaviour is analysed during an ac fault at the UK node in a scenario where the wind energy generation is high. In this case it cannot be guaranteed that the MTDC network is N-1 secure.

Instead of sending all the OWF power to the owner state, it is possible to share the produced energy via the MTDC grid. In case study 2b, the UK, Netherlands and Germany, share equally all the power being generated at the OWFs. In this case, the total production is 1.8 pu and each country receives a little less than 0.6 pu, which is due to the MTDC grid transmission losses of 0.85 pu on average. In case study 2c, the power flow in the MTDC network is arbitrarily set by the ISO. During the first 20 seconds, the power in the MTDC network is exactly as in case study 2a, where priority is given to the producing country.

Changing power flow

The third case study analyses the distributed voltage controller behaviour when the offshore wind farm power has to be curtailed. In the low-wind scenario, the British, Dutch and German OWFs are producing wind energy with an average value of about 0.5 pu, 0.8 pu and 0.4 pu, respectively, thus the total production of the OWFs is 1.8 pu. In case 3a, before the curtailment starts at t = 40 s, the Independent System Operator (ISO) is setting the DVC strategy to priority control as in case 2a; hence, until that point in time, the results of both cases are identical. Afterwards, from $40 \leq t \leq 60$ s, the Dutch and German OWFs are ordered to curtail their power outputs to 0.4 and 0.3 pu, respectively. The OWFs total power production after curtailment is 1.2 pu, so the power at the GS-VSC also needs to change to accommodate the curtailment. Nevertheless, even during the curtailment, the DVC strategy can control the power flow inside the MTDC network. In fact, when the curtailment starts, the ISO changes the direct voltage set-points of the

British and Dutch nodes in order to make each node receive respectively 1.0 pu and 0.4 pu of power, while the German node produces the additional 0.2 pu to compensate for some of the power that was curtailed. The results of case study 3a show (see Figure 27) that the changes in power are both fast and smooth, while the MTDC system voltage is controlled within the limit of ±10% the rated value. Meanwhile, the DVC strategy still guarantees that the MTDC network is operating with minimum losses for the chosen load-flow operating point whilst the MTDC system is N-1 secure. Finally, at t = 100 s, the OWF production is ramped back and the MTDC network is brought back to the initial operating point. In the high-wind-scenario case study (case study 3b), the total production at the OWFs is 2.4 pu. In the beginning of the simulation, a sharing control strategy is being used (as in case study 2b) and each onshore node receives approximately the same amount of power (circa 0.8 pu). The ISO then commands all OWFs to curtail their power to 0.4 pu from 40 ≤ t ≤ 60 s. Once more, the total power production after curtailment is 1.2 pu. Therefore, the ISO can send new voltage set-points to the GS-VSCs so the British and Dutch nodes receive 1.0 pu and 0.4 pu of power, respectively, while the German node produces 0.2 pu. This load-flow operating point can of course be arbitrarily chosen by the ISO, provided it respects the MTDC power balance and the GS-VSC power ratings. At t = 100 s, the OWF production is restored to the initial values and the sharing control strategy is re-established. Lastly, in case study 3b, the power flow in the MTDC network is arbitrarily set by the ISO. During the first 20 seconds the power in the MTDC network is exactly as in case study 2a, where priority is given to the producing country. From simulation time $20 \leq t \leq 80$ s, the UK onshore node starts receiving 1 pu from the MTDC network, whereas the Dutch node receives 0.9 pu. Since the power in the MTDC network has to be balanced at all times, the power flow in the German node is reversed. Therefore, during that period, the German onshore node will be injecting – i.e. selling – circa 0.20 pu of power to the MTDC grid. It is worth noting that in this case, all onshore nodes are effectively controlling their dc-side voltage and not directly the load-flow, as the DVC method dictates. Nevertheless, Germany is the node which is providing the extra power to balance the MTDC network losses. Towards the end of the simulation, the power from the German node is again reversed as the power to the British and Dutch node is set by the ISO as being equal to 0.5 pu.

Response to symmetrical terrestrial grid faults

The goal of the last case study is to analyse the DVC strategy behaviour during a fault in one ac network node. The fault takes place in the ac-side of the UK onshore node. The case study shows the response of the MTDC system to the fault during two different wind scenarios: low-wind scenario (total generation is 1.8 pu) and high-wind scenario (total generation is 2.4 pu). The fault lasts 40 s, starting from t = 40 s. The longer fault is applied to better visualize the transients involved when one MTDC network node is lost. Figure 28 shows the active power and direct voltage for both cases. It also shows that the DVC strategy can successfully ride through the fault in both cases, although the dynamic response varies according to the wind scenario. In the low-wind scenario, the sum of the remaining GS-VSC rated power is lower than the power being produced offshore. Therefore, the MTDC network is N − 1 secure and there is no need to change the OWF power output during the fault. In case 4a, as seen in Figure 28, when the fault happens in the UK node, the power at the Dutch and German onshore node rapidly changes to re-establish power balance in the dc grid. This occurs because all the GS-VSC are effectively controlling the dc system voltage, which is one of the DVC method's greatest advantages. During this very fast transient, the MTDC voltage reaches a peak of 1.11 pu, but is quickly restored back to values within the operating limit. When the fault is cleared, at t = 80 s, the MTDC system voltage undergoes another transient, this time only a direct voltage dip to about 1.04 pu, which is much less of concern than the voltage spike when the fault occurs. Finally, at t = 100, the priority control strategy is reinstalled by the DVC method and the MTDC network goes back to its initial operating point. Contrarily, in the high-wind scenario, the MTDC network is not N − 1 secure since the total power being produced, 2.4 pu, is higher than the remaining onshore VSC combined ratings, which is 2 pu. In that case, the DVC strategy cannot alone keep the MTDC network voltage secure by increasing active power absorption at the onshore GS-VSC

terminals. In case 4b (see Figure 28), when the fault happens, dc choppers are activated on the German and UK OWFs once the direct voltage exceeds 1.10 pu. Then, after the fault, the OWFs start to curtail their power outputs, which was not necessary before. Additionally, since in high-wind case more power was being produced prior to the fault than in comparison with the low-wind case, the MTDC voltage transient peak is higher, with a maximum of 1.12 pu being reached at the UK offshore node. Finally, when the fault is cleared, at t = 80 s, the offshore wind farm power output is kept constant for 20 s and then ramped up, starting from t = 100 s, to a new operating point, this time N-1 secure. A new load-flow scenario is established from t = 120 s onwards.

Transmission losses in MTDC network

The transmission losses and the power being traded in the MTDC network are shown in Figure 31 for all the analysed case studies. The transmission losses are given as a function of the total generated power at the offshore wind farms and the power trade is given in a per unit basis, assuming no converter losses at the WF-VSC. These (instantaneous values) are calculated as:

$$P_{loss} = \sum_{j=1}^{6} R_j * I_{DC_j}^2 / \sum_{j=1}^{3} P_{DC_j}^{OWF} \tag{5.1}$$

$$P_{trade} = \frac{1}{2} \sum_{j=1}^{3} (\left| P_{VSC_j} - P_{OWF_j} \right|) \tag{5.2}$$

The MTDC system losses are optimized by a multi-objective optimization algorithm[16], which has the transmission losses as objective function. Figure 31 shows that the MTDC transmission losses vary between 1% and 3% of the total generated power. The total MTDC system losses are higher since the VSC losses should also be taken into account. It is interesting to note that, as one would expect, the transmission losses and the power traded in the MTDC network have basically the same trend. This is due to the fact that trade, as calculated by Equation (5.2), happens through lines 3 and 6, i.e., the hub lines, which are the longest lines in the MTDC network.

Figure 25: Black-start

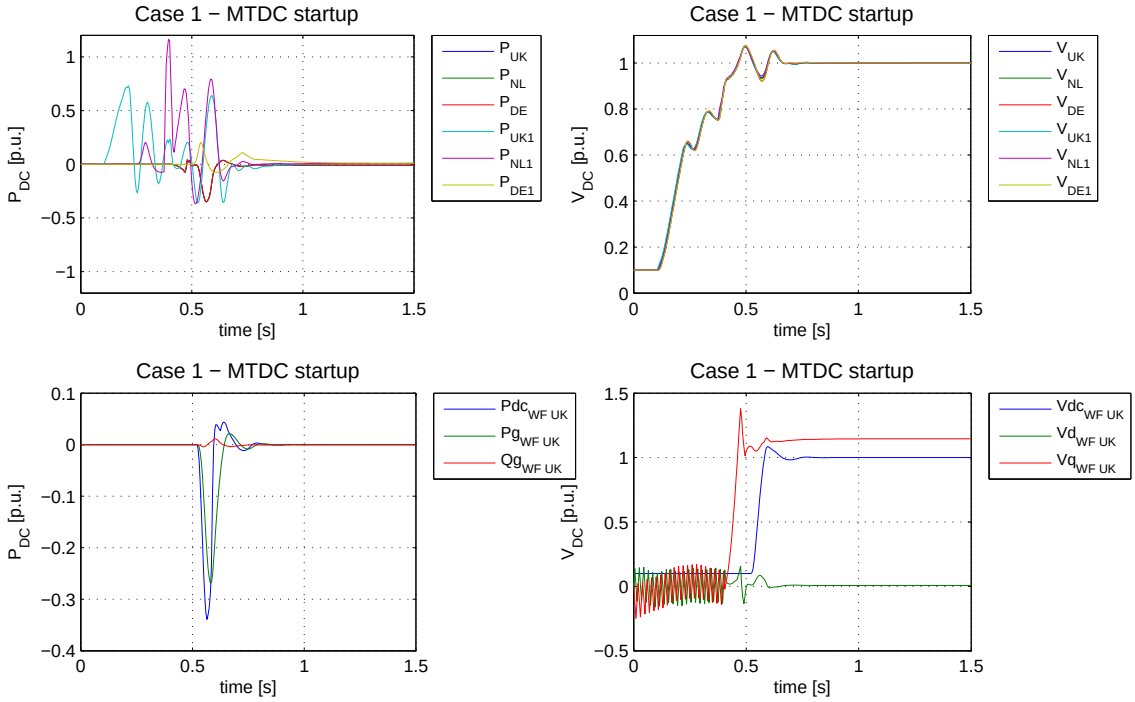

Figure 26: Steady-state operation

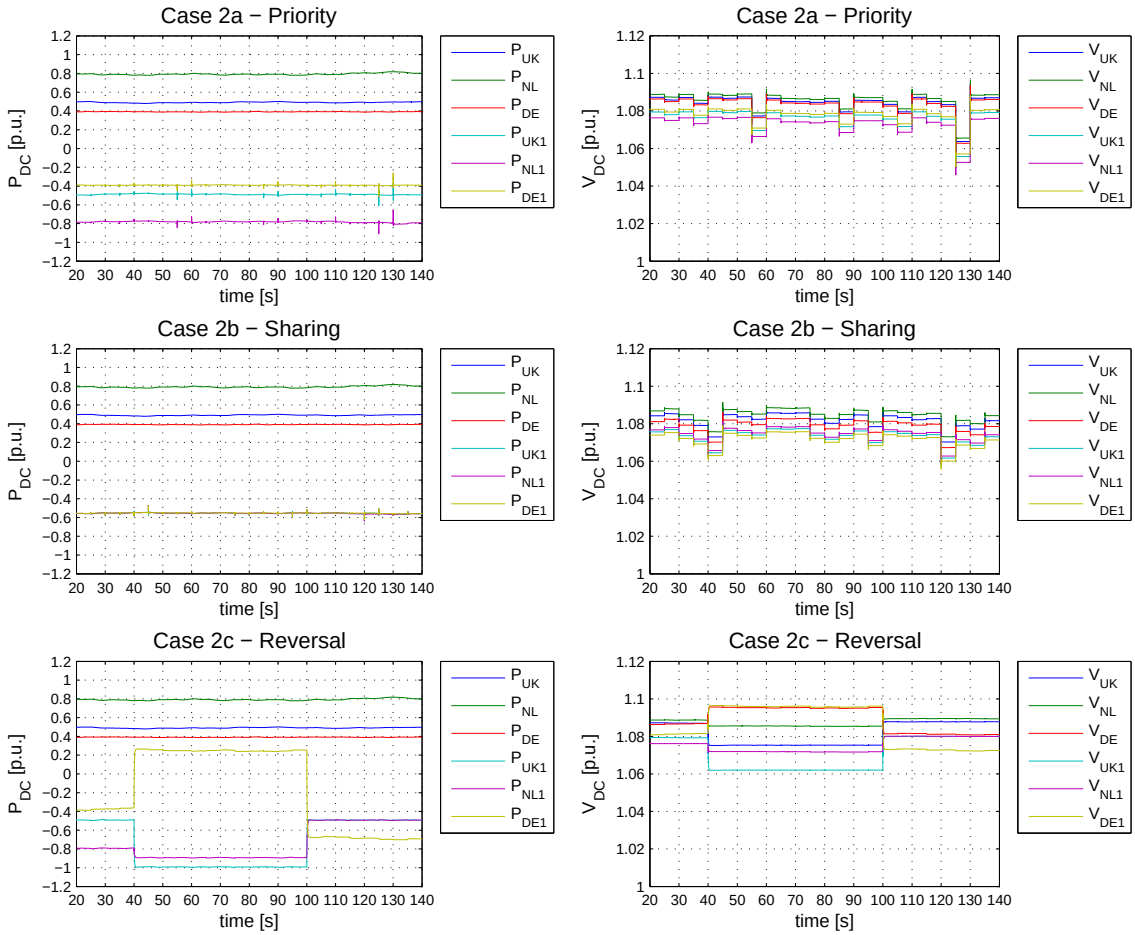

Figure 27: Changing power flow

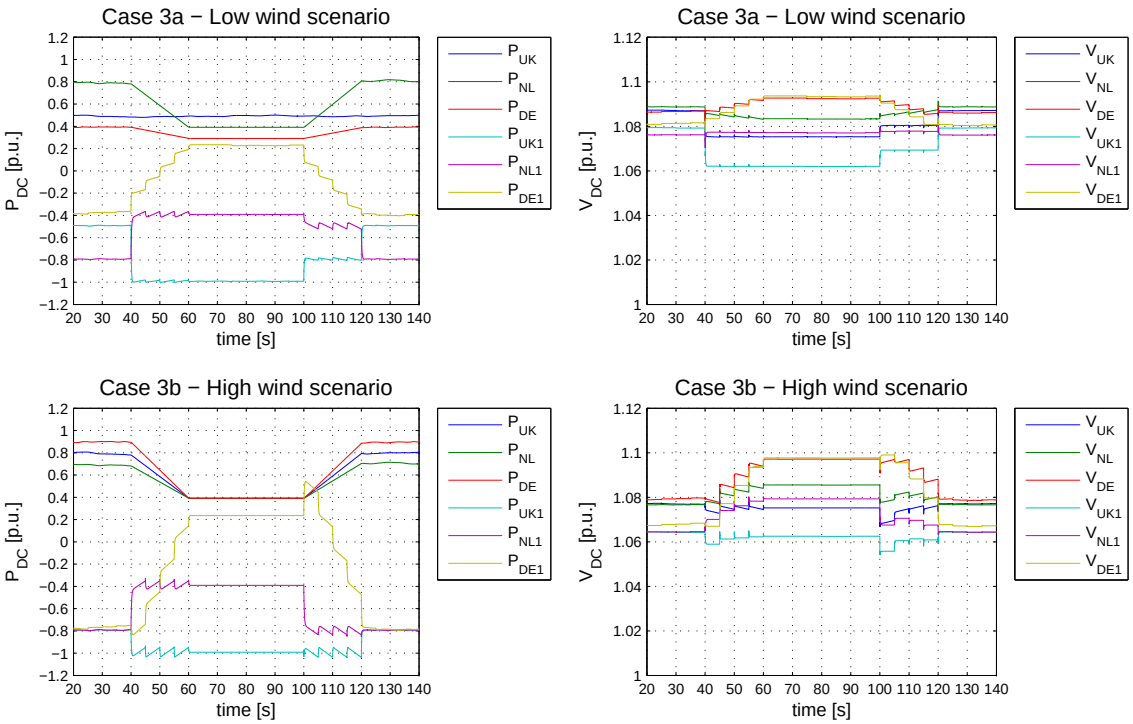

Figure 28: Fault response

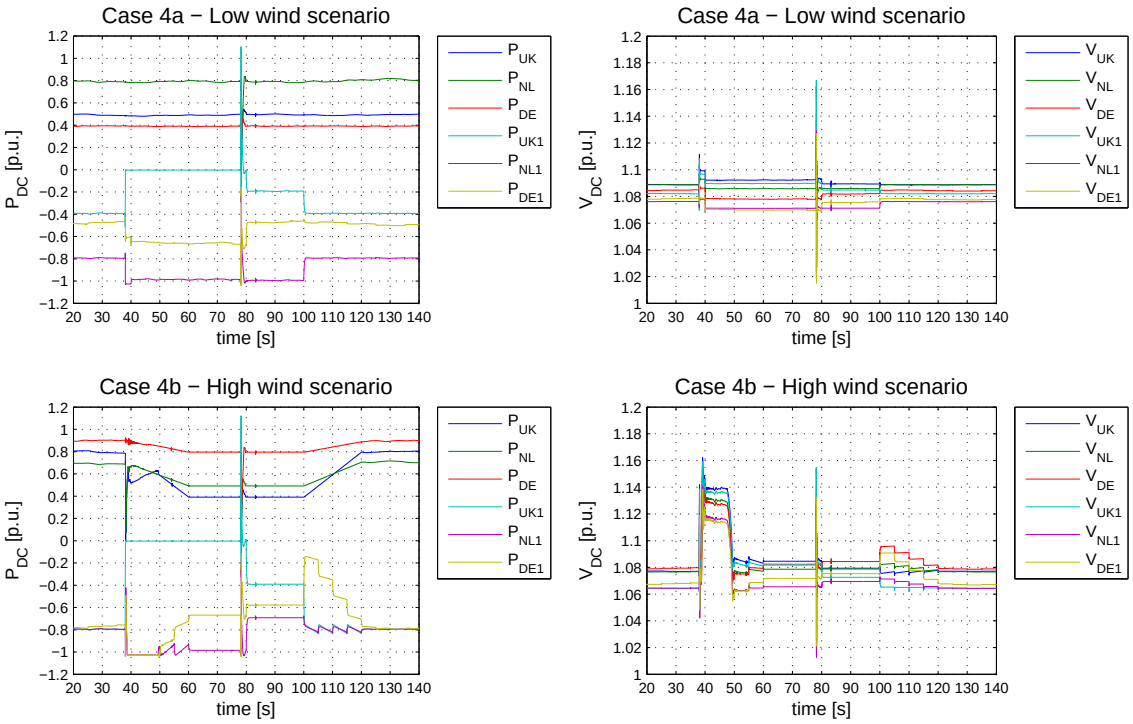

Figure 29: Fault response

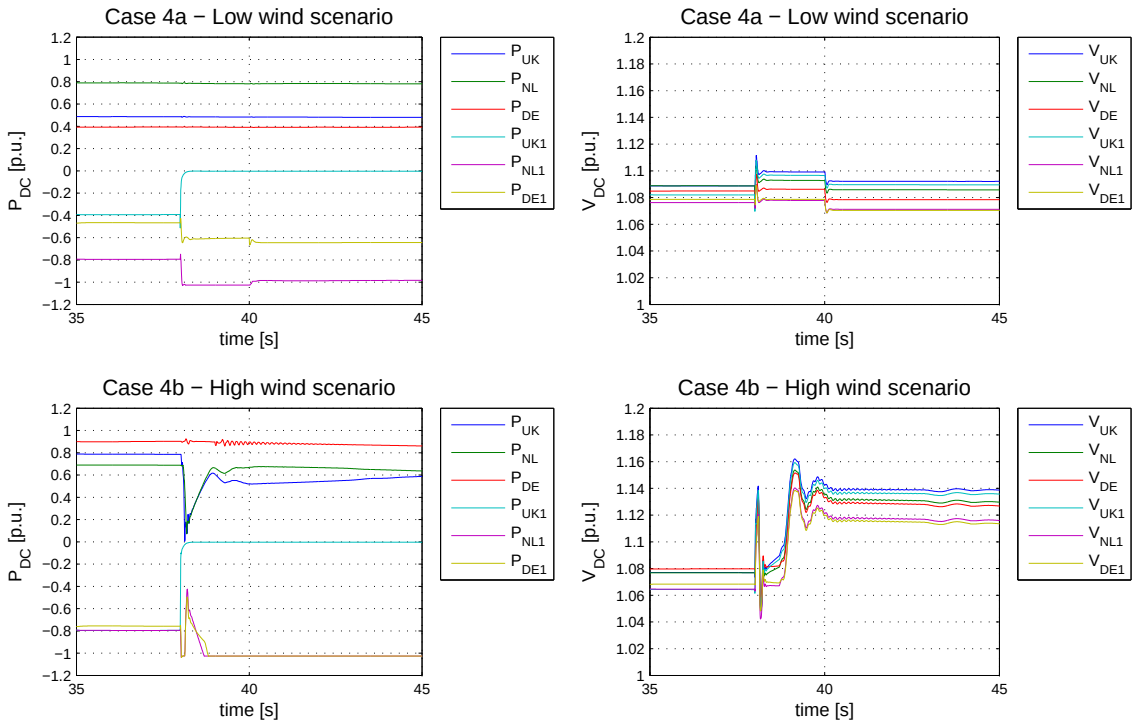

Figure 30: Fault response

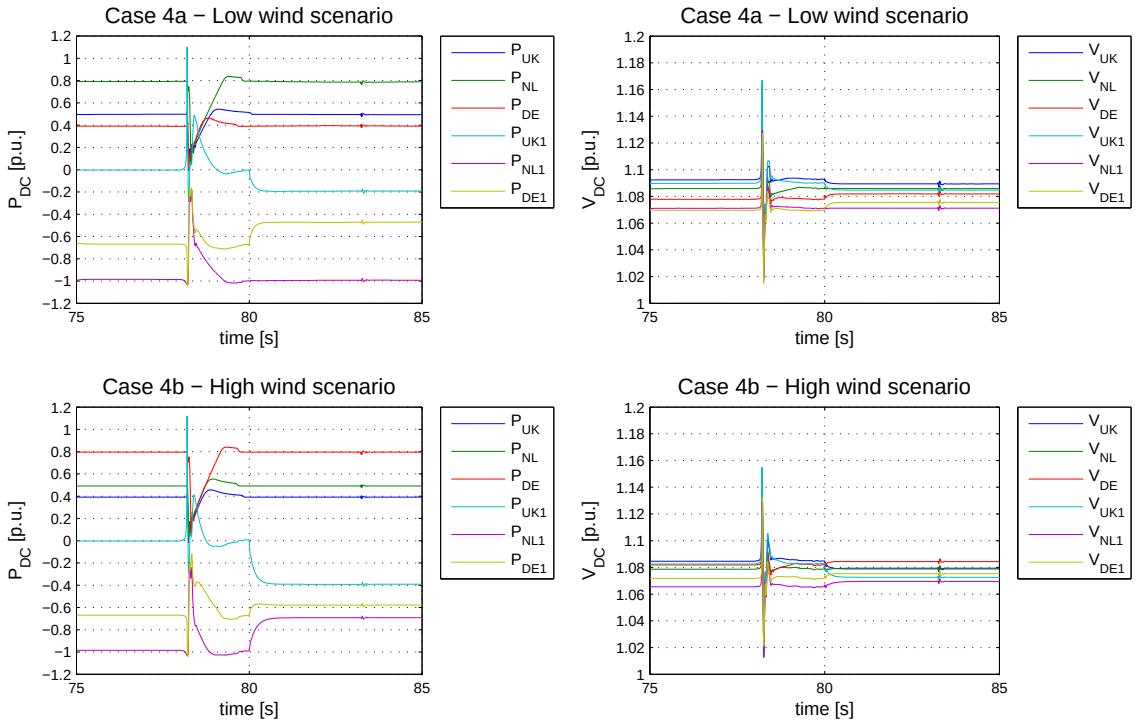

Figure 31: Losses in the MTDC system for all cases

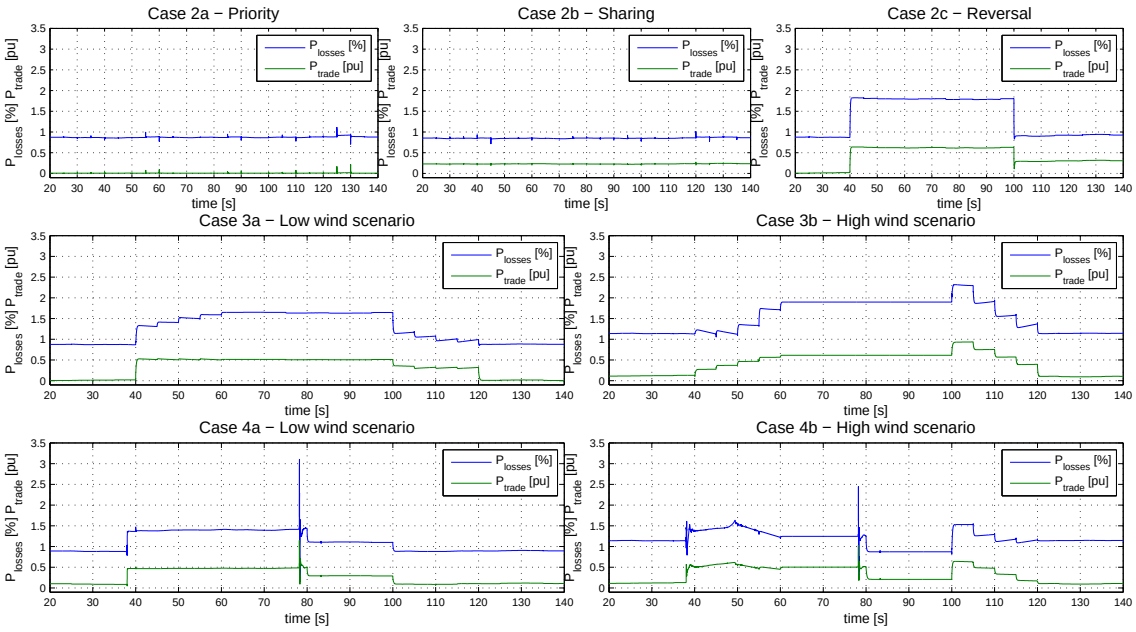

6

Conclusions

MTDC and wind farm technology

As part of WP3 of the NSTG project different technical solutions for a transnational grid have been presented with the focus on topologies, AC/DC converter types and wind turbine technologies. Although combinations of different converter technologies are possible, e.g. Voltage Source Converters (VSC) and Current Source Converters (CSC), both based on Forced Commutated switches, or even hybrid converter types, a grid based on VSCs has been selected. These hybrid systems may offer advantages, such as blocking DC faults, but for dynamic control using only VSCs are equally well-suited.

In WP3b an optimal power flow control method for MTDC grids based on VSCs, named Distributed Voltage Control, has been developed at TU-Delft. The underlying optimisation method is a genetic multi-objective optimisation algorithm that has been tailored for this application. Therefore, instead of a single VSC that controls the DC-voltage, all VSC stations connected to the onshore grids control the DC-voltage ion a coordinated manner, while the VSC connected to offshore wind farms behave as power sources.

The wind farm model is based on variable speed turbines with permanent magnet generators and full-rated converter that are connected to the HVDC grid through a rectifying VSC station. This wind turbine type is representative for current technology and shows good control capabilities, which are especially needed for balancing the power in the MTDC grid. Looking at the specific operating conditions of a wind farm connected through a VSC, DFIG wind turbines are expected to show similar dynamic performance.

Wind Farm modeling

The wind farm models have been built using a string of 5 wind turbines connected to a HVDC rectifying station. The power output of the single string has been upscaled to match the nominal power of the wind farm. In the final simulations the wind farm model was further aggregated to a single wind turbine, as the dynamic (electrical) interactions between the different wind turbines in the string feeder were not significant. To approximate the aggregated wind farm output a number of wind turbine power output signals have been combined in order to obtain the spatial smoothing that occurs in a wind farm. The wind farm model includes a power setpoint to enable a grid operator to curtail the wind farm power production when required.

MTDC grid modeling

The MTDC grid model includes the DC cabling, the grid-side VSC converter stations and a simplifies AC-grid model. The MTDC model has been applied to simulate the effect power flow control and power flow imbalances in the offshore MTDC grid due to grid events such as AC grid faults. The VSC models used at the AC-grid side as well as in the wind farms and in the wind turbines have been built almost similar, using a programmable configuration. The converter control settings have been chosen identical to those derived by TU-Delft, except for the generator-side control in the wind turbines. The converter models have been extended with a number of operational mode settings. As these settings are dependent on the specific type of equipment (converters as well as cables and switching equipment) and on the local grid requirements, estimates were required. These settings are required the resemble the converter behaviour during events, such as black-starts and AC-voltage dips.

Model coupling and Simulations

Integrating the wind farm model in the MTDC grid model, required tuning the AC-voltage control of the wind farm VSC, such that the AC-voltage remains stable under variable wind farm power production. Moreover, the AC-voltage control has been applied to mimic an AC-voltage dip in case of DC-overvoltages, forcing the wind turbines to limit their power production to help restoring the DC-power balance. Because of the short time constants in the DC-grid this needs precise tuning of the complete chain from the WF AC-voltage control, wind turbine VSC current limits, control and operational mode settings as well as the wind turbine torque and pitch control. The aim is to rapidly reduce the DC grid voltage while keeping the all voltages and currents in the wind farm and wind turbines as well as the mechanical loads stable and within safe limits. This has been achieved, although this tuning is inevitably specific to the turbine design and the wind farm electrical system.

The DVC power flow control method has been applied successfully in this simulation model, both under normal operation and for a number of events, such as optimal DC-power flow under certain restrictions and dynamic events such as AC-voltage dips and black-starts.

In order to simulate the model in combination with the DVC power flow optimization an offline coupling has been realized. The wind farm power production of the wind farm models under the case-specific wind conditions (and at for the lab-scale model in WP4 also from OWEZ data) has been fed to the DVC algorithm. In the second stage the optimized DC-voltage settings have been applied to each grid-side VSCs and simulated in the combination with the wind farm models. Here the simulated grid events were scheduled in between two DVC updates (at 5 seconds intervals). The simulation showed that using the DVC method the DC-voltages in the MTDC network showed little variation within the DVC update intervals. The DC-voltages were also kept within safe limits in case of rapid power setpoint changes and ac-grid voltage dips, where the wind farms did ride through these events.

Future work

In order to make the next step towards implementation, the modeling of the wind farms in combination with MTDC networks can be improved in many ways, see also section C.1. The most relevant aspects are considered to be:

- communication delays and limitations to the accuracy of the wind farm and MTDC grid SCADA system, both for power and voltage measurements and for setting wind farm power levels and VSC DC-voltage levels.
- Simulate high wind speed cut-out and the best use of wind power prediction for the MTDC grid operation.

- Modeling of converter losses and other HVDC converter technologies. i.e. multi-level VSCs
- Detailed cable modeling, both electro-magnetic and thermal
- Study the combination of storage systems connected to the MTDC grid and the consequences for its design and operation.

The DVC method can be developed further to handle these practical limitations. For mitigating the error in the DC-voltage control a simple feedback scheme is proposed and this could be simulated and tested in the laboratory, cf. section C.2.

For more complex MTDC networks solutions to preserve power flow control in mazed networks can be elaborated e.g. by applying parallel grids in order to ensure onshore grid stability without the need for numerous DC-breakers, cf. section C.3.

A

Model parameters

A.1 Wind farm model

The parameters of the wind farm model with HVDC connection are summarized in Table 2.

A.2 Wind farm control

The control parameters are summarized in Table 3.
The bandwidth of the inner loops controlling the current of the modelled converters is set to 500 rad/s, related to the switching frequency, while the bandwidths of the DC-voltage control loops are set to 150 rad/s, based on the inner loop bandwidth. The response of the DC-link control in the WT converter for changes in the generator power will be faster because of the feedforward term $k_{p_{FF}} P_{_{PMG}}$.
The filter time constant τ_p used in the calculation of the current references is set to 20ms for the converters that are directly connected to the grid and to 100ms for the WT converters that are connected to the grid via the HVDC link. This slower response is to prevent that the WT converter interferes with the ac-voltage control of the WF-VSC. The rate of change of the ac-voltage setpoint, which is controlled by the WF-VSC, is limited to $\pm 0.025[1/s]$ so that the connected WT controllers can follow the voltage change.

Parameter	**v**alue	**[**unit]
Rotor		
Aerodynamic control	collective pitch to vane	
Rated angular speed	1.24	$[rad/s]$
Inertia	$38.6\ 10^{6}$	$[kgm^2]$
Shaft stiffness	87.5	$[kNm]$
Generator (PMG 30 pole pairs)		
Inertia	$35\ 10^{3}$	$[kgm^2]$
Rated angular speed	2.85	$[rad/s]$
Rated voltage	4	$[kV]$
Rated power	2	$[MW]$
Power Factor	0.92	$[-]$
Converter (back-to-back VSC)		
Rated power	6	$[MVA]$
DC-link voltage	8.7	$[kV]$
DC-link capacitance	2	$[mF]$
Switching delay	1	$[ms]$
Series impedance	$0.0125\ +\ j\,0.6281$	$[\Omega]$
Braking resistor		
Rated power	0.25	$[p.u.]$
Power ramp rate	± 200	$[1/s]$
Unit transformer		
Rated power	7.5	$[MVA]$
Rated voltage	4 / 34	$[kV]$
Leakage reactance	0.074	$[p.u.]$
Copper resistance	0.003	$[p.u.]$
WT string cable		
Length (averaged)	6.3	$[km]$
Series impedance	$63\ +\ j\,100$	$[m\Omega/km]$
Susceptance	$j\,9.27\ 10^{-5}$	$[S/km]$
WF- and GS-transformer		
Rated power	430	$[MVA]$
Leakage reactance	0.13	$[p.u.]$
Copper resistance	0.0023	$[p.u.]$
HVDC converters (WF-VSC and GS-VSC)		
Rated power	1000	$[MVA]$
DC-link voltage	640	$[kV]$
DC-link capacitance	73	$[\mu F]$
Switching delay	1	$[ms]$
Series impedance	$0.0125\ +\ j\,6.28$	$[\Omega]$
HVDC cable		
Series impedance	$19.5\ +\ j\,59.9$	$[m\Omega/km]$
Susceptance	$j\,6.91\ 10^{-5}$	$[S/km]$
HVDC braking resistor		
Rated power	0	$[p.u.]$
Power ramp rate	± 200	$[1/s]$
Grid		
Nominal voltage	230	$[kV]$
Nominal frequency	50	$[Hz.]$
Short circuit power	3000	$[MVA]$
Impedance angle	85	$[deg.]$

Table 2: Wind farm parameters

Parameter description	symbol	value	[unit]
Generator control			
torque P-ctrl	k_{dq}	1	$[V/kNm]$
torque I-ctrl	k_{iq}	10	$[V/kNms]$
i_d P-ctrl	k_{pd}	0.2	$[V/A]$
i_d I-ctrl	k_{id}	2	$[V/As]$
U_{dc} limit	$U_{dc\,lim}$	1.20	$[p.u.]$
U_{dc} raised setpoint	$U_{dc\,raised}$	1.05	$[p.u.]$
Gain of fast U_{dc} rise		2.5	$[-]$
$T_{e\,ref}$ LPF time constant	τ_{Te}	500	$[ms]$
$T_{e\,ref}$ LPF switch rise/fall time	$t_{Te\,sw}$	+50, -200	$[ms]$
T_e ramp-down time constant	τ_{red}	10	$[ms]$
T_e ramp-up limit	τ	1.5	$[1/s]$
T_e damping feedback	k_{damp}	1.19610^6	$[kgm^2]$
T_e damping offset feedback	$\tau_{i\,drift}$	10	$[s]$
Feedback gain of estimated rotor flux position	$K_{p\,ThR}$	1	$[-]$
Time constant PLL to estimate rotor angle	τ_{ThR}	0.1	$[s]$
WT Converter			
U_{dc} P-ctrl	k_{pDC}	0.2	$[A/V]$
U_{dc} I-ctrl	k_{iDC}	0	$[A/Vs]$
P_{PMG} feedforward	k_{pFF}	1.0	$[-]$
Q/V control mode		const. ref.	$[-]$
Q_{ref} External ref.	$Q_{ref\,ext}$	0	$[-]$
Q_{ref} P-ctrl	k_{pQ}	4.0	$[-]$
Q_{ref} I-ctrl	k_{iQ}	8.0	$[1/s]$
u_{WT} and PQ_{ref} LPF time constant	τ_p	100	$[ms]$
u_d FB gain	$k_{p\,u}$	0.002	$[A/V]$
u_{dq} FB damping	$k_{damp\,u}$	0.1	$[-]$
i_{dq} P-ctrl	k_{pc}	1.0	$[V/A]$
i_{dq} I-ctrl	k_{ic}	3.12	$[V/As]$
current limit	i_{max}	1.2	$[p.u.]$
HVDC WF Converter, outer control loops			
u_{dq} P-ctrl	k_{pvg}	0.0088	$[A/V]$
u_{dq} I-ctrl	k_{ivg}	6.5767	$[A/Vs]$
U_{dc} limit	$U_{dc\,lim}$	1.20	$[p.u.]$
U_{dc} hysteresis	$U_{dc\,hys}$	0.05	$[p.u.]$
$u_{_{WF\,ref}}$ control rate limiter		± 40	$[1/s]$
HVDC GS Converter, outer control loops			
W_{dc} P-ctrl	k_{pDC}	0.0433	$[1/V]$
W_{dc} I-ctrl	k_{iDC}	2.5981	$[1/Vs]$
Q_{ref} P-ctrl	k_{prp}	0	$[1/V]$
Q_{ref} I-ctrl	k_{irp}	$7.38e-5$	$[1/Vs]$
$absu_{gref}$ P-ctrl	k_{pac}	0.0438	$[1/V]$
$absu_{gref}$ I-ctrl	k_{iac}	1.2265	$[1/Vs]$
HVDC WF and GS Converter, inner control loop			
i_{dqref} and PQ_{ref} LPF time constant	τ_p	20	$[ms]$
i_{dq} P-ctrl	k_{pc}	4.496	$[V/A]$
i_{dq} I-ctrl	k_{ic}	70.62	$[V/As]$
current limit	i_{max}	1.1	$[p.u.]$
u_g P-gain	k_v	1	$[VA]$
a_f $u_{feedfwd}$LPF BW	a_f	100	$[rad/s]$
Chopper braking resistor			
Gain of fast U_{dc} rise		2.5	$[-]$
Activation voltage	$U_{DC\,on}$	1.20	$[p.u.]$
De-activation voltage	$U_{DC\,off}$	1.10	$[p.u.]$
Power limitation FB-gain	k_p/C_{therm}	5	$[-]$

Table 3: Control parameters

B

Implementation

B.1 Simulation environment

The models are implemented in Matlab/Simulink® without the use of any specific libraries, such as SimPowerSystems. The wind turbine model is from a fictitious demo turbine and the wind turbine control has been designed in the ECN Control Design Tool. Figure 32 presents the process flow, starting with opening Matlab. After setting some environment variables like paths the user should select a project, which is in this case called 'DemoWtb'. Then the user is asked to select either to start a simulation with an existing controller or to perform a new controller design. The process flow of the control design has been included for completeness, but here simulation of a wind farm based on an existing design is chosen.

Figure 32: Flow diagram of model simulation

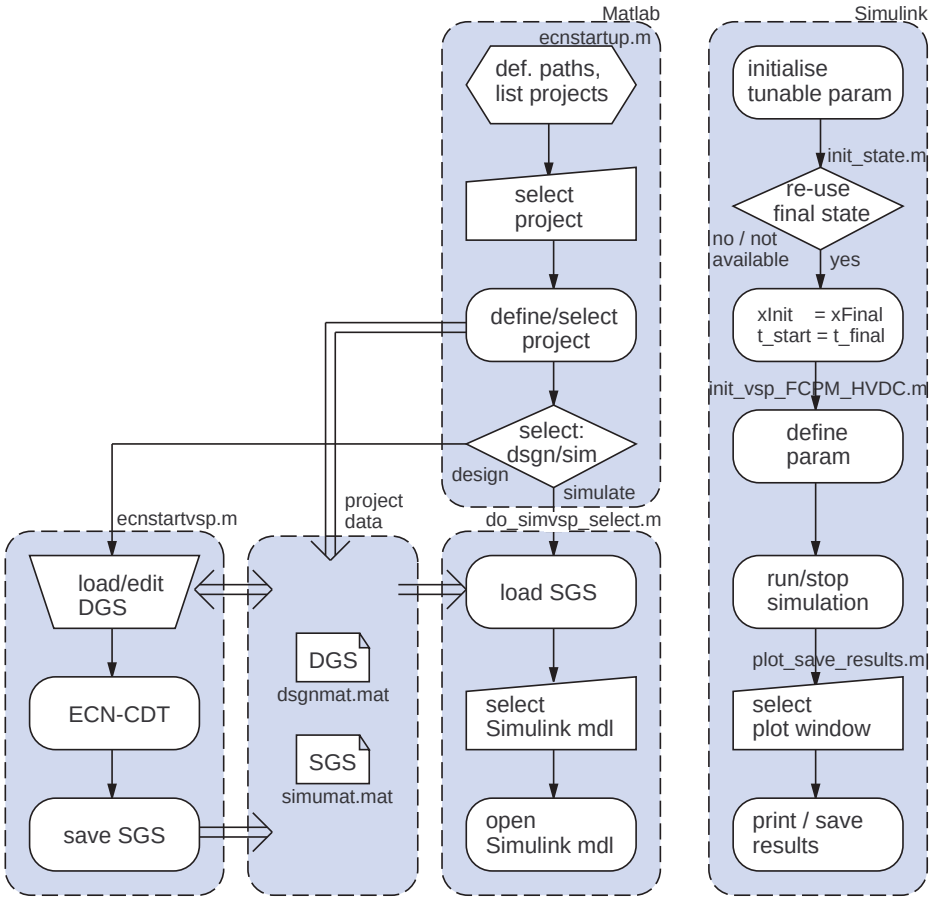

Initialisation

Before the model is opened so-called 'Simulation Global Structures' or SGS are loaded from ECN's Control Design Tool. These structs are loaded from the file *Simumat.mat* and contain the wind turbine design and controller parameters *turb, dcon, cmod, ctrp, ctrg* and settings for the simulation *ptune_<>, pconstr_<>, button_<> and partCtrl_<>*. Also several settings for the simulation environment, such as project name and paths, are loaded as globals: *FILENAME, FUNCTRL, GRAPH, PATHNAME, TEMP, TURBINE*. In this initialisation file also the user-specified Simulink model is opened and the appropriate reference variables are loaded. There references include wind time-series and either power reference signals or voltage setpoints from the DVC algorithm together with the appropriate VSC control mode settings.

Solver

As the model has a wide range of time constants a stiff solver *Ode23tb* with variable time step has been selected. The accelerator mode is selected, which leads to some time delay at the start of the simulation run, but overall it speeds it up.

Simulink initialisation

General
The initialisation of the Simulink model is performed in several the Simulink *InitFcn* call-back functions.First the function calls the M-script *InitState* to arrange that a previously saved final state *xFinal* is re-used as *xInitial* in case the model has not changed, which is visible from the * mark in the Simulink block diagram title bar, and a successful simulation run has been completed. In this case the user is prompted whether or not to over-

write the saved final state, otherwise the final state is saved automatically. This is useful when performing multiple (short) simulations, such as voltage dip responses, starting from the point in time when the wind farm has already started up. What follows is the parametrisation of the model and setting of initial states.

Wind turbine
The parameters of the electrical system and the dedicated controllers are loaded, and partly derived, in the M-file *init_VSP_FCPM_HVDC* .During the initialisation the following tunable parameters are set: faultstart, faultstop, baseLoad and faultLoad. Different faults in the ac-grid connected to converter *VSC Station UK1* can be simulated starting from a pre-loaded initial state by modifying these tunable parameters in the Matlab command window and starting the simulation run.

MTDC system
The initialisation of the MTDC system is performed in the top-level *InitFcn* call-back function wherein the script *RunMTDC_v3* is called. In this script the VSC stations are initialised and their control settings derived using the function *station_v3.m* . Also the external reference inputs of each VSC station are specified. Besides, each of the VSC subsystems is initialised separately through a local *InitFcn* call-back function. This call-back function reads the variable name that is entered in the block mask, see figure 34, e.g. *vsc3*, which is used to rename the workspace variable names to which data is saved through Scopes and ToWorkspace blocks. Also the mask variable name is displayed in the block icon for clarity, see figure 33. With this initialisation it is easy to expand the MTDC system, as the user only has to copy the VSC block and enter a unique variable in the mask. This variable has to be defined in the M-script RunMTDC_v3.m and also a valid variable name should be defined as reference input.

Post processing

The post processing at the end of the simulation does the plotting and printing of all scopes and ToWorkspace blocks in which the option *save to workspace as structure with time* is enabled. The printed figures for each run are saved in a single sub-directory with auto-generated name *Results_<ModelName>_<yyyymmdd_hhmmss>_<caseID>* , together with the final state and the workspace variables. A hyperlink to this directory is displayed in the Matlab command window.

B.2 Block structure

The Simulink model is organised in hierarchical levels to structure the block diagrams and limit the amount of information within a single block diagram, cf. figure 33. The actual values of the mask variables are shown in the blocks for clarity. Figure 34 shows the mask dialogue pane of the block 'VSC_Station_WF_UK1'. On the top level *From* and *To* blocks are used to split up the model, which is useful for the validation, which requires that the execution of the simulation is split over several processor cores.

Figure 33: Model overview model name 'NSTG_SSM'

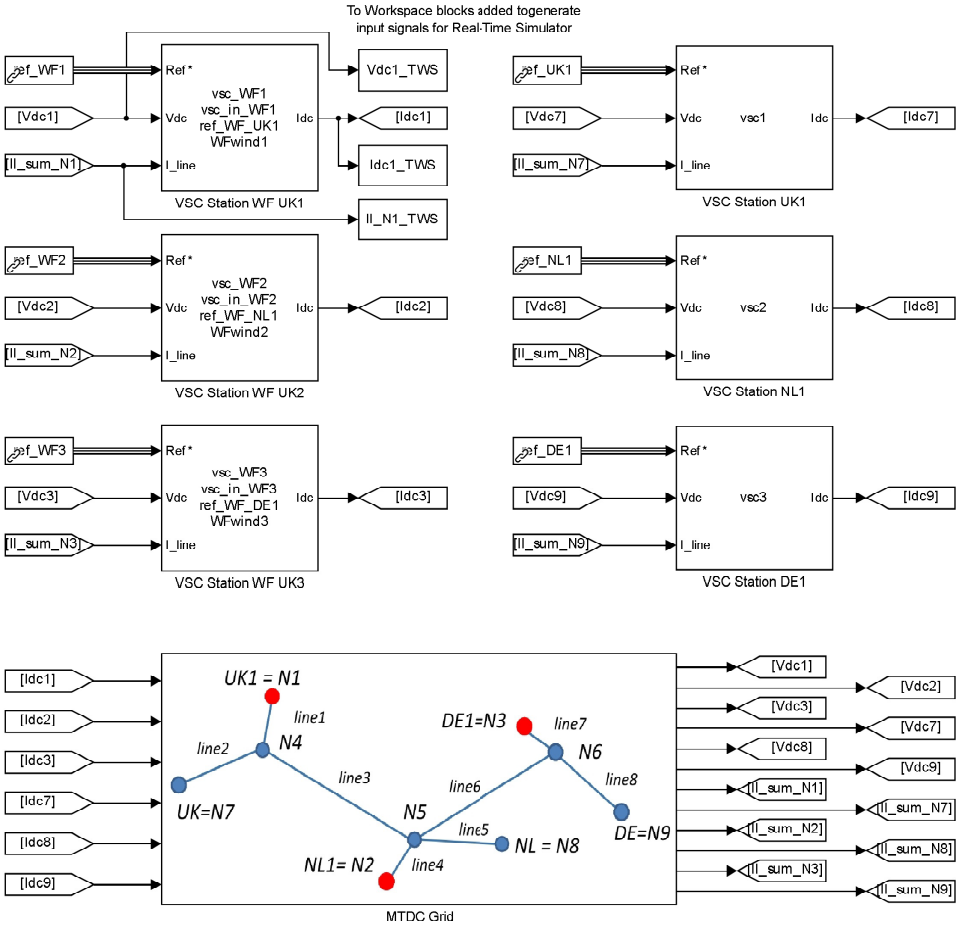

Figure 34: Wind Farm mask

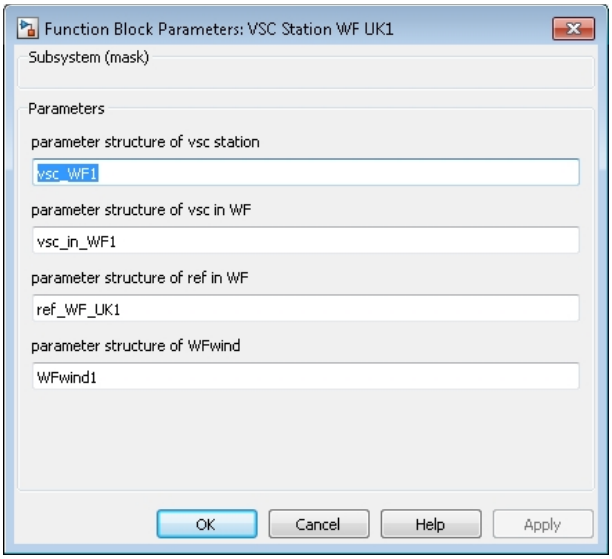

B.3 Wind farm

Figures 35 and 36 show the models of the wind farm and grid-side VSC station. Each wind farm and VSC station has a central reference input, which is shown in figure 37 and 38. The wind farm output power can be curtailed via the 'Pref' input. The VSC stations connected to the onshore grids receive their voltage set points from the central DC-power flow controller - which uses the novel DVC method - via the reference variable 'Wdcref'.

Figure 35: Wind Farm model, blockname: 'VSC_Station_WF_UK1'

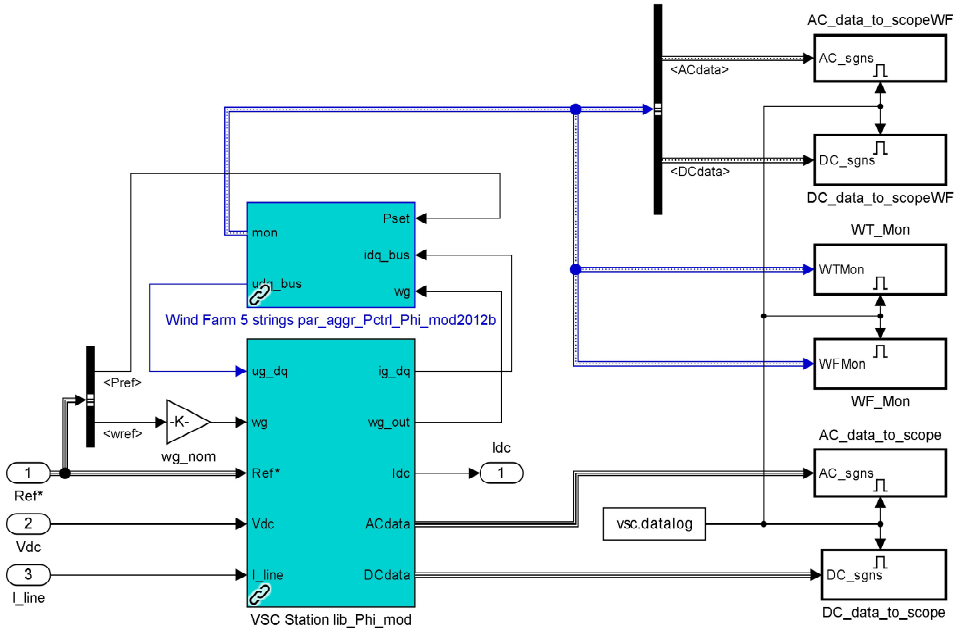

Figure 36: Wind Farm model, blockname: 'VSC_Station_UK1'

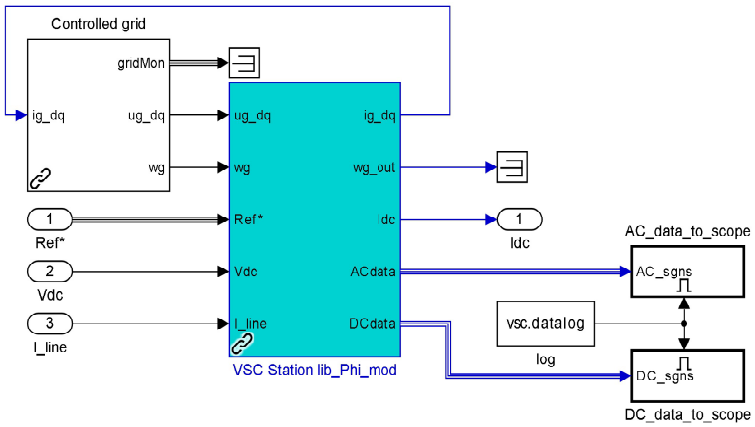

Figure 37: Wind Farm model reference, blockname: 'VSC_Station_WF1'

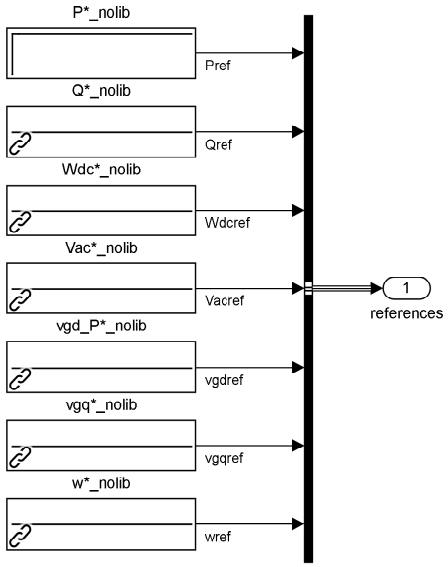

Figure 38: Wind Farm model reference, blockname: 'VSC_Station_UK1'

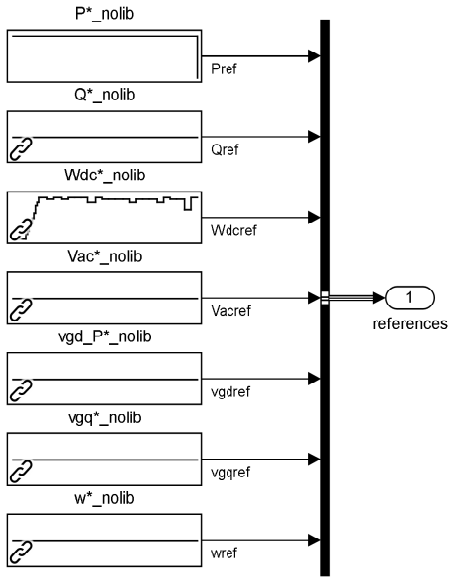

WF string

The five strings of wind turbines have been modeled both with individual wind turbines in figure 39 and as a single aggregated wind turbine with transformer which is connected through a single cable, cf. figure 40. The cable and transformer are modeled as a lumped LRC network, cf. figures 41 and 42.

WF trafo

The transformer at the WF collection bus is modeled as a Γ-circuit in which the filter capacitance in between the transformer and the smoothing reactance is included, cf. figure 42.

Figure 39: Wind Farm string 5WTs

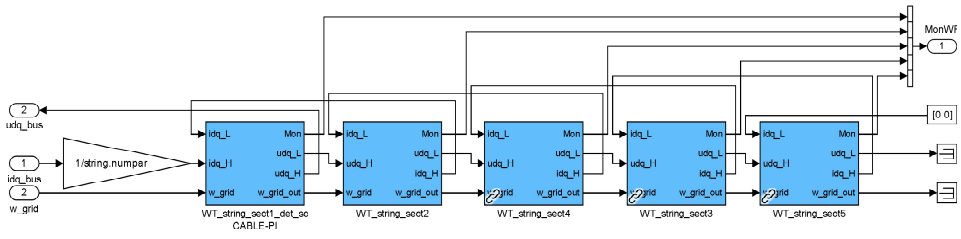

Figure 40: Wind Farm string

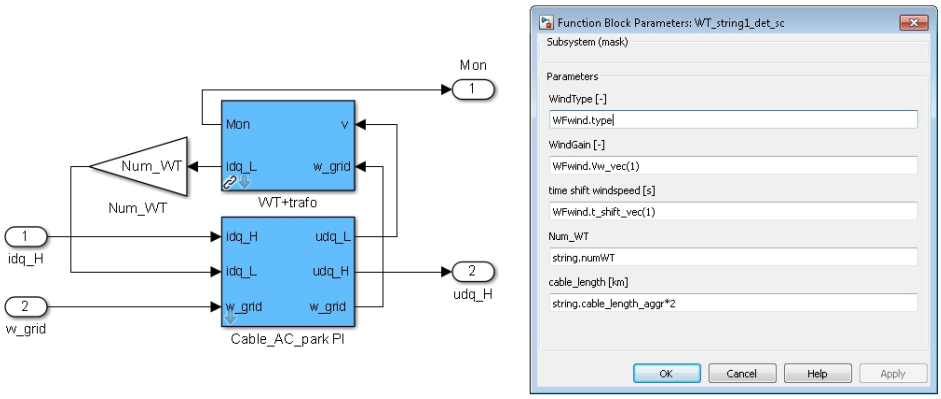

Figure 41: Wind Farm string cable, blockname: 'Cable_AC_park'

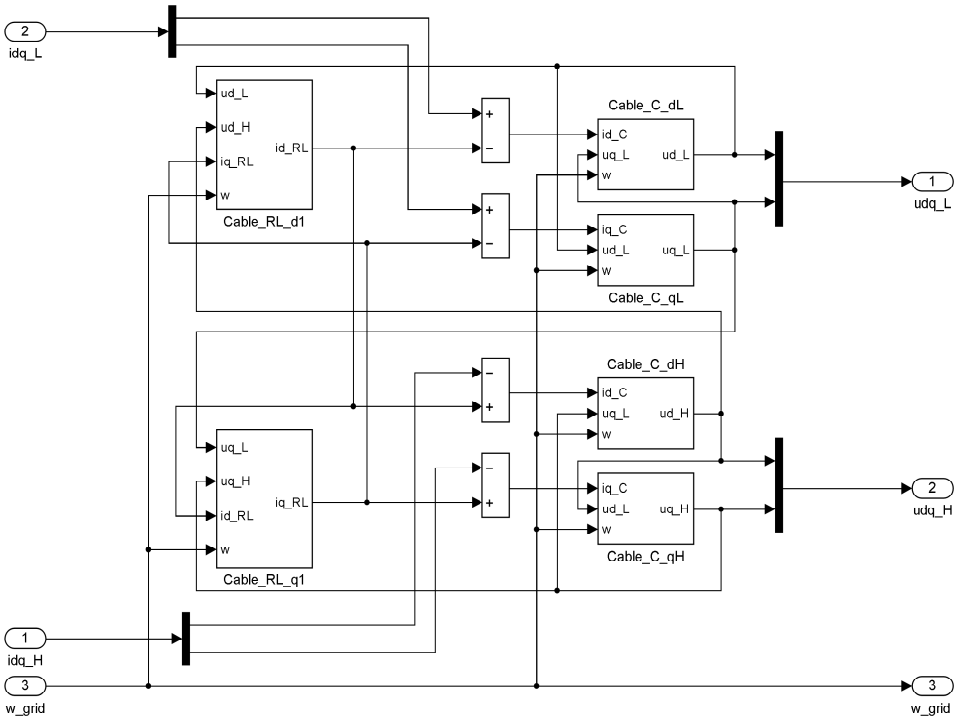

Figure 42: Wind Farm trafo, blockname: 'trafo_par_Cf'

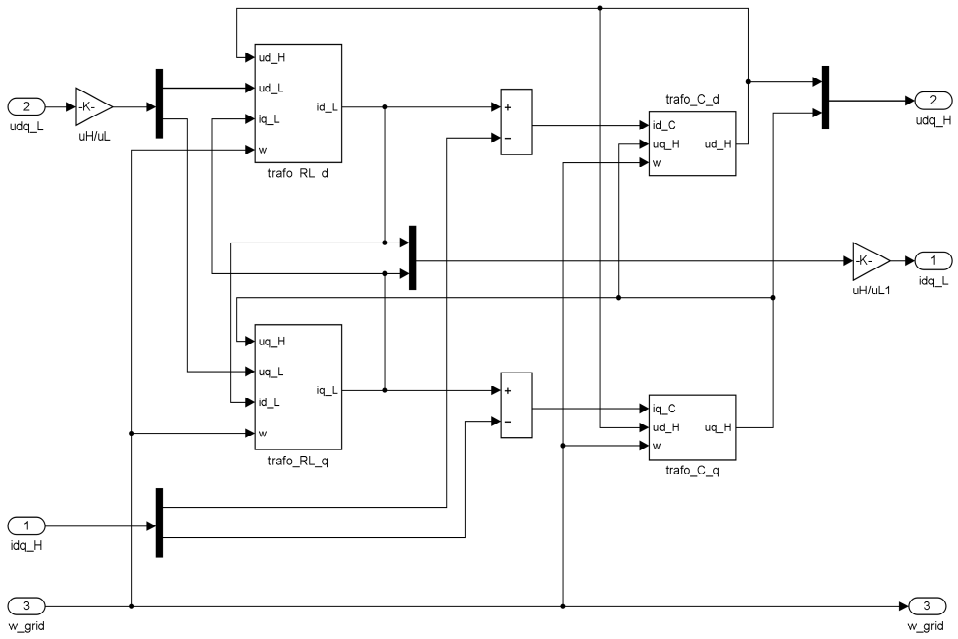

Figure 43: Wind Turbine model structure, blockname: 'WT+Ctrl'

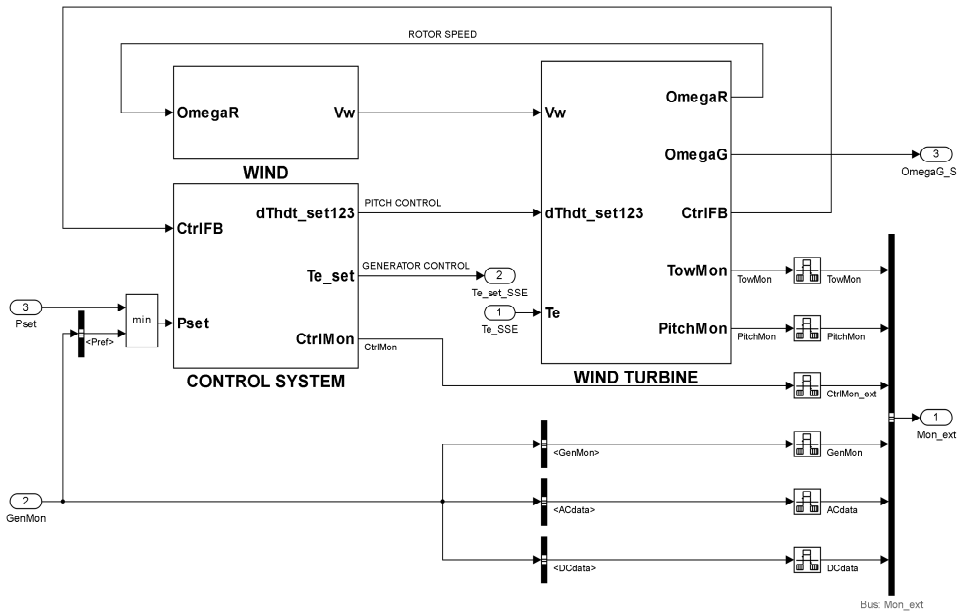

B.4 Wind turbine

WT model overview

Figure 43 shows the structure of the wind turbine model and figure 44 the aerodynamic and mechanic model of the wind turbine. The aerodynamic part basically consists of a dynamic inflow filter, lookup tables to derive the actual C_q and C_t coefficients and the calculation of the aerondynamic torque and thrust. The mechanical model contains a

Figure 44: Wind Turbine mechanical and aerodynamic model and control, blockname: 'WIND TURBINE'

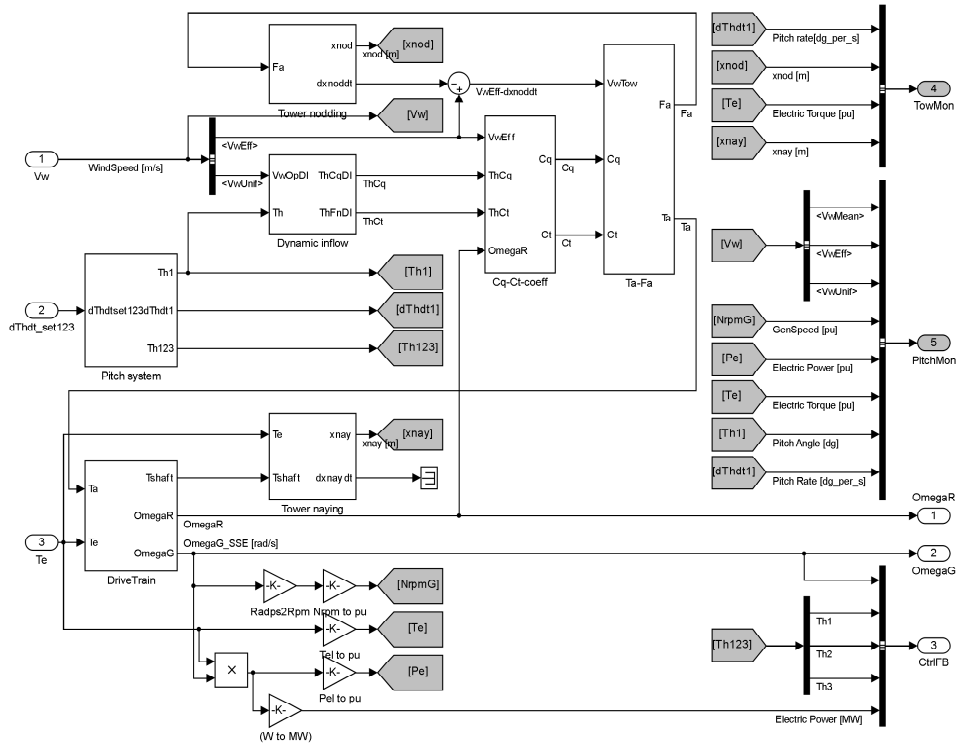

Figure 45: Wind Turbine wind model, blockname: 'WIND'

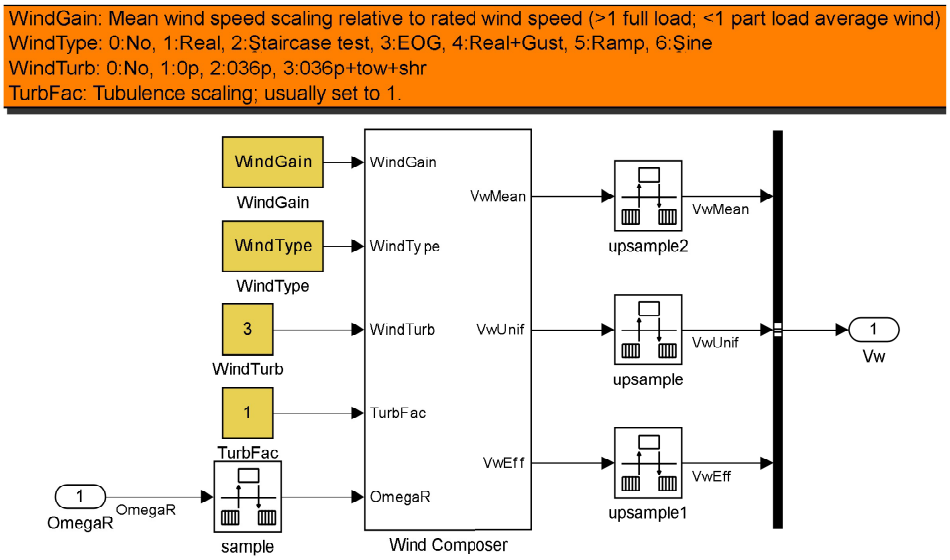

Figure 46: Wind Turbine generator inertia, blockname: 'Drive Train'

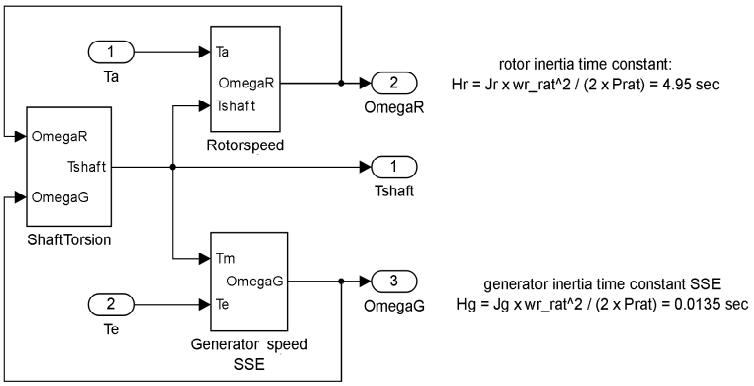

Figure 47: Wind Turbine generator inertia, blockname: 'Shaft Torsion'

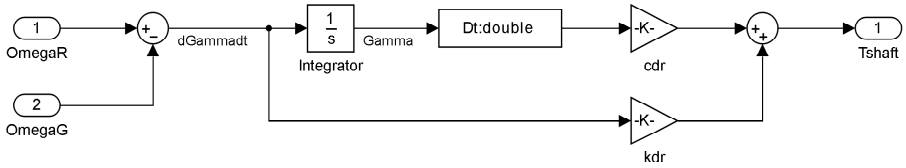

2-mass drive train model, shown in figures 46 - 49, a 1-mass tower model and a pitch actuator model. The wind model as shown in figure 45 generates the rotor effective wind speed. It has inputs to set the average wind speed as well as the type of wind, which is by default a realistic wind realisation with wind shear, rotor sampling and tower shear.

Figure 48: Wind Turbine generator inertia, blockname: 'Rotorspeed'

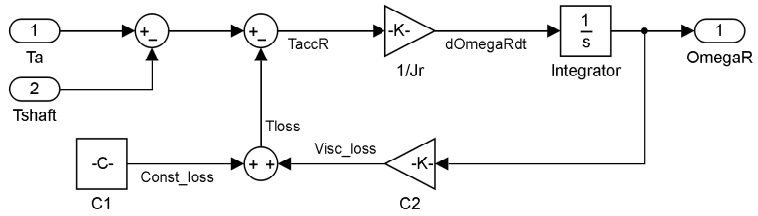

Generator

As the generator parameters used are from another turbine it needs conversion factors to adapt the nominal generator speed to the nominal rotor speed, cf. figure 49. For the same reason the nominal generator power is scaled, cf. figure 51.

Figure 52 shows the control loops to control the generator torque with v_q and generator reactive power with v_d. The torque setpoint from the turbine controller is reduced in case of power imbalance in the wind turbine converter. The reactive power setpoint is set to zero as the WF bus voltage is controlled by the HVDC WFC. The terms to decouple the two loops can be found in figure 53 and 59. The block PMG_Meas in figure 53 limits the bandwidth of the electrical signals to 1000 rad/s and of the mechanical signals to 100 rad/s. The rotor position, which is estimated from the measured currents and voltages and machine parameters, see also figure 60, is fed back through a low-pass filter to phase rotation blocks at the electrical inputs and outputs of the generator, cf. figure 54. This filter represents a PLL in its linear operating range. The initial position error is set to an arbitrary but small value, which is used in the flux calculation in figure 56. The dynamics of the rectifying converter have been neglected as these fast compared to the generator dynamics. Please note that compared to the synchronous generator model in [5] the stator flux is defined with opposite sign.

Figure 49: Wind Turbine generator inertia, blockname: 'Generator speed'

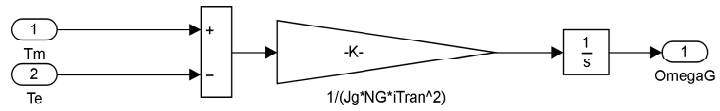

Figure 50: Wind Turbine generator and inverter, blockname: 'PM dq + conv'

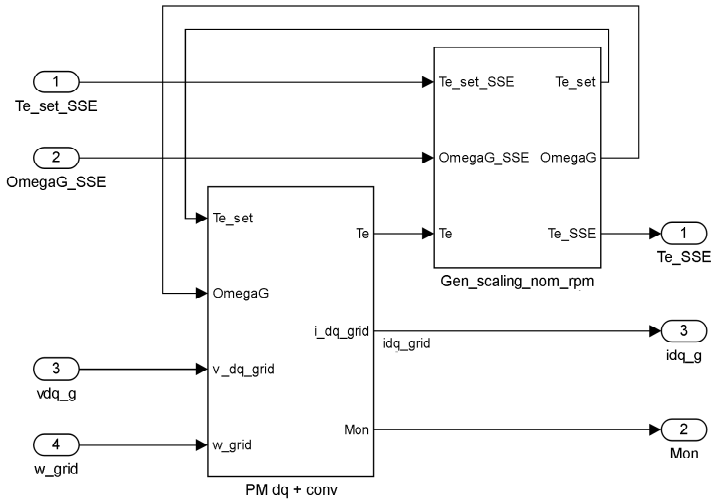

Figure 51: Wind Turbine generator with upscaling, blockname: 'Generator upscaling'

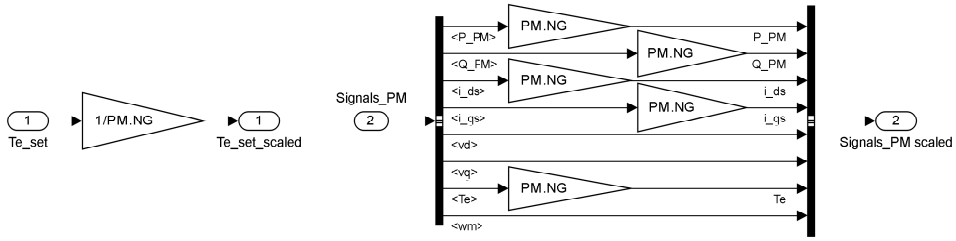

Figure 52: Wind Turbine generator with control, blockname: 'PMG 2MW + ctrl'

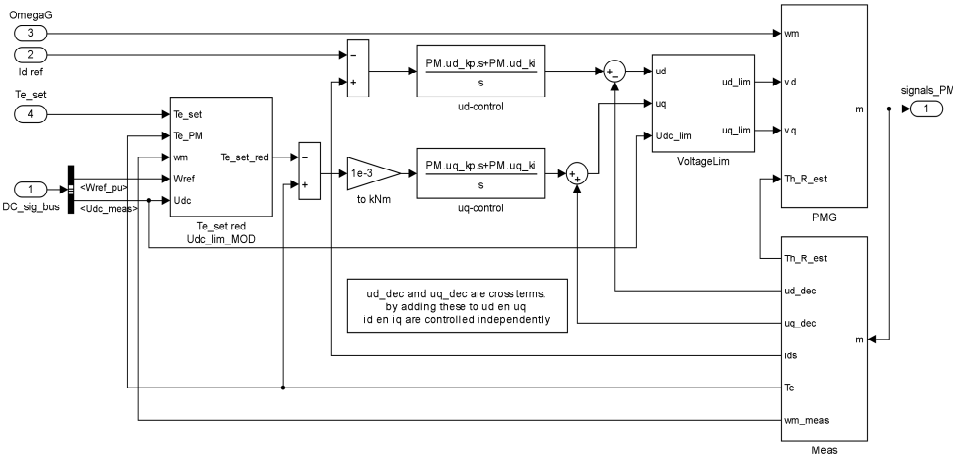

Figure 53: Wind Turbine generator and measurement block, blocknames: 'PMG' and 'PMG_Meas'

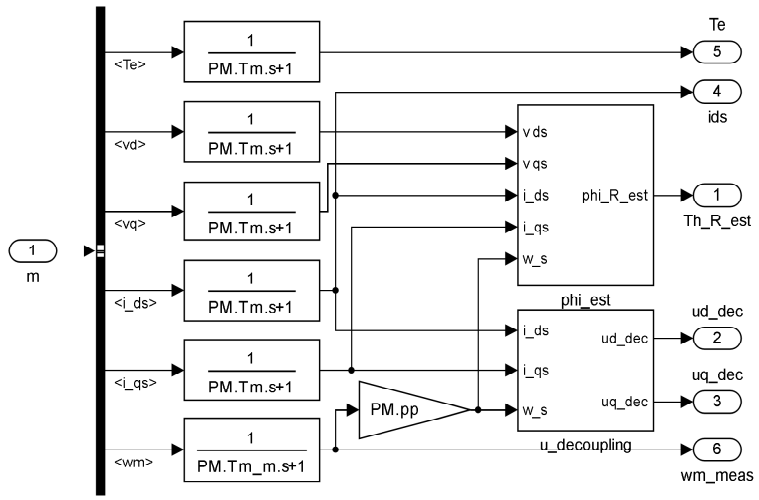

Figure 54: Wind Turbine generator, blockname: 'PM_2'

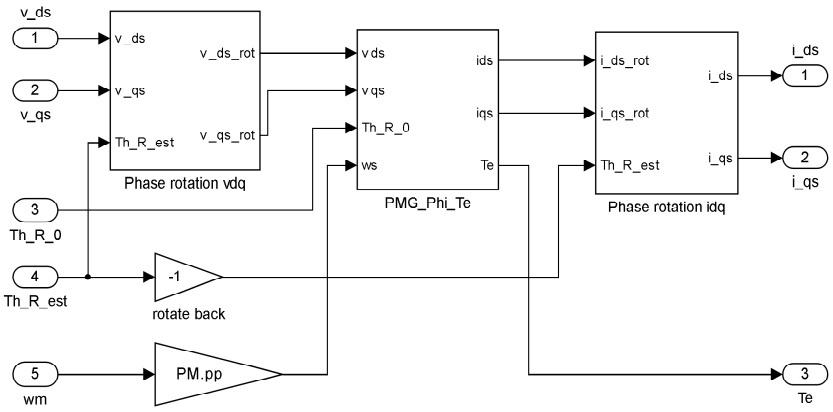

Figure 55: Wind Turbine generator flux and torque calculation, blockname: 'PM_phi_Te"

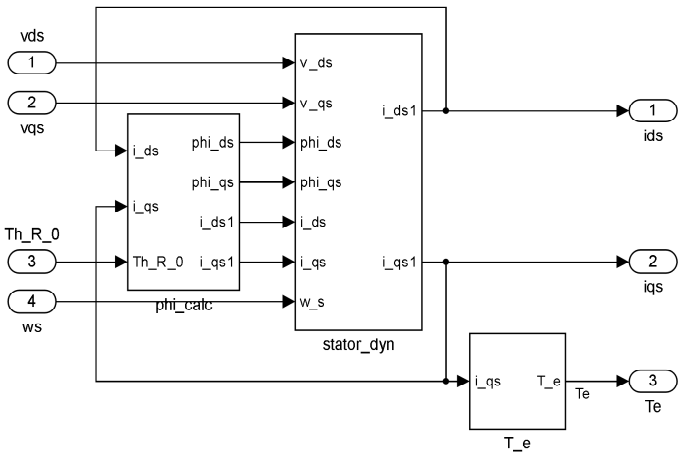

Figure 56: Flux calculation, blockname: 'phi_calc'

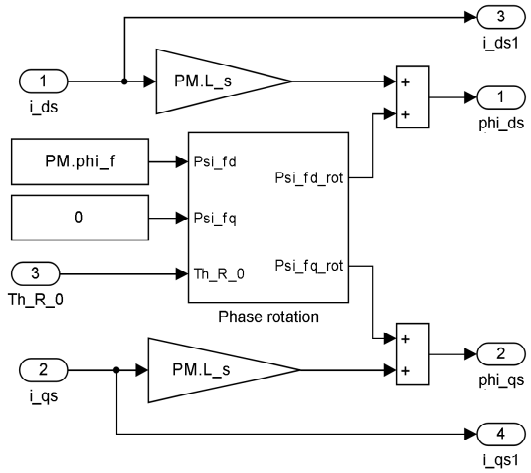

Figure 57: Wind Turbine generator stator dynamics, blockname: 'stator_dyn'

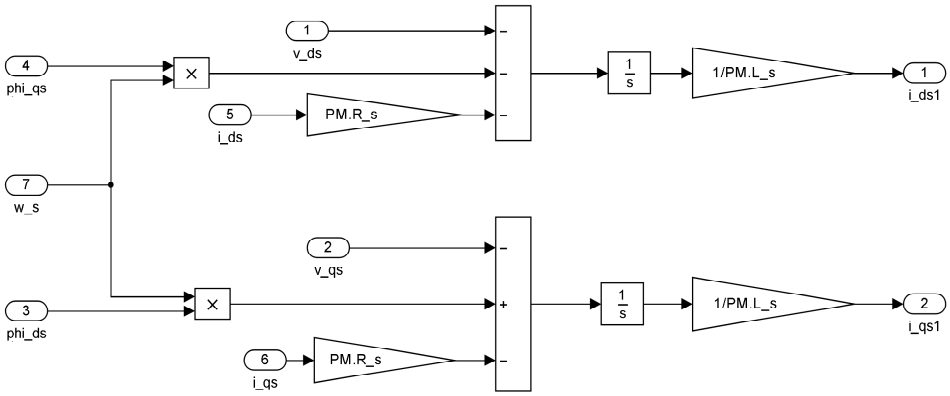

Figure 58: Wind Turbine generator torque calculation, blockname: 'T_e'

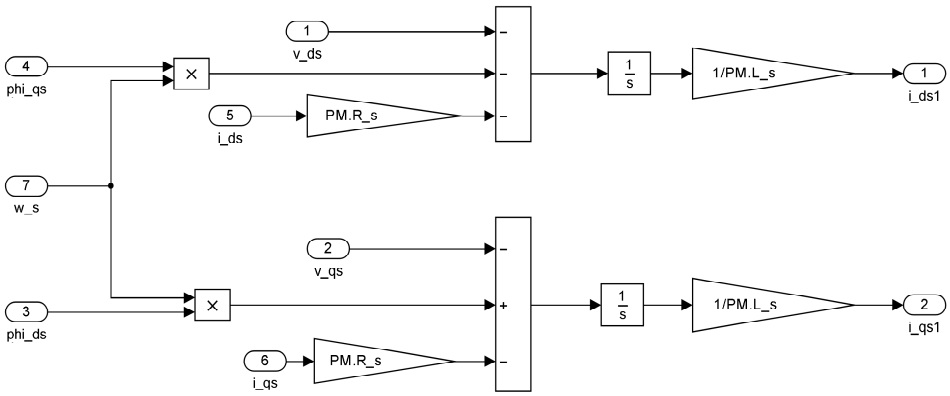

Figure 59: Wind Turbine generator decoupling, blockname: 'u_decoupling'

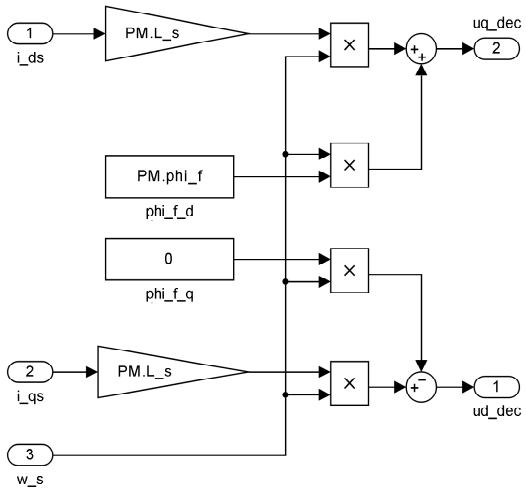

Figure 60: Wind Turbine generator flux calc, blockname: 'phi_est'

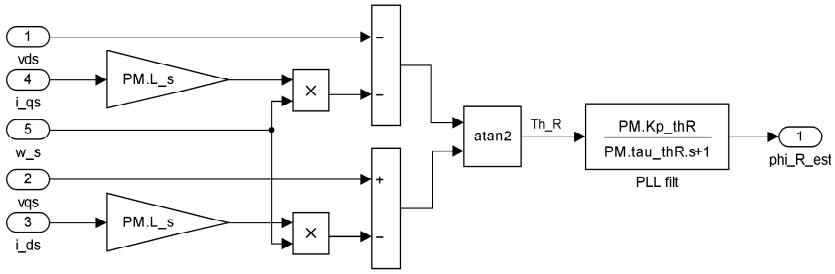

Figure 61: Wind Turbine generator flux angle estimation during startup: (top) rotor flux, (middle) measured and estimated rotor flux angle, (lower two) stator voltage and current

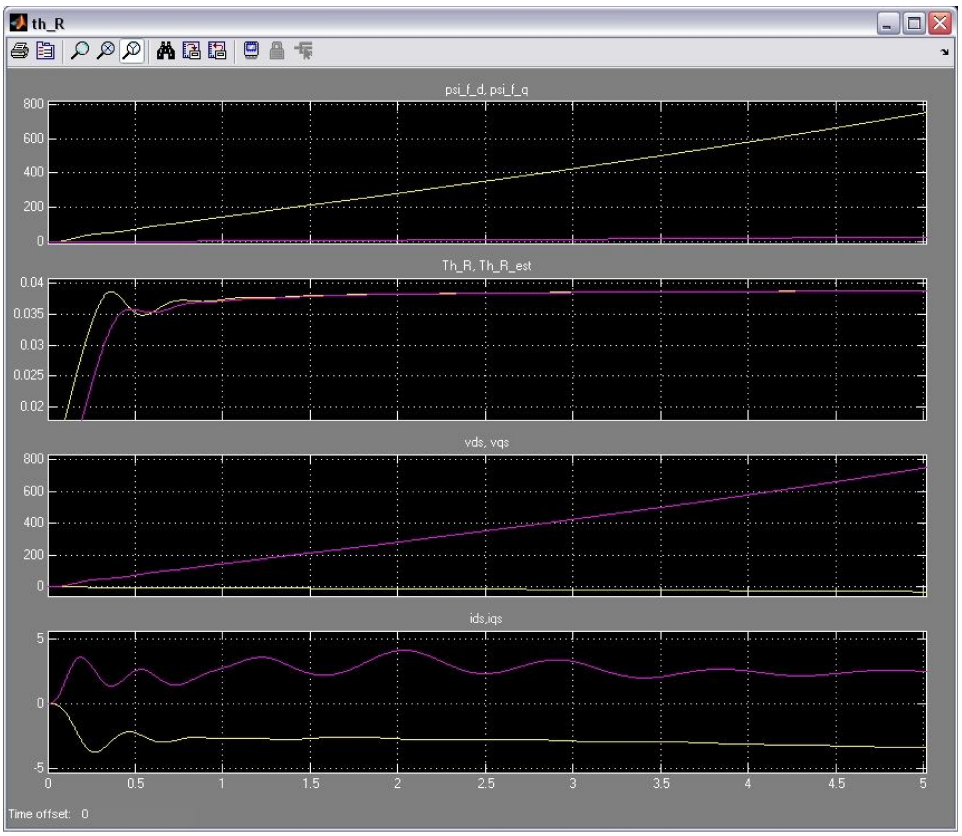

Figure 62: Wind Turbine generator flux angle estimation during voltage dip: (top) rotor flux, (middle) measured and estimated rotor flux angle, (lower two) stator voltage and current

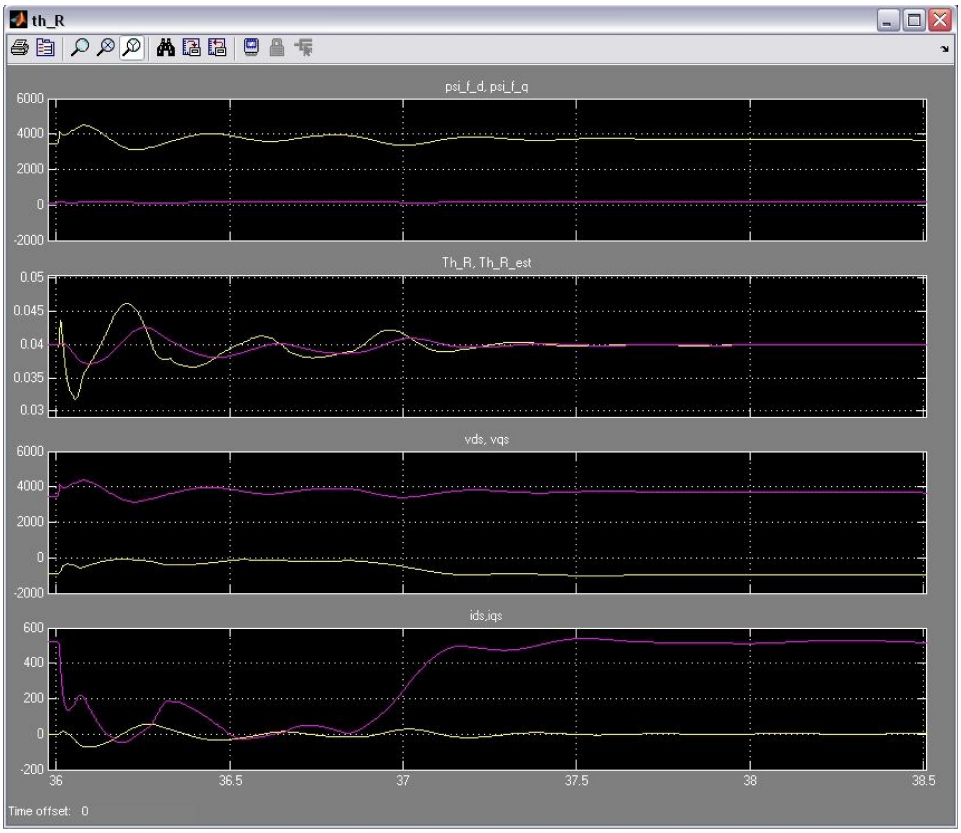

Figures 63 until 69 present the details of how the generator torque setpoint is reduced and ramped up again in case of a high or fast rising dc-link voltage. The purpose is to effectively limit the dc-link voltage while damping drive-rain oscillations. The block 'Pe_red' in figure 64 calculates an absolute reduction of the generator power that is basically proportional to the square of the dc-link voltage compared to a raised dc-voltage setpoint. The gain is chosen so to obtain a response time of the dc-voltage reduction of τ_{Udc}. The rising slope of the dc-voltage can be emphasised to obtain a faster response, while the negative slope is reduced to hold on the power reduction somewhat longer. The signal $T_{e\,red\,mode}$ is applied to activate the smoothing of the torque setpoint from the WT controller, cf. figure 66 and the damping of the drive-train oscillations, cf. figure 67. The reason for smoothing the WT controlled torque is that the WT controller responds to the generator speed rather than on the speed derivative. The drive-train oscillation damping basically adds a damping torque proportional to the derivative of the measured generator rotational speed. The speed derivative dw_m/dt is realised through a band pass filter, with the low cut-off frequency well above the mechanical oscillation frequency. The feedback gain k_{damp} to obtain critical damping has been derived from the drive-train parameters. Also the offset term in the damping torque is calculated and subtracted in order to suppress drift in the dc-link voltage. A third function the effect of the damping torque on the dc-link voltage is estimated and subtracted from the measured dc-link voltage to prevent interaction of the damping torque interaction with the the power reduction block. The low feedback gain is because the dc-link chopper also compensates for the oscillations from the damping torque. Finally a term T_{damp_lim}, cf. figure 67, is subtracted from the damping torque in case when the dc-voltage is close to its high limit value.

After the voltage dip clearance the WT grid converter ramps up the power leading to a decrease of the dc-link voltage. This again leads to a ramp up of the generator torque setpoint. The block 'Limit Pramp_up' anticipates on possible drive-train oscillations during ramp-up and therefore limits the ramp-up rate especially at (positive) torque levels close to the rated torque, which is realized through the square and square-root function blocks, cf. Figure 68. Finally the generator torque and the generator power are limited, cf. figure 69. The generator power limitation is imposed separately, because of the generator speed oscillations during and after the dip.

Figure 63: Wind Turbine generator torque reduction, blockname: 'Te_set red Udc_lim_MOD'

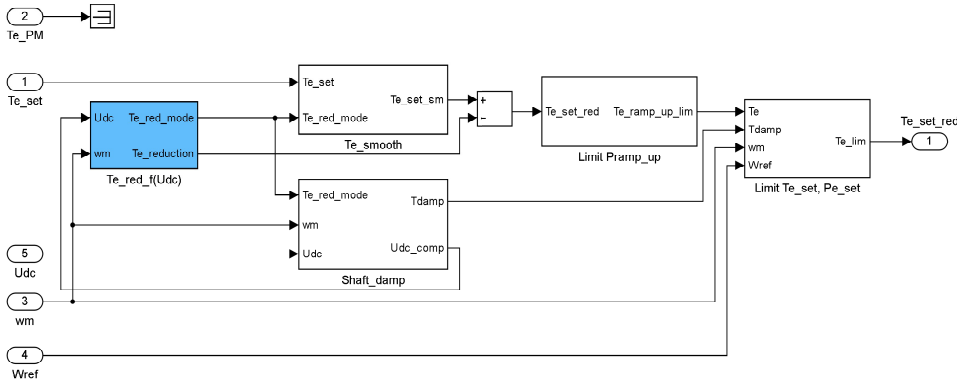

Figure 64: Wind Turbine generator electrical power reduction, blockname: 'Pe_red'

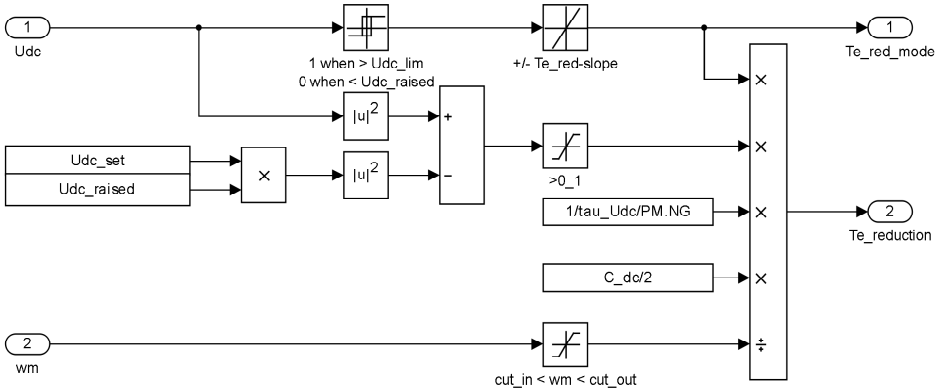

Figure 65: Wind Turbine generator electrical power reduction during voltage dip: top: U_dc measured (yellow), emphasized (magenta) and emph. and slopehold (green)

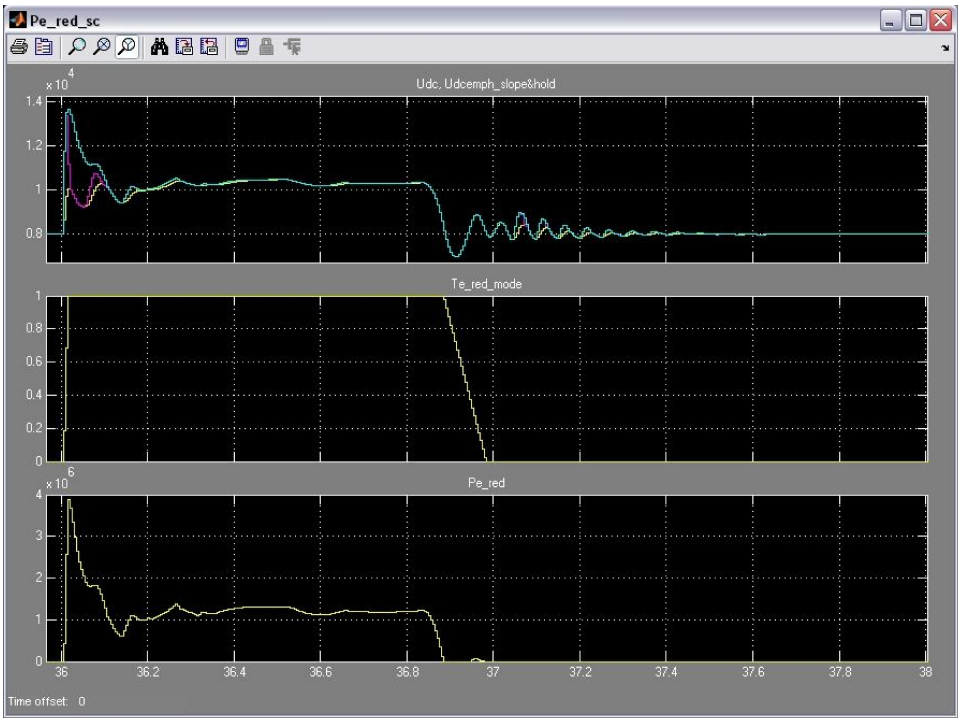

Figure 66: Wind Turbine generator torque setpoint smoothing, blockname: 'Te_smooth'

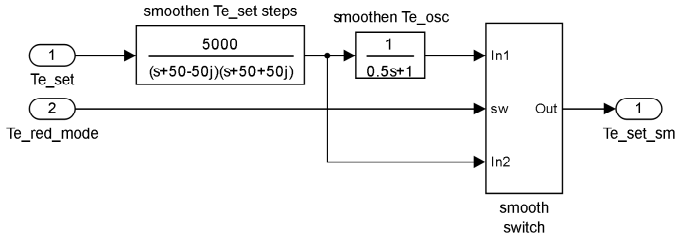

Te_red_mode = 0 (Normal operation), only filter out small quantifation steps from WT controller
Te_red_mode = 1 (Torque reduction): also filter out WT controller response to shaft oscillations

Figure 67: Wind Turbine generator damping, blockname: 'Shaft_damp'

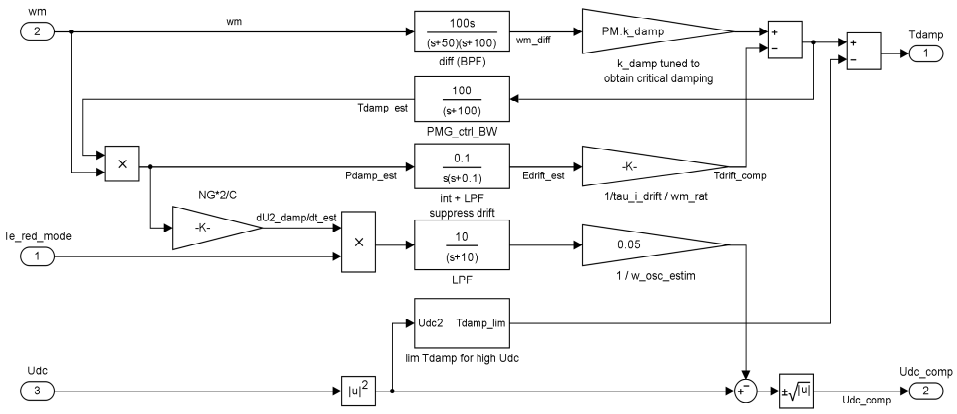

1: detect shaft oscillations through band pass filter with phase lead in freq. range of the oscillations

2: apply propoertonal damping torque

3: Estimate the generator response and compensate low-frequency content in damping toraue that would lead to excessive DC-voltage variations

4: Actively limit the damping torque in case of DC-overvoltage

5: Subtract the estimated DC-voltage variation caused by the damping, so that this is not fed back into the DC-voltage control loop

Figure 68: Wind Turbine generator torque ramp-up limit, blockname: 'Limit Pramp_up'

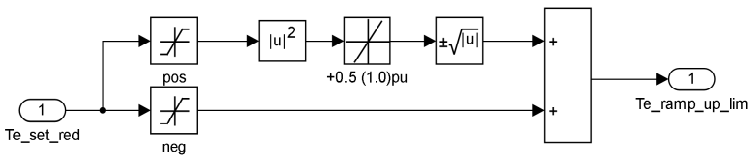

Limit the ramp-up rate of the torque setpoint,

The ramp rate limit is scaled with the reciprocal value of the torque (by measns of the (u)2 and sqrt(u) blocks)

Figure 69: Wind Turbine generator torque and power limit, blockname: 'Limit Te_set, Pe_set'

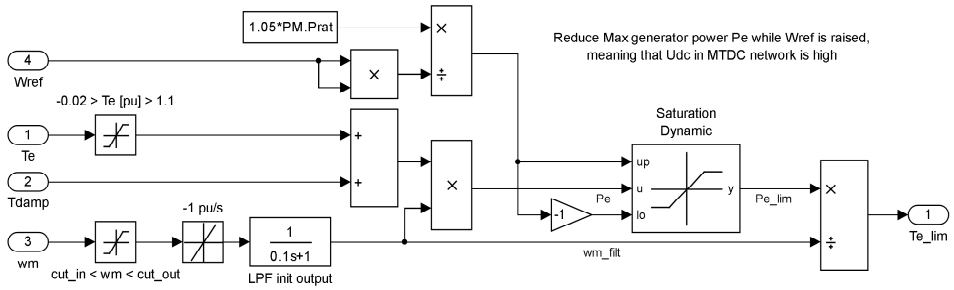

Figure 67 illustrates the various functions within the torque block. The smoothing of the torque setpoint under normal conditions is visible in figure 70, while during a voltage dip smoothing with a longer time constant is applied, which is visible figure 71. Starting from the smoothed torque setpoint, which is the purple line in the upper right plot, the lower right plot shows the steps how the torque is reduced. The yellow line is basically the reduced torque with the reduction proportional to the square DC voltage error. The purple line, which partly overlaps this curve, shows the effect of the ramp-up limit, especially at the start of the dip and during the power ramp up after the dip, starting around 36.8 sec. The magenta curve also includes the damping torque, which is active both during and after the dip.The red curve is the actual torque.

Figure 70: Wind Turbine generator torque reduction, partial to full load transition: (top) WT-controller Torque setpoint (yellow), smoothed torque setpoint (magenta), (bottom) red line shows some reduction of torque oscillations

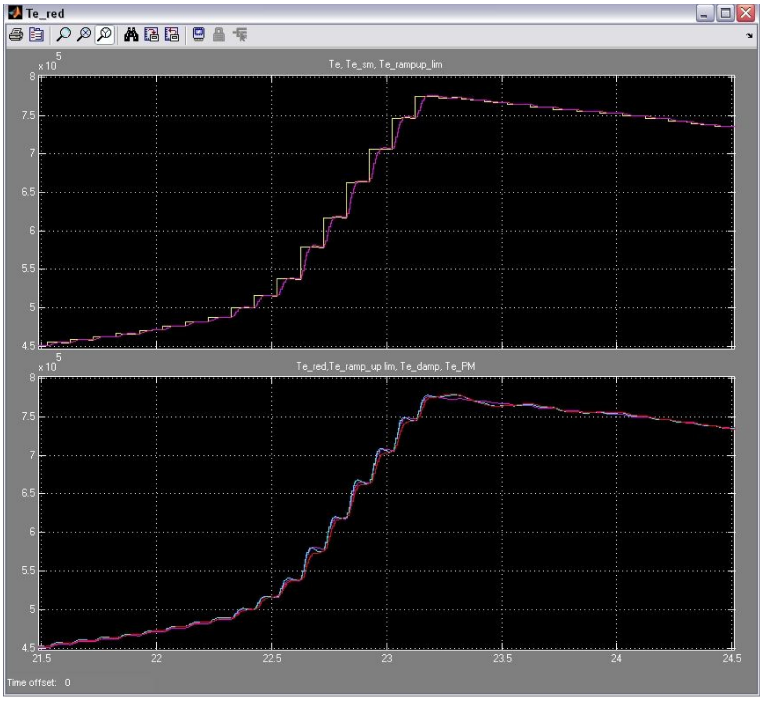

Figure 71: Wind Turbine generator torque reduction, voltage dip response: (top)

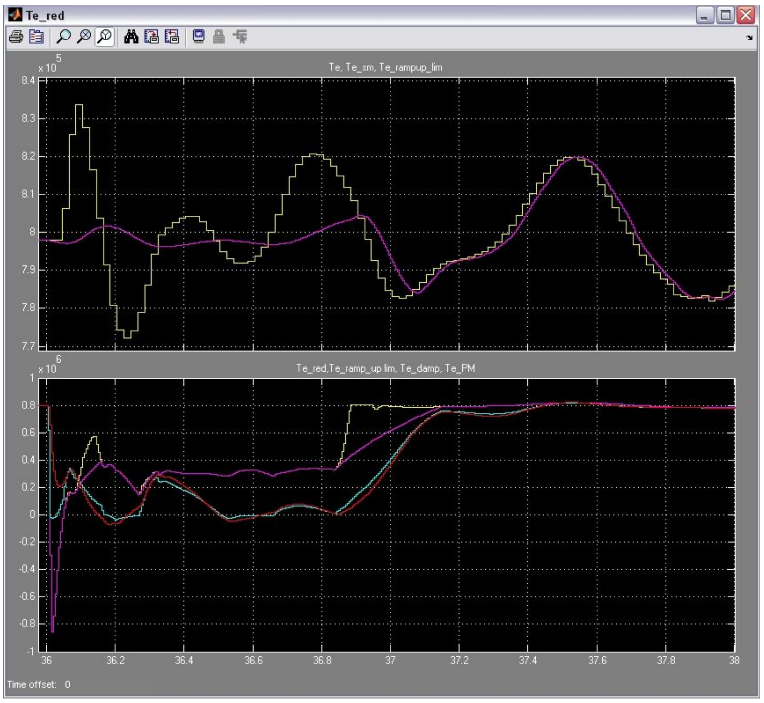

Full-scale converter

The figures 72 until 81 present the model of the WT grid converter. The voltage source converter controls the current over a series impedance, see the block 'Grid Imp Mod' in figure 73, which is the inner control loop, see also figure 75. The outer loop generates the current setpoint values from the power setpoints and measured grid voltages, see figure 76. To decouple the i_d and i_q control loops two decoupling terms are applied: $u_{d\,dec} = -\omega \cdot L_{conv}$ and $u_{q\,dec} = \omega \cdot L_{conv}$. In this model the WF bus voltage is controlled centrally by the HVDC-WFC. Therefore the reactive power is set to zero. The feedback terms k_q are added to reduce voltage disturbances and in addition damping terms k_{damp} are introduced to counteract instabilities caused by the constant power control of the WTGCs, cf. figure 76.

Figures 77 and 79 show the power setpoint limiter, the block 'PQ_lim' in figure 73, and the current limiter with alternating priority. The power references and transitions are smoothed and also the fast current limitation has some filtering (t_lim = 0.5 ms) to represent the inverter response time. The power limitation block 'PowerLim' in figure 76, shown in detail in figure 80, is a droop control which is intended to respond to the grid voltage decrease controlled by the HVDC-WFC in case of a DC-power imbalance.

Figures 81 and 82 show the converter control on the DC-side. The DC-link voltage control is a proportional feedback loop combined with a feedforward term, as in the back-to-back configuration the incoming power from the generator is measured. The operational mode control of the WT grid converter holds switching between rectifier operation (start-up) and inverter (normal) operation. Secondly, the reference DC-voltage is raised in case when a voltage dip is detected. Finally the reactive power setpoint is reduced in case when the dc-link voltage drops below its setpoint.

Because the AC-Voltage is controlled by the Wind Farm VSC, the reactive power and Ac voltage controllers are disabled with a fixed to zero reactive current.

Figure 72: Wind Turbine grid full-scale converter with dc-link and controllers, blockname: 'Gridconv + DC link from HVDC mdl'

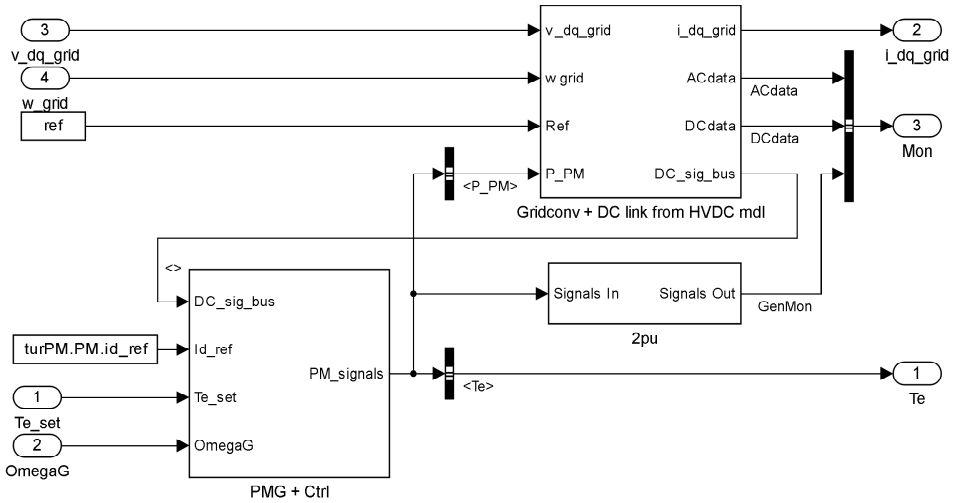

Figure 73: Wind Turbine grid side converter, blockname: 'Grid converter'

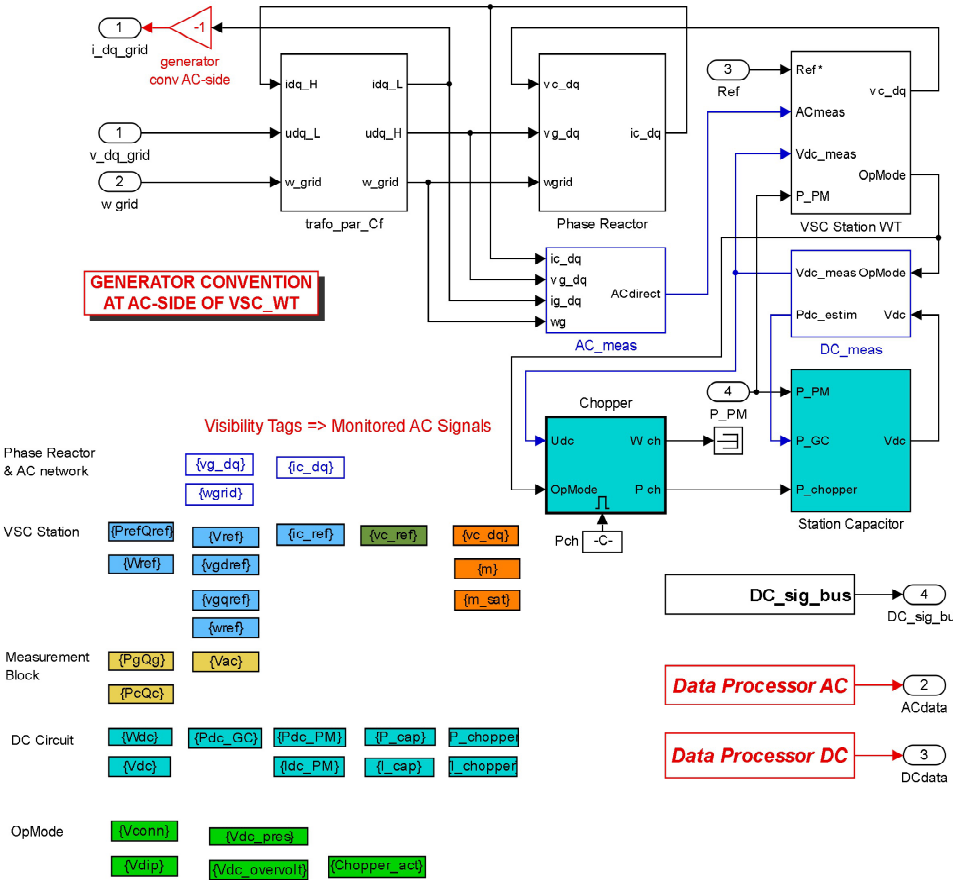

Figure 74: Wind Turbine grid side converter, blockname: Voltage Modulator

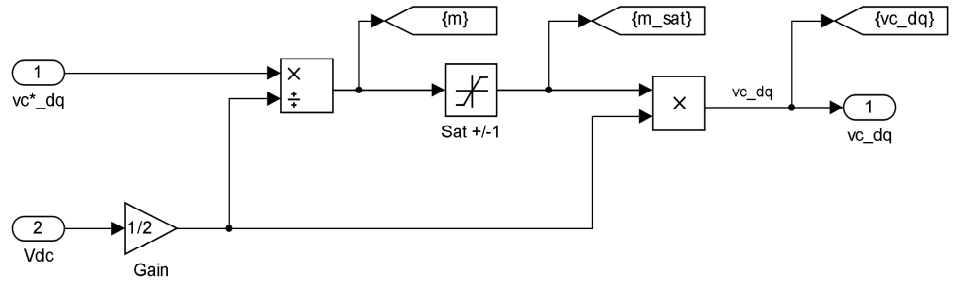

VSC non-switching modulator:

> modulation index |m| limited to 1
this corresponds to the maximum modulation of the fundamental frequency.
A higher modulation index would be possible if high (e.g. 3rd) harmonics are allowed.

> As vc_dq is defined by an amplitude-invariant dq-transform,
the maximum amplitude of vc_dq is equal to Vdc/2

Figure 75: Wind Turbine grid side converter current control, blockname: 'Inner_Controller'

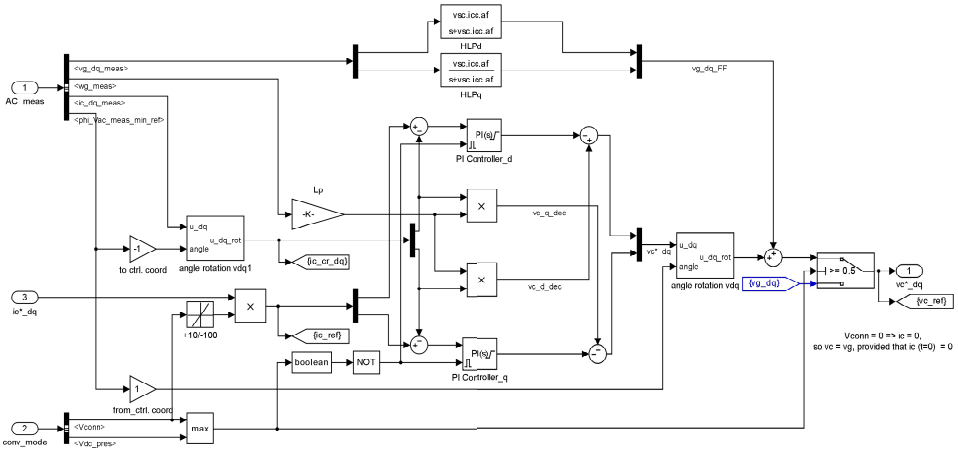

Figure 76: Wind Turbine grid side converter current control, blockname: 'Outer_Controller'

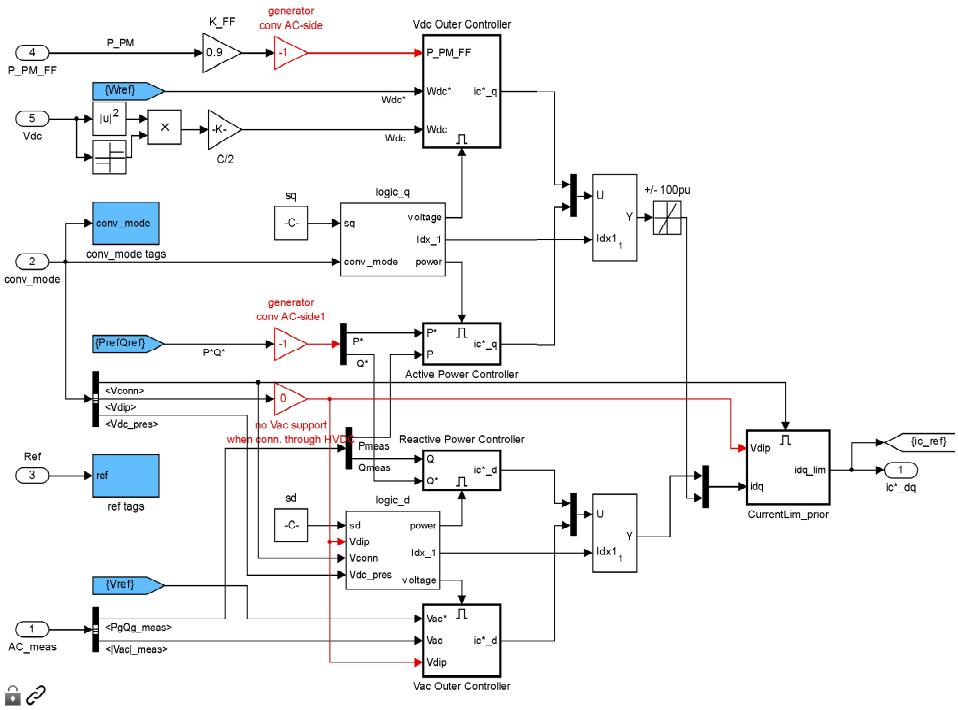

Figure 77: Wind Turbine grid side converter power limiter with PQ-priority selection, blockname: 'PQ_ref_lim_f(Vdc_Vqd)_WT'

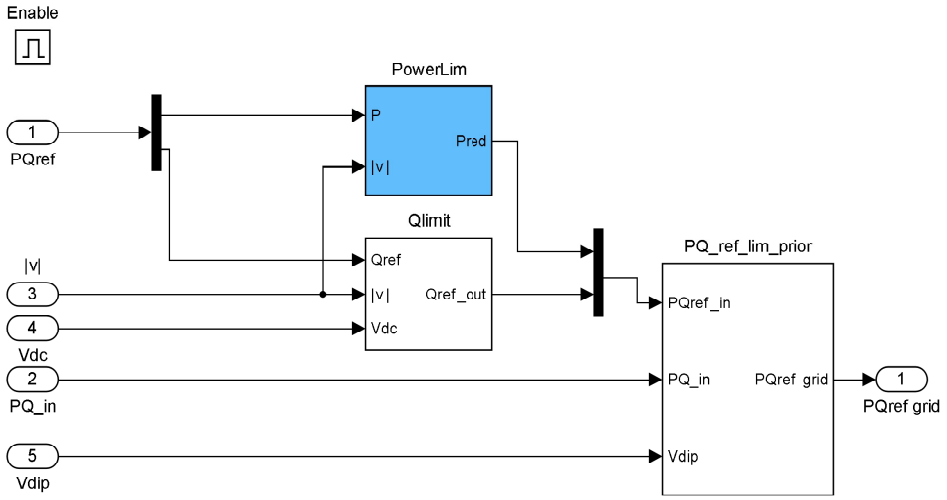

Figure 78: Wind Turbine grid side converter power limiter with PQ-priority selection detail, blockname: 'PQ_ref_lim_prior'

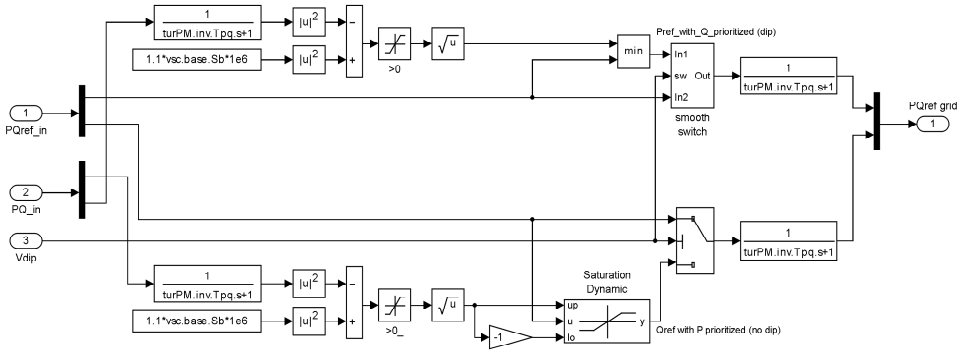

Figure 79: Wind Turbine grid side converter current limiter with PQ-priority selection detail, blockname: 'CurrentLim_prior'

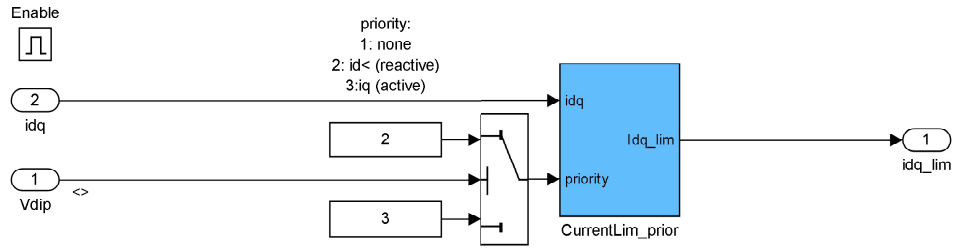

Figure 80: Wind Turbine grid side converter active power reduction at low grid voltage, blockname: 'PowerLim'

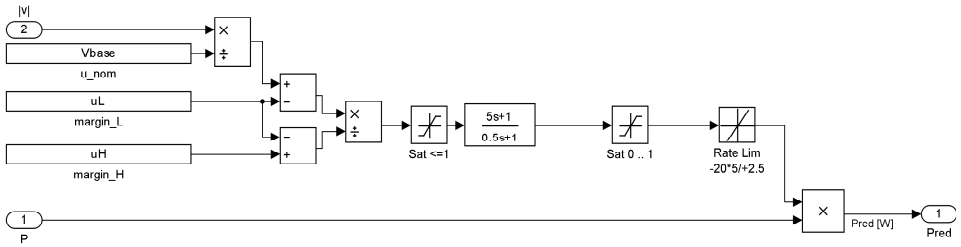

Figure 81: Wind Turbine grid side converter dc-voltage control, blockname: 'Vdc_Outer_Controller'

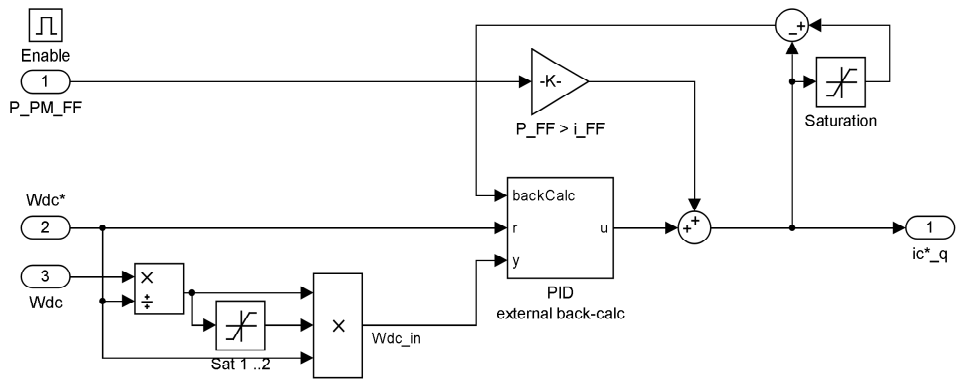

Figure 82: Wind Turbine grid side converter operating mode control, blockname: 'Conv_operating_mode_WT'

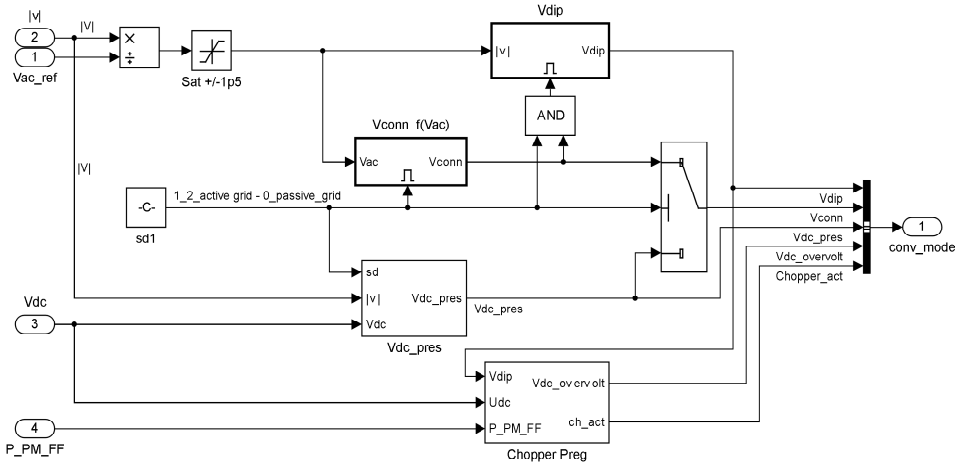

Figure 83: Wind Turbine grid side converter dc-voltage control, blockname: 'calc_actual_Refs_WT'

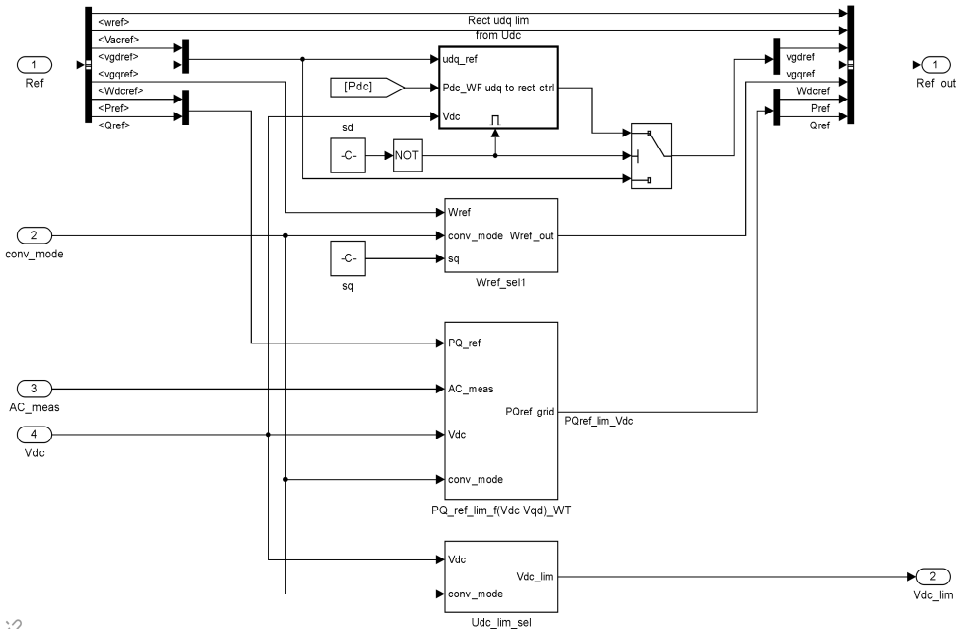

Figures 84 to 86 show the DC-link of the WTGC with chopper model. The chopper activation is a hysteresis control with ramp limiter to represent the modulation dynamics. The dc-voltage rising slope is emphasized using a filter to obtain an earlier activation. The power setpoint is proportional to the square dc-voltage error. Compensation of the voltage oscillations from the drive-train damping is implemented by a band pass filter. The low pass filter and and min block are applied to prevent negative values for the power setpoint of the chopper. The DC-link in the wind turbine converter is basically the capacitor as shown in figure 88.

Figure 84: Wind Turbine grid side converter dc-voltage control, blockname: 'Chopper'

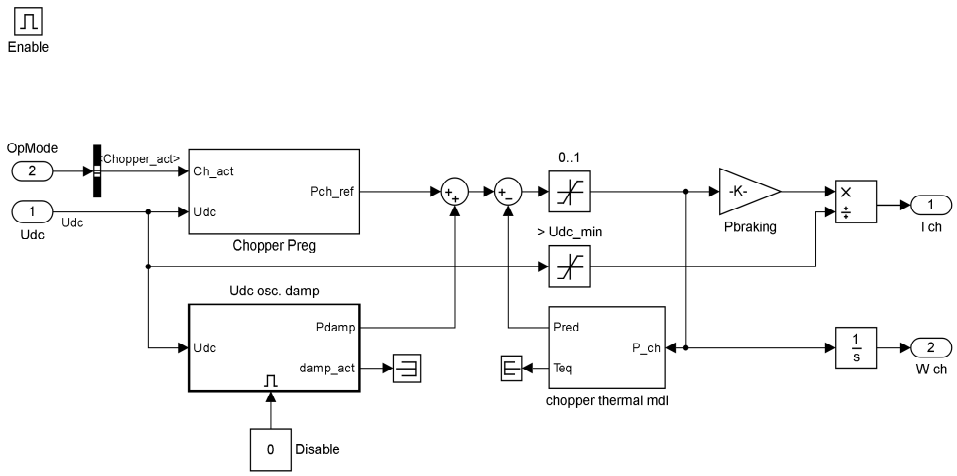

Figure 85: Wind Turbine grid side converter dc-voltage control, blockname: 'Chopper_Preg'

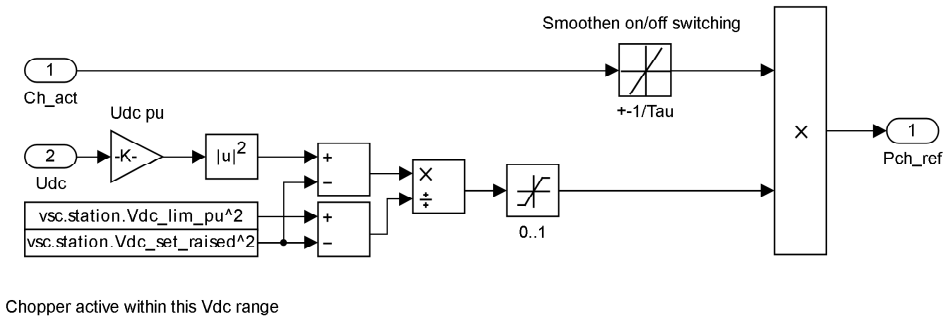

Figure 86: Wind Turbine grid side converter dc-voltage control, blockname: 'chopper_thermal_mdl'

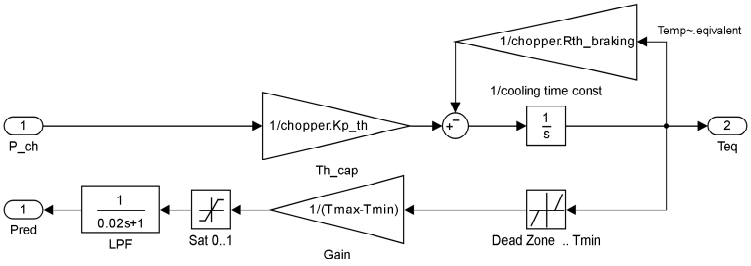

Figure 87: Wind Turbine grid side converter dc-voltage control, chopper operation during voltage dip: (top) dc-voltage, (bottom) PMG power (Yellow), chopper dissipated power (magenta) and grid converter power (cyan)

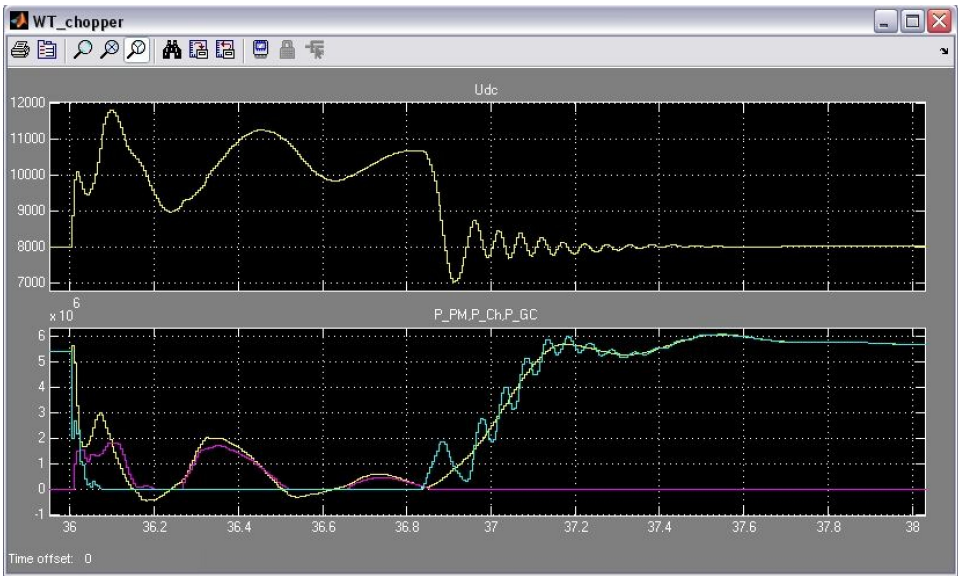

Figure 88: Wind Turbine grid converter dc-link, blockname: 'Station_Capacitor'

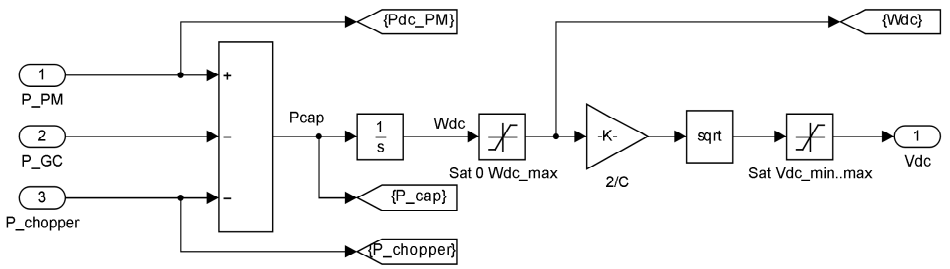

B.5 MTDC model

Figure 89 shows the structure of the Multi-terminal HVDC model, which consists of two state-space models with an operational mode switch to approximate the dynamic - but not the transient - behaviour in case of several types of faults. cf. figures 90, 91 and 92. The Station capacitors are added to the pi-model of the connected DC-cables, which leaves a simple subtraction for the VSC station DC-output current $I_{station}$, see figure 93.

Wind Farm Converter station (WF-VSC)

The wind farm converter model has a similar structure as the wind turbine VSC, although with opposite sign convention and different control settings. The rectifier current control model of figure 94 is almost similar to the WT grid converter and the HVDC grid converter model. Differences are that the dc-voltage control does not have the feedforward term of the rectifier power as it is no back-to-back configuration. Secondly, the reactive current setpoint is non-zero and is applied to control the ac-voltage. The ac-voltage control shown in figure 95 combines a PI-feedback loop and a feedforward term to compensate the dq-cross-coupling and the voltage drop over the WF transformer series impedance. Also the reference current setpoints are calculated differently, i.e. the damping terms needed to stabilise the interaction between two converters are absent and here a model for estimating the grid voltage angle is included. The ac-voltage reference control includes an estimation of the dc-link voltage at the HVDC grid converter. This dc-voltage is used as input to a hysteresis control of the ac-voltage setpoint. When the dc-voltage exceeds the limit value Udc_{lim} the ac-voltage setpoint is gradually decreased to 0.5pu, shown in figure 98. After the dc-voltage has decreased below a lower limit the ac-voltage setpoint is gradually restored. Actual ac-voltage limits, see figure 96 represent the VSC capability limits.

Figure 89: MTDC Grid model, blockname: 'MTDC_Grid'

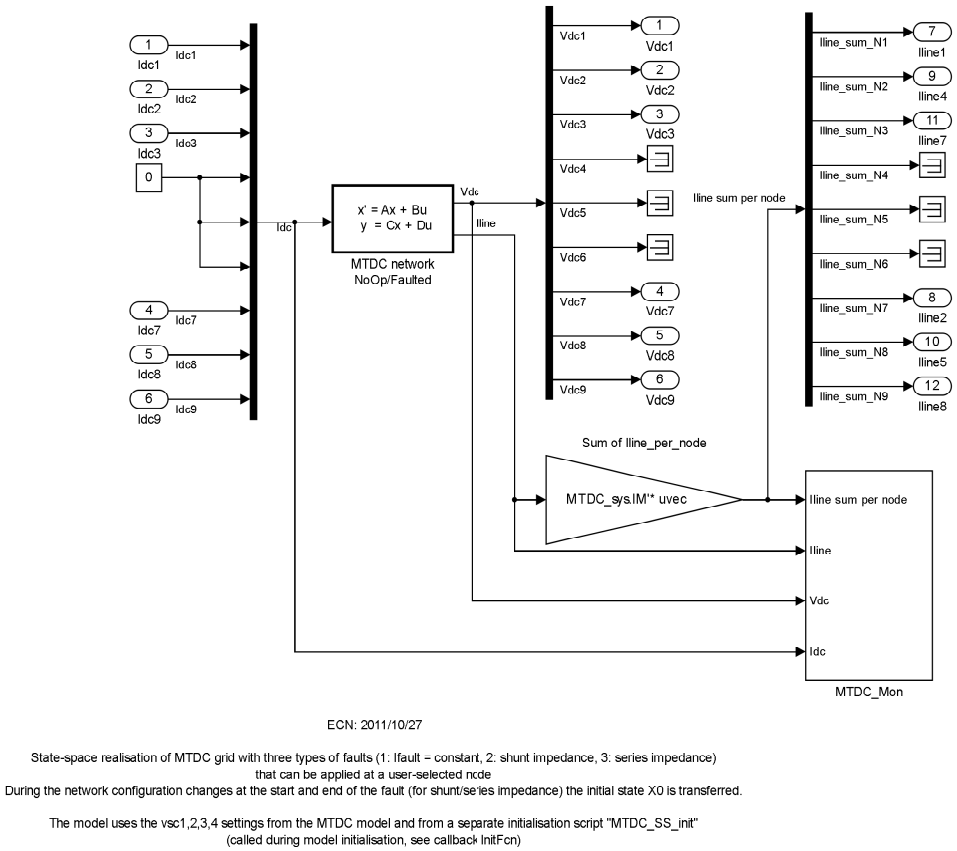

Figure 90: MTDC Grid model, blockname: 'MTDC_Grid'

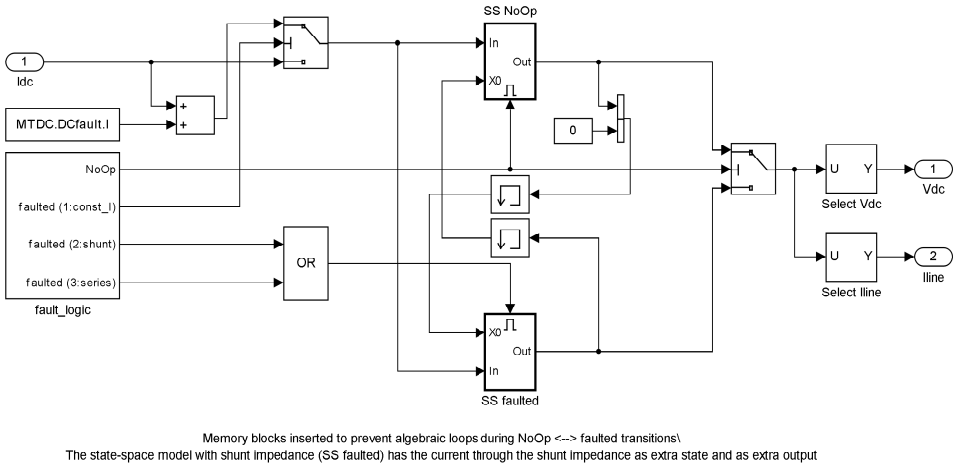

Figure 91: MTDC Grid model, blockname: 'MTDC_Grid'

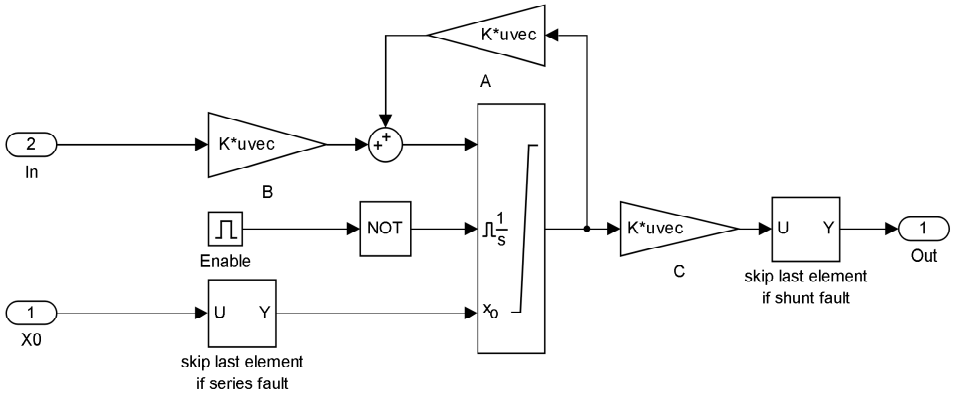

Figure 92: MTDC Grid model, blockname: 'MTDC_Grid'

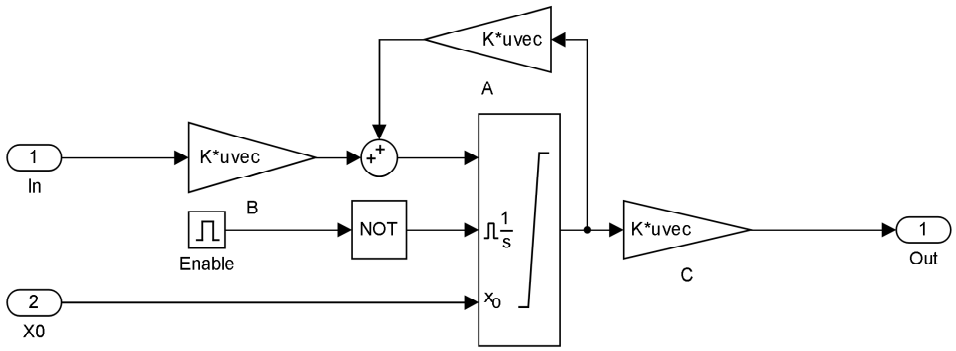

Figure 93: HVDC link, blockname: 'DC_Circuit'

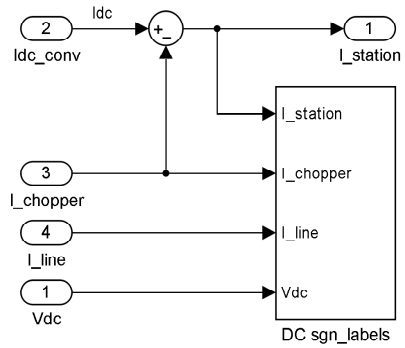

Station capacitor is included in the MTDC network model and not here

Figure 94: HVDC WFC, blockname: 'WF Rectifier'

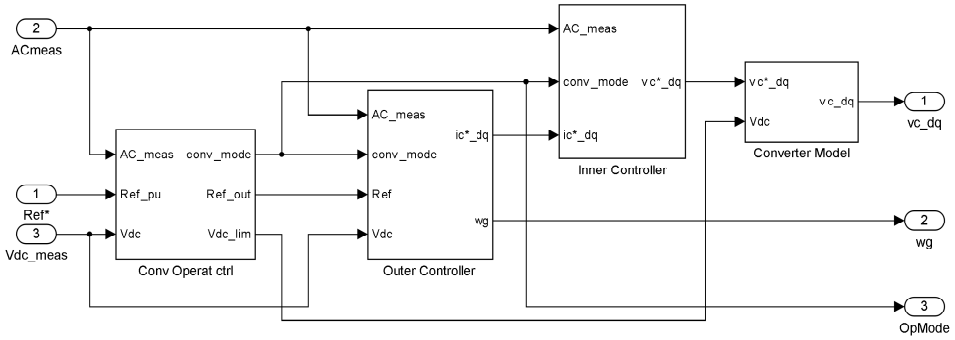

Figure 95: HVDC WFC outer controller with voltage decoupling and FF series reactance voltage drop, blockname: 'Outer_Controller'

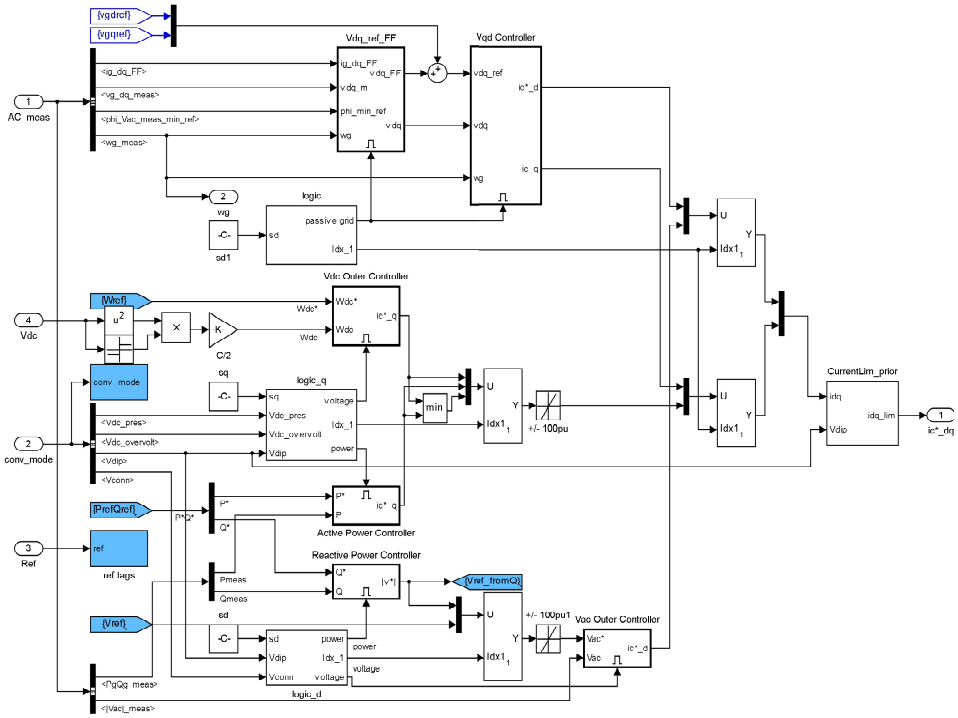

Figure 96: HVDC WFC calculation of control references: 'calc_actual_Refs1'

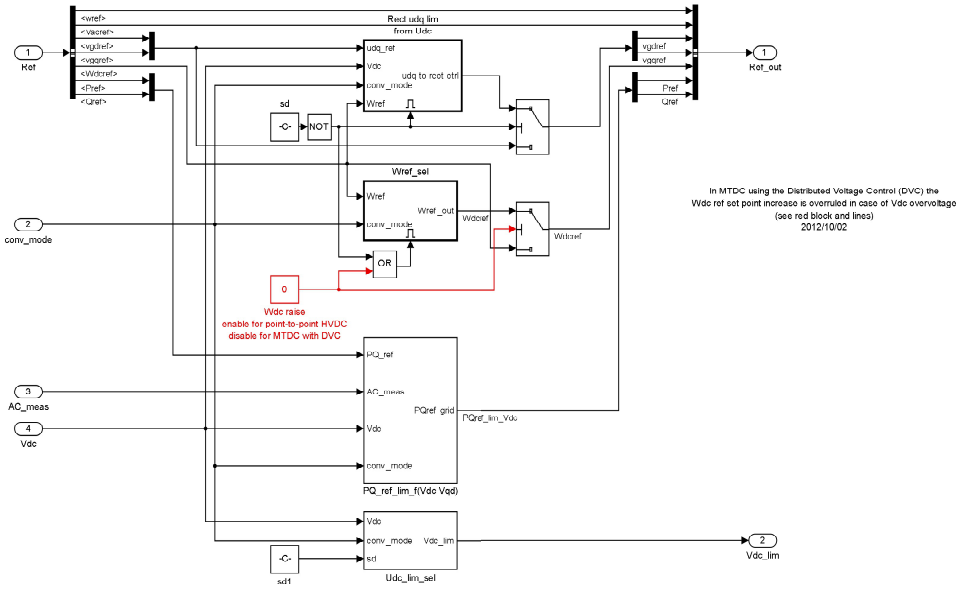

Figure 97: HVDC WFC calculation of reduced ac-voltage setpoint: 'udq_red'

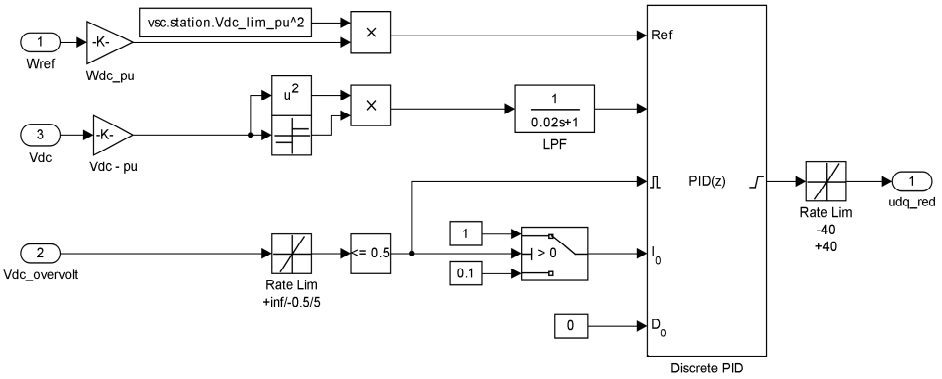

Figure 98: HVDC WFC calculation of actual voltage limits: 'voltLim'

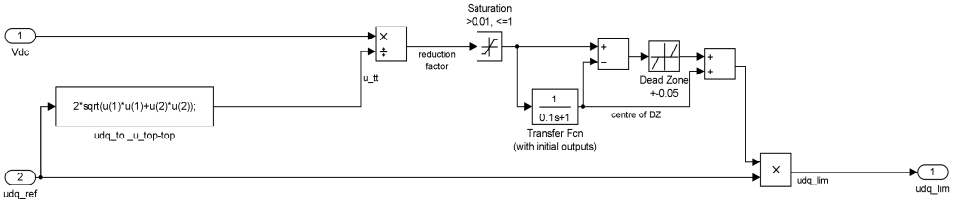

GS-VSC

The HVDC grid side converter model is identical to the Wind farm VSC model, although with different control mode settings and control references. The grid side VSC are set to control dc-voltage, for which the DVC method provides the references, and reactive power in order to support the onshore grid as prescribed by the relevant grid code.

Grid model

The onshore grid for the UK connection is modeled as a single synchronous generator that is connected via an overhead line. To simulate voltage dips a symmetrical shunt impedance with a timed switch is along this line. The actual generator characteristics and line impedance have been chosen such that the short circuit ratio is high enough for proper operation of the VSC and that still some interaction occurs (in both the voltage at PCC and in the grid frequency). The grid model does not relate to actual UK grid characteristics. For the two grid connections (NL and GE) no grid fault is applied and therefore the grid is simply modeled as an infinite bus.

C

Suggested improvements and next steps

C.1 Wind Farm dynamic models

Wind Farm

- Detail model, f.i. by including earthing and protection equipment
- Model high wind speed cut-out behaviour and simulate at WF scale in MTDC grid

Wind turbines

- Simplification of WT models to speed up calculations
- Reactive power control: check capabilities with common grid code requirements
- Improve WT controller tuning of 6MW demo WT
- Include existing DFIG WT models and eventually SCIG WT models in WF model

HVDC converters and MTDC-grid

- Test optimized converter control settings
- Add alternative WF power regulation methods, e.g. variable WF grid frequency
- Model HVDC protection system response for different configurations, e.g. bi-polar, mono-polar, etc.
- Model alternative converter choices, e.g. FC-VSC FC-CSC combinations
- Check typical time constants of PLL and stability regions

AC-grid

- Simulate MTDC with voltage control in weak grids

Validation

- Implement WF model in real-time simulator
- perform calculations with several other wind farm configurations,e.g.: faults in the WF, e.g. tripping of a string feeder

C.2 DVC power flow control with measurement errors

In real systems both measurements and control settings include errors. Because of the low impedances in the MTDC grid any voltage error may lead to serious errors in the actual power flow. In the following a feedback structure and controller settings are proposed for the voltage measurement error, according to the block scheme in figure 99. In theory itwill significantly reduce the errors in the DVC method in presence of (especially DC-voltage) measurement errors, although the bandwidth it limited and also the accuracy is limited by the power measurement errors.

The inner loop, controlling the DC voltage V_i of VSC station i:

$$\frac{dV_i^2(t)}{dt} = \frac{2}{C_i}\Big\{P_i(t) - \sum_{j\neq i} P_j(t)\Big\} \tag{C.1}$$

$$s\,V_i^2 = \frac{2}{C_i}\Big\{G_v(s)\cdot\{(V_{set,i}^2 - (V_i + V_{err,i})^2)\} - \sum_{j\neq i} V_i(V_i - V_j)Y_{ij}\Big\} \tag{C.2}$$

with $V_{err,i} \ll V_i$:

$$s\,V_i^2 \approx \frac{2}{C_i}\Big\{G_v(s)\cdot\{(V_{set,i}^2 - V_i^2 - 2V_iV_{err,i}))\} - \sum_{j\neq i} V_i(V_i - V_j)Y_{ij}\Big\} \tag{C.3}$$

with $|V_i - V_j| \ll V_i$ and $|V_i - V_{set,i}| \ll V_{set,i}$:

$$s\,V_i^2 \approx \frac{2}{C_i}\Big\{G_v(s)\cdot\{(V_{set,i}^2 - V_i^2 - 2V_{set,i}V_{err,i}))\} - \frac{1}{2}\sum_{j\neq i}(V_i^2 - V_j^2)Y_{ij}\Big\} \tag{C.4}$$

$$V_i^2(s+\frac{2}{C_i}G_v(s)+\frac{1}{C_i}\sum_{j\neq i}Y_{ij}) \approx \frac{2}{C_i}\Big\{G_v(s)\cdot\{(V_{set,i}^2-2V_{set,i}V_{err,i}))\}+\frac{1}{2}\sum_{j\neq i}V_j^2Y_{ij}\Big\} \tag{C.5}$$

with $G_v(s) = K_v \gg \sum_{j\neq i} Y_{ij}$:

$$V_i^2 \approx \frac{V_{set,i}^2 - 2V_{set,i}V_{err,i} + \frac{1}{2K_v}\sum_{j\neq i}V_j^2Y_{ij}}{s\frac{C_i}{2K_v} + 1} \tag{C.6}$$

The outer loop, controlling the power P_i of VSC station i:

$$P_i + P_{err,i} = G_v(s) \cdot \{(V_{set,i}^2 - (V_i + V_{err,i})^2)\} \tag{C.7}$$

with $G_v(s) = K_v \gg \sum_{j \neq i} Y_{ij}$ and $V_{err,i} \ll V_i$ and then substituting (C.6) in (C.8):

$$P_i + P_{err,i} \approx K_v \cdot \{(V_{set,i}^2 - V_i^2 - 2V_{set,i}V_{err,i})\} \tag{C.8}$$

$$P_i + P_{err,i} \approx K_v \cdot \{(V_{set,i}^2 - \frac{V_{set,i}^2 - 2V_{set,i}V_{err,i} + \frac{1}{2K_v}\sum_{j \neq i} V_j^2 Y_{ij}}{s\frac{C_i}{2K_v} + 1} - 2V_{set,i}V_{err,i})\} \tag{C.9}$$

$$P_i + P_{err,i} \approx \frac{s\,C_i\{\frac{1}{2}V_{set,i}^2 - V_{set,i}V_{err,i}\} + \frac{1}{2}\sum_{j \neq i} V_j^2 Y_{ij}}{s\frac{C_i}{2K_v} + 1} \tag{C.10}$$

$$P_i + P_{err,i} \approx \frac{s\,C_i\{\frac{1}{2}\,G_p(s) \cdot \{(P_{set,i} - (P_i + P_{err,i}))\} + V_{nom}^2 - V_{set,i}V_{err,i}\} + \frac{1}{2}\sum_{j \neq i} V_j^2 Y_{ij}}{s\frac{C_i}{2K_v} + 1} \tag{C.11}$$

with $G_p(s) = K_i/s$ and $K_i\frac{C_i}{2} \gg 1$:

$$(P_i + P_{err,i}) \cdot (s\,\frac{C_i}{2K_v} + K_i\frac{C_i}{2} + 1) \approx \frac{s\,C_i\{\frac{1}{2}\,G_p(s) \cdot P_{set,i} + V_{nom}^2 - V_{set,i}V_{err,i}\} + \frac{1}{2}\sum_{j \neq i} V_j^2 Y_{ij}}{s\frac{C_i}{2K_v} + 1} \tag{C.12}$$

$$(P_i + P_{err,i}) \cdot (\frac{s}{K_v K_i} + 1) \approx P_{set,i} + \frac{s}{K_i}\{V_{nom}^2 - 2V_{set,i}V_{err,i}\} + \frac{1}{K_i C_i}\sum_{j \neq i} V_j^2 Y_{ij} \tag{C.13}$$

$$P_i - P_{set,i} \approx \frac{\frac{s}{K_v K_i}\{-P_{set,i} + K_v V_{nom}^2\} + \frac{1}{K_i C_i}\sum_{j \neq i} V_j^2 Y_{ij}}{\frac{s}{K_v K_i} + 1} - P_{err,i} \tag{C.14}$$

Figure 99: *Control scheme to reduce measurement errors*

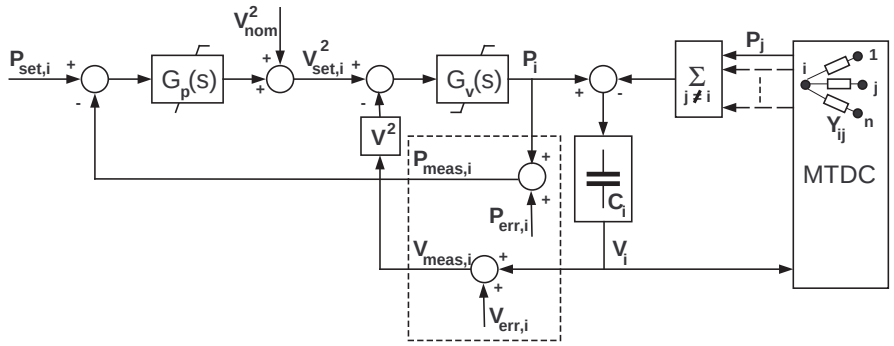

C.3 DC loop flows

When the NSTG expands to more complex topologies it may contain mazes. Simply interconnecting the DC cables will prevent loop flows as there is no voltage source in the maze that drives this loop flow. In other words, the system is overdetermined, i.e. each new line between two existing nodes does not increase the number of DC-voltages that can be controlled, which results that the load flow through this new line cannot be controlled independently, limiting the so-called Net Transfer Capacity of the MTDC grid.

Proposed solutions

The proposed solutions below add extra degrees of freedom, such that any load flow demanded by TSOs can be realized, within the rated line and converter capacities. Two solutions will be explained with the “Full ring” topology, see also figure 100.

1) Parallel node splitting: The voltages of the parallel nodes, 1, 1a and 1b, can be controlled independently, thereby controlling the power flows. The grouping of the VSC stations and the connected wind farms over the nodes is chosen proportional to the capacities of the connected trading lines, in order to make the best use of the available transport capacity.

2) Serial node splitting: By inserting DC/DC-converters in each maze of the NSTG an extra degree of freedom is added to control the DC voltage at node 1a and 1b and thereby the power flow.

Discussion

Solution 2 is much more expensive than solution 1 as it requires extra converter stations. With this solution the maximum line capacities are always available to realize the requested power flow from the market model. Solution 1 works well for large nodes, i.e. with a significant number of parallel VSCs. If solution 1 is applied at a node with only one converter station it does require an extra converter station, but such station can be installed onshore. Trading power between two neighbouring nodes, e.g. from No to Dk via UK results in extra converter losses, as the nodes are coupled by the onshore AC bus. Parallel circuits may also be inevitable because of limited capacity ratings of converters and cables and also to preserve onshore grid stability in case of a converter or DC cable failure.

What matters for the power flow is that solutions exist to resolve de restrictions (dependencies) in the MTDC power flow with the same (solution 2) transport capacities between the countries. The result is that the NTC that are available are equal to the rated capacities (1 pu.) with subtraction of the cable and converter losses. Obviously also the limitations in the connected onshore grid should be taken into account.

Figure 100: Solutions for loop flow limitations in MTDC grid

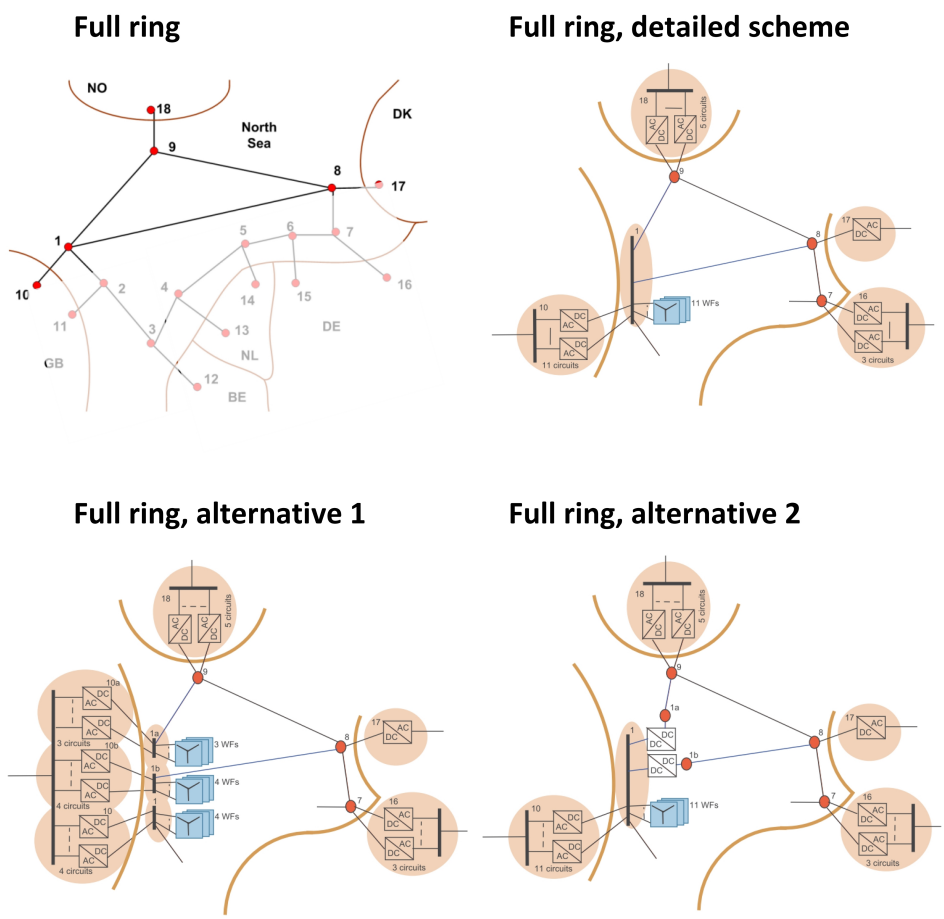

Index

Bibliography

1 M. Aredes, Portela C., Aquino A.F.C., and Peixoto C.A.O. *A 500 kV Soft-Switching HVDC Tap*. *CIGR 14-115*, 2002.

2 R. Blasco-Gimenez, S. Ano-Villalba andJ. Rodriguez, D. Derlee, S. Bernal-Perez, and F. Morant. *Diode-Based HVdc Link for the Connection of Large Offshore Wind Farms*. *IEEE TRANSACTIONS ON ENERGY CONVERSION*, VOL. 26, NO. 2:615–626, 2011.

3 S.K. Chaudhary. *Control and Protection of Wind Power Plants with VSC-HVDC Connection*. PhD thesis, Aalborg University, 2011.

4 O. Gomis-Bellmunt, Liang J., J. Ekanayake, R. King, and N. Jenkins. *Topologies of multiterminal HVDC-VSC transmission for large offshore wind farms*. *Electric Power Systems Research*, EPSR-3125:11, 2010.

5 Kundur. *Power System Stability and Control*. EPRI, 1994.

6 WECC Modeling and Validation Work Group WECC. *WECC Wind Power Plant, Dynamic Modeling Guide*. Technical report, Western Electricity Coordinating Council, http://renew-ne.org/wp-content/uploads/2012/05/WECCWindPlantDynamicModelingGuide.pdf, 2010.

7 NSCOGI. *Final report - grid configuration, NSCOGI, Technical Report*. Technical report, North Seas Countries Offshore Grid Initiative, http://www.benelux.int/NSCOGI/NSCOGI_WG1_OffshoreGridReport.pdf, 2012.

8 Pedro Andre Carvalho Rosas P. Soerensen, A.D. Hansen. *Wind Models for Prediction of Power Fluctuations of Wind Farms*. *J. Wind Eng. Ind. Aerodyn.*, No. 90:1381–1402, 2002.

9 J.T.G. Pierik. *North Sea Transnational Grid (NSTG) WP2 - Part 1: Wind farm locations and NSTG development*. Technical report, ECN, 2010.

10 J.T.G. Pierik and J. Morren. *Validation of dynamic models of wind farms (Erao-3): Executive summary, benchmark results and model improvements*. Technical Report ECN-E-07-006, *ECN*, 2007.

11 J.T.G. Pierik and J. Morren. *Variable Speed Wind Turbine Dynamic Model Validation; JWT measurements and simulations*. Technical Report ECN-E-07-008, *ECN*, 2007.

12 J.T.G. Pierik, J. Morren, E.J. Wiggelinkhuizen, S.H.W. de Haan, T.G. van Engelen, and J. Bozelie. *Electrical and Control Aspects of Offshore Wind Turbines II (Erao-2). Volume 1: Dynamic models of wind farms* . Technical Report ECN-C- -04-050, ECN, 2004. available at the web site of ECN (*www.ecn.nl*, use search option).

13 J.T.G. Pierik, J. Morren, E.J. Wiggelinkhuizen, S.H.W. de Haan, T.G. van Engelen, and J. Bozelie. *Electrical and Control Aspects of Offshore Wind Turbines II (Erao-2). Volume 2: Offshore wind farm case studies* . Technical Report ECN-C- -04-051, ECN, 2004. available at the web site of ECN (*www.ecn.nl*, use search option).

14 J.T.G. Pierik, Y. Zhou, and P. Bauer. *Wind Farm as Power plant, Dynamic modelling studies*. Technical Report ECN-E- -08-017, ECN, 2008. available at the web site of ECN (*www.ecn.nl*, use search option).

15 JTG Pierik, Y. Zhou, and P. Bauer. *Wind Farm as Power Plant: Dynamic modelling studies* . Technical Report ECN-E-08-017, *ECN* , 2008.

16 R. Teixeira Pinto. *M ulti-terminal DC networks: System integration, dynamics and control*. PhD thesis, Delft University of Technology, 2014.
17 R. Teixeira Pinto, S.F. Rodrigues, E.J. Wiggelinkhuizen, P. Bauer, and J.T.G. Pierik. *Operation and Power Flow Control of Multi-Terminal DC Networks for Grid Integration of Offshore Wind Farms Using Genetic Algorithms*. *Energies*, 6:1–26, 2013.
18 B. Qahraman. *Series / Parallel Hybrid VSC-LCC for HVdc Transmission Systems*. PhD thesis, University of Manitoba, 2010.
19 G. Ramtharan, N. Jenkins, and O. Anaya-Lara. *Modelling and Control of Synchronous Generators for Wide-range Variable-speed Wind Turbines*. *Wind Energy'*, VOL. 10, No. 3:231246, 2007.
20 P. Soerensen, B. Andresen, J. Fortmann, and P. Pourbeik. *Modular structure of wind turbine models in IEC 61400-27-1*. *Power and Energy Society General Meeting (PES), 2013 IEEE*, pages 1–5, 2013.
21 C. J. A. Versteegh. *Design of the Zephyros Z72 wind turbine with emphasis on the direct drive PM generator*. *NORPIE 2004, NTNU Trondheim Norway*, 2004.
22 D.A.J. Wouters and T.G. van Engelen. *Modern wind turbine controller design*. *Global Wind Power 2008, China Wind Power 2008*, 2008. Report nr. ECN-M–08-060.
23 Chunming Yuan, Xiaobo Yang, Dawei Yao, and Chengyan Yue. *Review on Hybrid HVDC Technology for Integration of Offshore Wind Power Plant*. *12th Wind Integration Workshop, London, UK*, 2013.
24 Yi Zhou. *Wind Power integration from individual Wind Turbine to Wind Park as a Power Plant*. PhD thesis, TU-Delft, 2009.

List of Tables

1 Description of the analysed case studies 31

2 Wind farm parameters 44
3 Control parameters 45

List of Figures

1 North Sea Transnational Grid and wind farm locations (photo: NASA) 6

2 Possible basic topologies in the NSTG 8
3 Possible basic topologies in the NSTG 9
4 Wind farm technologies and grid connection options 10

5 Topology of the modeled MTDC grid 13
6 Components of the modelled MTDC grid (DE nodes) 14
7 Model of the MTDC network including AC-grids 15

8 Wind farm component aggregation 18
9 Wind farm smoothing, step 1: generation of wind turbine power series 18
10 Wind farm smoothing, step 2: combining wind turbine power 19

11 Wind farm power per wind turbine 19
12 Wind farm power per line of 20 wind turbines 20
13 Wind turbine and wind farm power 20
14 Wind turbine and wind farm power spectra 21
15 Wind turbine schematic overview 21
16 Wind turbine model blocks 22
17 Wind turbine and rectifier control 23
18 Generator torque reduction and damping 24
19 Wind turbine converter control 25
20 Wind turbine grid-side converter operational mode 26
21 HVDC Wind Farm Converter 26
22 HVDC Grid Side Converter 27
23 HVDC Grid Side Converter operation 27
24 HVDC DC-link with chopper 27

25 Black-start 34
26 Steady-state operation 34
27 Changing power flow 35
28 Fault response 35
29 Fault response 36
30 Fault response 36
31 Losses in the MTDC system for all cases 37

32 Flow diagram of model simulation 48
33 Model overview model name 'NSTG_SSM' 50
34 Wind Farm mask 50
35 Wind Farm model, blockname: 'VSC_Station_WF_UK1' 51
36 Wind Farm model, blockname: 'VSC_Station_UK1' 52
37 Wind Farm model reference, blockname: 'VSC_Station_WF1' 52
38 Wind Farm model reference, blockname: 'VSC_Station_UK1' 52
39 Wind Farm string 5WTs 53
40 Wind Farm string 53
41 Wind Farm string cable, blockname: 'Cable_AC_park' 54
42 Wind Farm trafo, blockname: 'trafo_par_Cf' 54
43 Wind Turbine model structure, blockname: 'WT+Ctrl' 55
44 Wind Turbine mechanical and aerodynamic model and control, blockname: 'WIND TURBINE' 55
45 Wind Turbine wind model, blockname: 'WIND' 56
46 Wind Turbine generator inertia, blockname: 'Drive Train' 56
47 Wind Turbine generator inertia, blockname: 'Shaft Torsion' 56
48 Wind Turbine generator inertia, blockname: 'Rotorspeed' 57
49 Wind Turbine generator inertia, blockname: 'Generator speed' 57
50 Wind Turbine generator and inverter, blockname: 'PM dq + conv' 57
51 Wind Turbine generator with upscaling, blockname: 'Generator upscaling' 58
52 Wind Turbine generator with control, blockname: 'PMG 2MW + ctrl' 58
53 Wind Turbine generator and measurement block, blocknames: 'PMG' and 'PMG_Meas' 58
54 Wind Turbine generator, blockname: 'PM_2' 59
55 Wind Turbine generator flux and torque calculation, blockname: 'PM_phi_Te" 59
56 Flux calculation, blockname: 'phi_calc' 59
57 Wind Turbine generator stator dynamics, blockname: 'stator_dyn' 60
58 Wind Turbine generator torque calculation, blockname: 'T_e' 60
59 Wind Turbine generator decoupling, blockname: 'u_decoupling' 60
60 Wind Turbine generator flux calc, blockname: 'phi_est' 61
61 Wind Turbine generator flux angle estimation during startup: (top) rotor flux, (middle) measured and estimated rotor flux angle, (lower two) stator voltage and current 61
62 Wind Turbine generator flux angle estimation during voltage dip: (top) rotor flux, (middle) measured and estimated rotor flux angle, (lower two) stator voltage and current 62

63 Wind Turbine generator torque reduction, blockname: 'Te_set red Udc_lim_MOD' 63
64 Wind Turbine generator electrical power reduction, blockname: 'Pe_red' 64
65 Wind Turbine generator electrical power reduction during voltage dip: top: U_dc measured (yellow), emphasized (magenta) and emph. and slopehold (green) 64
66 Wind Turbine generator torque setpoint smoothing, blockname: 'Te_smooth' 64
67 Wind Turbine generator damping, blockname: 'Shaft_damp' 65
68 Wind Turbine generator torque ramp-up limit, blockname: 'Limit Pramp_up' 65
69 Wind Turbine generator torque and power limit, blockname: 'Limit Te_set, Pe_set' 65
70 Wind Turbine generator torque reduction, partial to full load transition: (top) WT-controller Torque setpoint (yellow), smoothed torque setpoint (magenta), (bottom) red line shows some reduction of torque oscillations 66
71 Wind Turbine generator torque reduction, voltage dip response: (top) 67
72 Wind Turbine grid full-scale converter with dc-link and controllers, blockname: 'Gridconv + DC link from HVDC mdl' 68
73 Wind Turbine grid side converter, blockname: 'Grid converter' 68
74 Wind Turbine grid side converter, blockname: Voltage Modulator 69
75 Wind Turbine grid side converter current control, blockname: 'Inner_Controller' 69
76 Wind Turbine grid side converter current control, blockname: 'Outer_Controller' 70
77 Wind Turbine grid side converter power limiter with PQ-priority selection, blockname: 'PQ_ref_lim_f(Vdc_Vqd)_WT' 70
78 Wind Turbine grid side converter power limiter with PQ-priority selection detail, blockname: 'PQ_ref_lim_prior' 71
79 Wind Turbine grid side converter current limiter with PQ-priority selection detail, blockname: 'CurrentLim_prior' 71
80 Wind Turbine grid side converter active power reduction at low grid voltage, blockname: 'PowerLim' 71
81 Wind Turbine grid side converter dc-voltage control, blockname: 'Vdc_Outer_Controller' 71
82 Wind Turbine grid side converter operating mode control, blockname: 'Conv_operating_mode_W
83 Wind Turbine grid side converter dc-voltage control, blockname: 'calc_actual_Refs_WT' 72
84 Wind Turbine grid side converter dc-voltage control, blockname: 'Chopper' 73
85 Wind Turbine grid side converter dc-voltage control, blockname: 'Chopper_Preg' 74
86 Wind Turbine grid side converter dc-voltage control, blockname: 'chopper_thermal_mdl' 74
87 Wind Turbine grid side converter dc-voltage control, chopper operation during voltage dip: (top) dc-voltage, (bottom) PMG power (Yellow), chopper dissipated power (magenta) and grid converter power (cyan) 74
88 Wind Turbine grid converter dc-link, blockname: 'Station_Capacitor' 74
89 MTDC Grid model, blockname: 'MTDC_Grid' 75
90 MTDC Grid model, blockname: 'MTDC_Grid' 76
91 MTDC Grid model, blockname: 'MTDC_Grid' 76
92 MTDC Grid model, blockname: 'MTDC_Grid' 76
93 HVDC link, blockname: 'DC_Circuit' 77
94 HVDC WFC, blockname: 'WF Rectifier' 77
95 HVDC WFC outer controller with voltage decoupling and FF series reactance voltage drop, blockname: 'Outer_Controller' 77
96 HVDC WFC calculation of control references: 'calc_actual_Refs1' 78
97 HVDC WFC calculation of reduced ac-voltage setpoint: 'udq_red' 78
98 HVDC WFC calculation of actual voltage limits: 'voltLim' 78

99 *Control scheme to reduce measurement errors* 85
100 Solutions for loop flow limitations in MTDC grid 87

ECN
Westerduinweg 3
1755 LE Petten
The Netherlands

P.O. Box 1
1755 ZG Petten
The Netherlands

T +31 88 5154949
info@ecn.nl
www.ecn.nl